NEW SOLVENTS FOR SURFACTANT SELF-ASSEMBLY: MOLTEN HYDRATED SALTS AND CONCENTRATED AQUEOUS ELECTROLYTE SOLUTIONS

A DISSERTATION SUBMITTED TO
THE DEPARTMENT OF CHEMISTRY
AND THE GRADUATE SCHOOL OF ENGINEERING AND SCIENCE
OF BILKENT UNIVERSITY
IN PARTIAL FULFILLMENT OF THE REQUIREMENTS
FOR THE DEGREE OF
DOCTOR OF PHILOSOPHY

By
CEMAL ALBAYRAK

January 2013

I certify that I have read this thesis and that in my opinion is it is fully adequate, in scope and quality, as a thesis for the degree of Doctor of Philosophy.

……..

Prof. Dr. Ömer Dağ

Supervisor

I certify that I have read this thesis and that in my opinion is it is fully adequate, in scope and quality, as a thesis for the degree of Doctor of Philosophy.

……..

Prof. Dr. Saim Özkar

Examining Committee Member

I certify that I have read this thesis and that in my opinion is it is fully adequate, in scope and quality, as a thesis for the degree of Doctor of Philosophy.

……..

Prof. Dr. Ahmet M. Önal

Examining Committee Member

I certify that I have read this thesis and that in my opinion is it is fully adequate, in scope and quality, as a thesis for the degree of Doctor of Philosophy.

……..

Assoc. Prof. Dr. Margarita Kantcheva

Examining Committee Member

I certify that I have read this thesis and that in my opinion is it is fully adequate, in scope and quality, as a thesis for the degree of Doctor of Philosophy.

……..

Assist. Prof. Dr. Emrah Özensoy

Examining Committee Member

Approved for the Graduate School of Engineering and Science

……..

Prof. Dr. Levent Onural

Director of the Graduate School

ABSTRACT

NEW SOLVENTS FOR SURFACTANT SELF-ASSEMBLY: MOLTEN HYDRATED SALTS AND CONCENTRATED AQUEOUS ELECTROLYTE SOLUTIONS

CEMAL ALBAYRAK

Ph.D., Department of Chemistry

Supervisor: Prof. Dr. Ömer Dağ

January, 2013

Lyotropic liquid crystalline (LLC) mesophases are formed by at least two components: a surfactant and a solvent. Common solvents in the surfactant self-assembly include water, organic liquids, and ionic liquids. In this work, we show that molten hydrated salts of the type $[M(H_2O)_m](X)_n$ (where, M is a transiton metal cation and X is a suitable anion such as NO_3^-, Cl^-, and ClO_4^-), which have melting points close to room temperature (RT), can organize surfactant molecules into LLC mesophases. As an example, we have focused on the $[Zn(H_2O)_6](NO_3)_2$-$C_{12}EO_{10}$ system (where, $C_{12}EO_{10}$ is decaethylene monododecyl ether; H_3C-$(CH_2)_{11}$-$(OCH_2CH_2)_{10}$-OH). A binary phase diagram was constructed between -190^{o}C and 110^{o}C using differential scanning calorimetry (DSC), polarized optical microscopy (POM), X-ray diffractometry (XRD), fourier transform infrared spectroscopy (FT-IR), and raman spectroscopy. The phase diagram closely resembles the phase diagram of H_2O-C_mEO_n systems, exhibiting typical phases such as spherical cubic, hexagonal, and bicontinuous cubic. It is also observed that the phase transitions are dictated by the critical packing parameter (CPP) as the solvent concentration is changed. The mesophases are unusually stable at low temperatures, where a LLC to mesostructured solid transformation has been observed with a glass transiton at -52^{o}C. The mesostructured solid phase is also stable at -190^{o}C. The confinement of

the salt species in the LLC domains prevents the crystallization of the salt at low temperatures.

In the second part, from the analogy between $[M(H_2O)_m](X)_n$ type salts and concentrated electrolyte solutions of alkali metal salts, the mixtures of concentrated aqueous solutions of some Li^+ salts (LiCl, LiBr, LiI, $LiNO_3$ and $LiClO_4$) with $C_{12}EO_{10}$ surfactant, were investigated. The mixtures exhibited LLC mesophases in a broad range of compositions. A ternary phase diagram was constructed for the $LiNO_3$-H_2O-$C_{12}EO_{10}$ system at room temperature using XRD and POM tecniques. In the LLC mesophases formed with the Li^+ salts, the water remains as hydrated under ambient conditions and open atmosphere. In addition, the effect of anions on the phase behaviour follows a Hofmeister series except for the ClO_4^- ion. Ionic conductivty of the LiX-H_2O-$C_{12}EO_{10}$ (where X is Cl^- and NO_3^-) mesophases has been determined in a broad range of the salt concentrations (5 to 7 salt/surfactant mole ratio) and temperature (-13 to 100^oC). The LiCl-H_2O-$C_{12}EO_{10}$ LLC samples have also been used as a gel-electrolyte to run a polymer electrochromic device. The mesophase shows excellent performance in this device.

The investigations were further extended to include some of the Ca^{2+} salts, namely $CaCl_2$ and $Ca(NO_3)_2$. The concentrated aqueous solutions of both salts with $C_{12}EO_{10}$ and water exhibited LLC mesophases similar to the molten hydrated salts and concentrated solutions of Li^+ salts. In the $CaCl_2.xH_2O$-$C_{12}EO_{10}$ system, an LLC to mesocrystalline phase transformation was observed, for the first time, where the salt, water and surfactant species freezes to a mesocrystalline phase at RT.

Lastly, many other salt.xH_2O-surfactant LLC mesophases were investigated using the following salts: NaCl, NaBr, NaI, CH_3COONa, NaSCN, $NaClO_4$, $NaNO_3$, KNO_3, KCl, KSCN, KI, $MgCl_2$, $Mg(NO_3)_2$ and NaOH. In addition, the LLC mesophases of concentrated H_3PO_4 acid and $C_{12}EO_{10}$ were also investigated. Among these compounds, H_3PO_4 systems exhibited air stable LLC mesophases at RT and 25% relative humdity (RH). The $MgCl_2$ system was found to exhibit air stable LLC mesophases for a couple of hours. The NaI, KSCN and $NaClO_4$ systems were found to be stable at low salt concentrations with little or no mesostructured order. Other salt systems were unstable and leached out salt

crystals rapidly. The NaOH system is unstable because of a reaction with CO_2 in the air. In summary, we have found a correlation between the deliquescent relative humidity value of the salt and its LLC mesophase formation ability under ambient conditions.

Keywords: Lyotropic Liquid Crystals, Molten Salts, Concentrated Aqueous Electrolytes, Self Assembly, Transition Metal Aqua Complex Salts, Alkali Metal Salts, Alkaline Earth Metal Salts.

ÖZET

YÜZEY AKTİFLER İÇİN YENİ ÇÖZÜCÜLER: ERİYİK HİDRATLI TUZLAR VE DERİŞİK ELEKTROLİT SOLÜSYONLARI

CEMAL ALBAYRAK

Doktora, Kimya Bölümü

Tez Yöneticisi: Prof. Dr. Ömer Dağ

Ocak , 2013

Liyotropik sıvı kristal (LSK) arahaller (mesophase) en az iki bileşenden oluşur. Bunlardan biri yüzey aktif (surfactant), diğeri ise bir çözücüdür. Yüzey aktiflerin kendiliğinden düzenlenmesini sağlayan sıvılar arasında en çok bilinen çözücüler su, organik sıvılar, ve iyonik sıvılardır. Bu çalışmada erime noktaları oda sıcaklığı civarında olan ve $[M(H_2O)_m](X)_n$ olarak gösterilen (M bir geçiş metali, X ise NO_3^-,Cl^-,ClO_4^- vb. uygun bir karşı anyon olmalıdır) eriyik hidratlı tuzların, yüzey aktifleri LSK arahallere düzenleyebildiği gösterilmektedir. Bu amaçla örnek olarak $[Zn(H_2O)_6](NO_3)_2$-$C_{12}EO_{10}$ sistemini seçtik ($C_{12}EO_{10}$ dekaetilen monododesil eter olup; molekül yapısı H_3C-$(CH_2)_{11}$-$(OCH_2CH_2)_{10}$-OH dır). Bu sistemin ikili hal diyagramı -190^{o}C ile 110^{o}C arasında diferansiyel tarama kalorimetresi, polarize optik mikroskobu, X-ışını kırınım yöntemi, FT-IR ve raman spektroskopisi kullanılarak ortaya çıkarıldı. Hal diyagramı H_2O-C_nEO_m sistemlerinin hal diyagramlarına benzemekle birlikte bu hal diyagramlarına özgü küre kübik-hegzagonal ile hegzagonal-süreğen kubik halleri göstermektedir. Ek olarak, hal geçişlerinin kritik toplanma etkeninin (critical packing parameter) buyruğunda olduğu da görülmüştür. Diğer sistemlerden farklı olarak bu arahaller düşük sıcaklıklarda yüksek kararlılık göstermişlerdir. LSK arahallerde ilk defa arayapılı katı bir hale geçiş (-52^{o}C'de bir camsı-geçiş şeklinde) gözlemlenmiştir. Arayapılı katı fazın da -190^{o}C'de dahi kararlı olduğu gösterilmiştir. Tuz ögesinin liyotropik sıvı kristal hal içersinde kısıtlanması onun düşük sıcaklıklarda kristallenmesini engeller.

Çalışmanın ikinci kısmında, $[M(H_2O)_m](X)_n$ türü tuzlar ile derişik elektrolit çözeltiler arasındaki benzerlikten yola çıkılarak, çeşitli derişik Li^+ tuzu

çözeltilerinin (LiCl, LiBr, LiI, $LiNO_3$ and $LiClO_4$) $C_{12}EO_{10}$ yüzey aktifi ile oluşturduğu karışımlar incelenmiştir. Karışımların geniş bir derişim aralığında LSK arahali gösterdiği tespit edilmiş, bu doğrultuda, $LiNO_3$-H_2O-$C_{12}EO_{10}$ sistemiyle ilgili üçlü bir hal diyagramı, X-ışını kırınımı ve polarize optik mikroskobu tekniği ile inşa edilmiştir. Li^+ tuzlarının yönlendirdiği LSK fazlarda (oda koşullarında ve açık havada) su ögesi hidrat suyu olarak bulunur. Ayrıca, ClO_4^- iyonu haricinde anyonların hal davranışına etkisi Hofmeister dizisini takip eder. LiX-H_2O-$C_{12}EO_{10}$ (X'in Cl^- yahut NO_3^- olduğu) sistemlerde iyonik elektriksel iletkenlik derişime (5 ile 7 tuz/yüzey aktif oranı arasında) ve sıcaklığa (-13^oC ile 100^oC arasında) göre takip edilmiştir. Yüksek iletlenlikleri sebebiyle bu sistemler polimer tabanlı bir elektrokromik cihazda test edilmiştir. Arahaller bu cihazda yüksek başarım göstermiştir.

Araştırmalarımızı daha sonra bazı Ca^{2+} tuzlarını kapsayacak şekilde genişlettik. $CaCl_2$ ve $Ca(NO_3)_2$ tuzları da geçiş metal tuzları ve alkali tuzlar gibi $C_{12}EO_{10}$ yüzey aktifi ile LSK arahaller gösterdi. $CaCl_2.xH_2O$-$C_{12}EO_{10}$ sisteminde LSK bir arahalden arakristal (mesocrystal) hale, ilk defa olarak, bir geçiş gözlemlendi. Bu arakristallerde su-tuz-yüzey aktif üçlüsünün oda sıcaklığında beraberce bir mezokristale dönüştüğü anlaşılmıştır.

Son olarak, olası diğer tuz.xH_2O-yüzey aktif LSK arahalleri şu tuzlarda araştırılmıştır: NaCl, NaBr, NaI, CH_3COONa, NaSCN, $NaClO_4$, $NaNO_3$, KNO_3, KCl, KSCN, KI, $MgCl_2$, $Mg(NO_3)_2$ ve NaOH. Ek olarak derişik H_3PO_4 asidi ile $C_{12}EO_{10}$ yüzey aktifinin olası LSK hallerine de bakılmıştır. Tüm bu karışımlar arasında H_3PO_4 sistemi oda koşulları ve %25 bağıl nemde LSK hal göstermiştir. Diğer yandan, $MgCl_2$ sisteminin de oluşturduğu LSK arahaller birkaç saat kararlıdır. NaI, KSCN and $NaClO_4$ sistemlerinin ise düşük tuz oranlarında kararlı olmalarına karşın çok düşük arayapılı düzen içerdiği saptanmıştır. Kalan sistemler ise kararsızdır ve tuzlar kısa sürede kristallenir. NaOH sistemi ise havadaki CO_2 ile doğrudan reaksiyona girdiğinden kararsızdır. Özetle, bu tuzların higroskopik meyilleri ile LSK fazların oluşumu ve kararlılıkları arasında bir ilişki olduğu gösterilmiştir.

Anahtar Kelimeler: Liyotropik Sıvı Kristaller, Eriyik Tuzlar, Derişik Elektrolit Çözeltileri, Kendiliğinden Düzenlenme, Geçi Metali Sulu Kompleksleri, 1A Grubu Tuzları, 2A Grubu Tuzları

ACKNOWLEDGEMENTS

I remember the first time I looked through the microscope in my Junior year. It has been 7 years since then but still, it was just an hour ago that I did the same. In between these two glances and through the life of these half-alive amphiphiles, I got deeply connected to the subject, such that it became a part of me. This was only possible with the efforts of my supervisor. During all these years, he was always supportive, patient and considerate. I cordially thank him as he kept supporting me. I have learned a lot both in chemistry and in scientific methods under his supervision. Our elaborate dialogs shone light on the darkest problems and allowed us to discover new geographies in scientific research. I am leaving our lab with thousands of valuable questions and sincerely wishing that I could stay more.

I would also like to thank Prof. Atilla Cihaner for his help in the conductivity measurements. He was always kind and in good synergy with us throughout our discussions. Furthermore, I owe earnest thankfulness to Prof. Necati Özkan for his help and elaborate discussions on thermal measurements.

Special thanks should be given to the examining committiee members for their valuable suggestions and corrections on the thesis.

Among our research group members, I am especially thankful to Gözde Barım for her collaboration in the alkali metal salt systems. I also thank all the past group members for their help, friendship and support. I would like to thank Övgü Yılmaz for the preparation of some samples in this summer. I am also indepted to Ethem Anber, who has always been helpful with his creative ideas and indisputable handcraft. Lastly, I'd like to wish good luck to all newcomers; they are lucky to have Bilkent Chemistry as their academic family.

The financial support of the TUBITAK and Bilkent University is also highly appreciated.

I am also truly grateful for the serene nature of Bilkent. It has been a home for me for the last ten years with its elder trees and blossoming plants. I must say that I loved walking along the quiet lake, resting on the grassy hills and discovering all the hidden nooks and lonely corners of our big garden. I am happy to say that I was lucky enough to observe the nature in our campus thrive and become fully alive during these years.

Here, I feel obliged to thank to my dear friends from our department, Okan Çiftçi, Fatih Genişel, Hikmet Sezen, Emre Emmez, Emrah Parmak and Cüneyt Karakaya. Also, I cannot forget to express my blessings to my best friends Yiğit Subaşı, Can Rıza Afacan, Emre Say, Ozan Dündar,Ozan Şentürk and Can Baldan.

My family and Aslı'm: Your endless love has given me a *place to be*. This work would be impossible without your support and I am blessed to have you by my side.

I dedicate this thesis to the loving memory of my father and my brother Deniz.

TABLE OF CONTENTS

LIST OF FIGURES

LIST OF TABLES

1. Introduction

1.1 Surfactants and Micellar Phases

An interface is the boundary between two immiscible phases. A surface on the other hand is an interface where one of the phases is a gas. The molecules at an interface or surface are more energetic than the ones in the bulk because the interfacial molecules are unsaturated in terms of intermolecular interactions and form fewer bonds with the surronding molecules. The work required to create a unit surface area is called as the *surface free energy* which can be reduced when an appropriate molecule is able to compensate it by forming new bonds with the surface molecules. Such molecules lower the energy gap between the two phases in consideration.

Due to their amphiphilic nature, surfactant molecules (an abbreviation for surface active agents) can be adsorbed at the air-water interface and reduce the surface free energy. A surfactant molecule has hydrophilic and hydrophobic groups that can interact selectively with different sides of an interface. **Figure 1.1** shows various types of surfactant molecules. Surfactants can be classified according to their charge on hydrophilic region(s) (head groups). An anionic surfactant has a negatively charged head group, similarly a cationic surfactant has a positively charged head group. Surfactants, which contain both positively and negatively charged regions are classified as zwitterionic (zwitter: *hybrid*). If there is no charge at all, the surfactant is classified as nonionic.

The phase behaviour of surfactants in water differs in a delicate manner depending on the variations in the fundamental thermodynamic parameters such as; temperature, pressure, concentration etc. At very low concentrations in water, surfactant molecules migrate toward the air-water interface. The hydrophilic regions are hydrated by water molecules and the hydrophobic regions tends to stay away from the water by aligning vertically on the surface forming a monolayer of surfactant molecules, see **Figure 1.2**. Increasing the surfactant concentration increases the surface coverage and reduces the surface energy. In addition, the concentration of the surfactant molecules dissolved in the bulk liquid also increases. At a critical concentration, a microphase separation occurs, if the surfactant is

sufficiently soluble and surfactant molecules start to form aggregated structures – called *micelles*, see **Figure 1.3**- where hydrophobic regions tend to decrease their interaction with water by coalescing. It will be useful to understand the underlying mechanism behind the formation of micelles.

It is well known that, oil and water do not mix. However, contrary to the popular belief, spotaneous separation of both components is not solely driven by the enthalpy. Indeed, water and oil can attract each other. For instance, dissolving small non-polar molecules in water is an exothermic process.[1-3] Even for hexane, the enthalpy of transfer of this molecule to the aqueous solution is close to zero.[3] Therefore, entropic effects should be taken into account to understrand the nature of the phase separation. It is known that, the transfer of nonpolar molecules from organic to the aqueous phase results in a negative entropy.[2] This is usually explained by the increase in the order of water molecules around the free nonpolar molecules.[1-4] However, it should also be noted that the size of the nonpolar molecules may determine the dominancy of the contributions among the enthalpy and the entropy.[4] In the self-assembly of surfactant molecules, the confinement of the free moving surfactant molecules to the micellar volume restricts the movements of both hydrophilic and hydrophobic segments.[4] Therefore, the coalescence of the free moving surfactant molecules may at first seem to be entropically unfavorable. However as mentioned, the hydrophobic (nonpolar) segments can also induce some order in water.[4-6] At a certain surfactant concentration, contributions arising from the water ordering around the hydrophobic segments overcomes the aforementioned restrictions and overall the micelle formation increases the entropy at ambient conditions.[1,4-6] It is known that enthalpic and entropic contributions to micelle formation does not vary significantly with temperature (for nonionic surfactants) because these two thermodynamic parameters cancel out each other[1] and as a result the intermolecular interactions among the hydrophobic moieties becomes a significant factor in micelle formation.[7]

The concentration about which surfactants start to form micelles is the critical micelle concentration (CMC); a value that is determined by the nature of the surfactant, the nature of the solvent, temperature of the media, and other additives. **Table 1.1** shows the CMC of some surfactant molecules at room temperature. In

general, the CMC decreases rapidly with increasing hydrophobic chain length, so the less soluble the surfactant is, the lower the CMC is.[7] For nonionic surfactants, that have an ethyleneoxide chain as their hydrophilic region, the length of the chain increases the solubility in water and so the CMC.[7] In general, the charged surfactants have higher CMC as compared to nonionic surfactants,[7] this is due to the higher solubility of these molecules in water and extensive repulsive interactions among the charged head groups when a micelle is formed. For charged surfactants, addition of electrolytes decrease the repulsion among the head groups and therefore the CMC. The geometry, aggregation number (average number of surfactant molecules per micellar unit) and the size of the micelles depend on temperature and the type of the surfactant but additionally on the surfactant concentration. There is a tendency towards higher aggregation numbers and larger (or longer) micelles as the surfactant concentration is increased. [7]

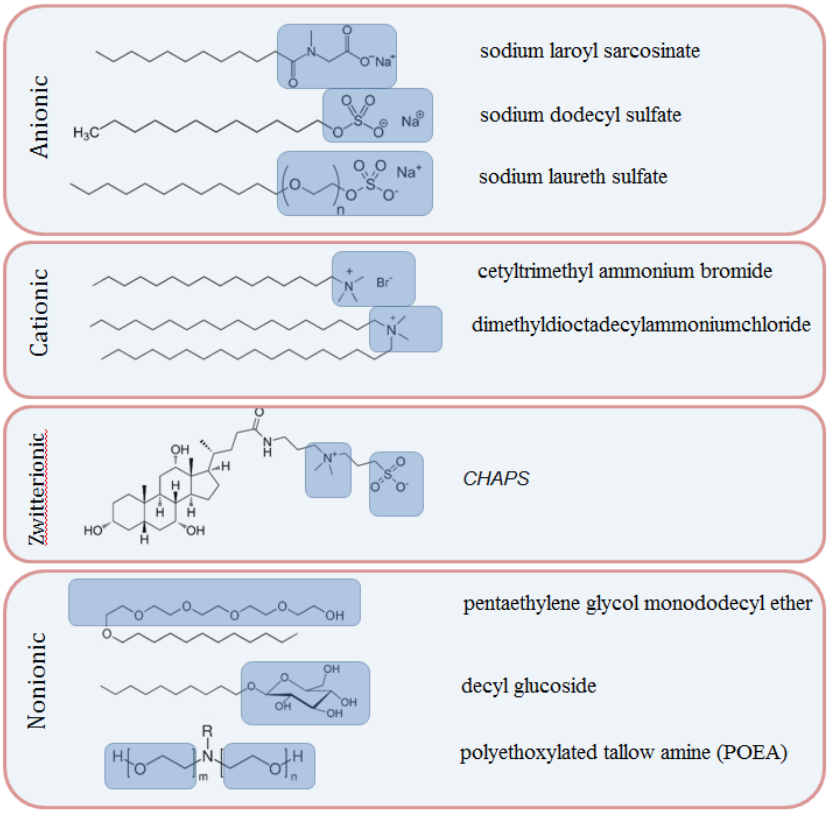

Figure 1.1. Typical surfactant molecules. Encapsulated parts depict the hydrophilic regions in the molecules.

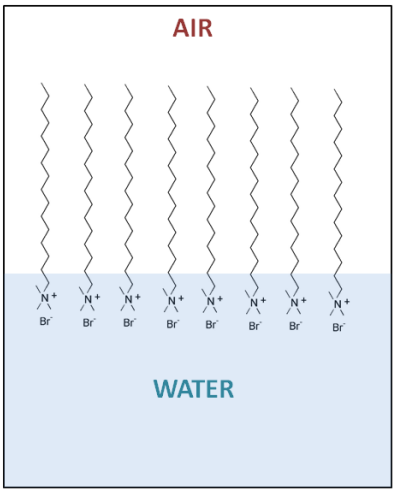

Figure 1.2. The alignment of surfactant molecules (CTAB) at the air-water interface

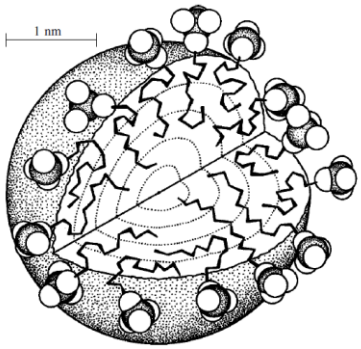

Figure 1.3.[*] An illustration of core (inner region) and corona (ball shaped hydrophilic regions) for the micelle formed by dodecyl sulphate (anionic) surfactant molecules. (Reprinted from ref. 11, with permission from Elsevier)

For nonionic surfactants,[7] the CMC is not significantly affected by the electrolytes as in charge surfactants but the eletrolyte effects are found to follow certain trends, which will be discussed in detail in the following chapters.

At the CMC, physical properties of surfactant solutions are greatly altered. **Figure 1.4** illustrates these changes on a plot. The sharp changes are followed in determination of the CMCs of surfactants. Above the CMC, the surface tension of

[*] Reprinted from Israelachvili, J.N. 20 - Soft and biological structures. in *Intermolecular and Surface Forces (Third Edition)* 535-576 (Academic Press, San Diego, 2011) with permission from Elsevier (2011).

the solution remains more or less the same, because additional surfactant molecules tend to form micellar aggregates in the bulk solution and air-water interface is already saturated with surfactant molecules. Turbidity (reduced transparency) of the solution also increases because of the emergence of colloidal size micelles. If the surfactant molecules are ionic, it is plausible to follow the ionic conductivity of the solution. The self diffusion of surfactant molecules will decrease upon micelle formation and therefore their ionic conductivity. While most of these properties can be followed for any surfactant type, it is more plausible to follow the sharpest change.

Increasing the surfactant concentration above the CMC increases the number of micelles in the solution.[7] At sufficiently high concentrations intermicellar interactions becomes dominant and micellar domains organize themselves into ordered mesostructures in response to these interactions. The viscosity of the solutions drop significantly and a liquid to liquid crysalline phase transition occurs.[7,8]

Table 1.1.[*] Critical micelle concentrations of various surfactant molecules at room temperature.[7]

Surfactant	CMC[a]
Dodecylammonium chloride	1.47×10^{-2} M
Dodecyltrimethylammonium chloride	2.03×10^{-2} M
Decyltrimethylammonium bromide	6.5×10^{-2} M
Dodecyltrimethylammonium bromide	1.56×10^{-2} M
Hexadecyltrimethylammonium bromide	9.2×10^{-4} M
Dodecylpyridinium chloride	1.47×10^{-2} M
Sodium tetradecyl sulfate	2.1×10^{-3} M
Sodium dodecyl sulfate	8.3×10^{-3} M
Sodium decyl sulfate	3.3×10^{-2} M
Sodium octyl sulfate	1.33×10^{-1} M
Sodium octanoate	4×10^{-1} M
Sodium nonanoate	2.1×10^{-1} M
Sodium decanoate	1.09×10^{-1} M
Sodium undecanaote	5.6×10^{-2} M
Sodium dodecanoate	2.78×10^{-2} M
Sodium *p*-octylbenzene sulfonate	1.47×10^{-2} M
Sodium *p*-dodecylbenzene sulfonate	1.20×10^{-3} M
Dimethyldodecylamineoxide	2.1×10^{-3} M
$CH_3(CH_2)_9(OCH_2CH)_6OH$	9×10^{-4} M
$CH_3(CH_2)_9(OCH_2CH)_9OH$	1.3×10^{-3} M
$CH_3(CH_2)_{11}(OCH_2CH)_6OH$	8.7×10^{-5} M
$CH_3(CH_2)_7C_6H_4(CH_2CH_2O)_6$	2.05×10^{-4} M
Potassium perfluorooctanoate	2.88×10^{-2} M

[a] In mol/dm^3 (M) or mol/kg H_2O (m)

[*] Reprinted from Krister Holmberg, B.J., Bengt Kronberg, Björn Lindman. *Surfactants and Polymers in Aqueous Solution*, (John Wiley & Sons, Ltd, 2003), with permission from John Wiley & Sons(2003) .

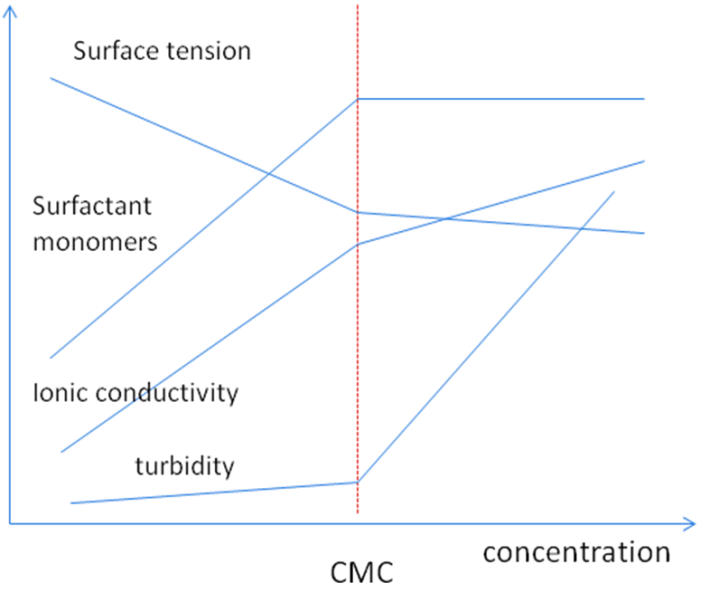

Figure 1.4. Graph representing the change in the physical properties of an aqueous solution with respect to surfactant concentration.

1.2. Lyotropic Liquid Crystalline (LLC) Mesophases

1.2.1. Formation of LLC mesophases

Liquid crystalline (LC) phase is a phase of matter, which has intermediate properties in between those of a crystalline solid and isotropic liquid.[9] In the LC state, the positional order in crystalline state is greatly lost, that is the molecules (or building units) are considerably mobile, however, the molecules are able to align themselves in certain directions and the orientational order is preserved to some extend, **Figure 1.5**. Usually the enthalpy change in **Solid → LC** transition is nearly 10 times greater than the enthalpy change in **LC → Liquid** transition.[10] This means that most of the energy is hidden in the positional ordering of the building units.

There are two main classes of LCs, namely Thermotropic LCs (TLCs) and Lyotropic LCs (LLCs). The TLCs are molecules that contain flexible (aliphatic groups) and rigid regions (aromatic groups) together. At crystalline state the positional and orientational order is maintained by both regions. Increasing the temperature may result in a **Solid → LC** transition. At the LC state the segmental motion of the flexible aliphatic groups decreases the positional order of the

molecules, so the molecules are more free to move around. At the same time the interactions among the rigid aromatic groups helps the molecules to align themselves in certain directions. Further increasing the temperature may result in a **LC→ Liquid** transition,[10]if the molecules do not decompose thermally. **Figure 1.6** shows some of the most typical molecules that show TLC phases.

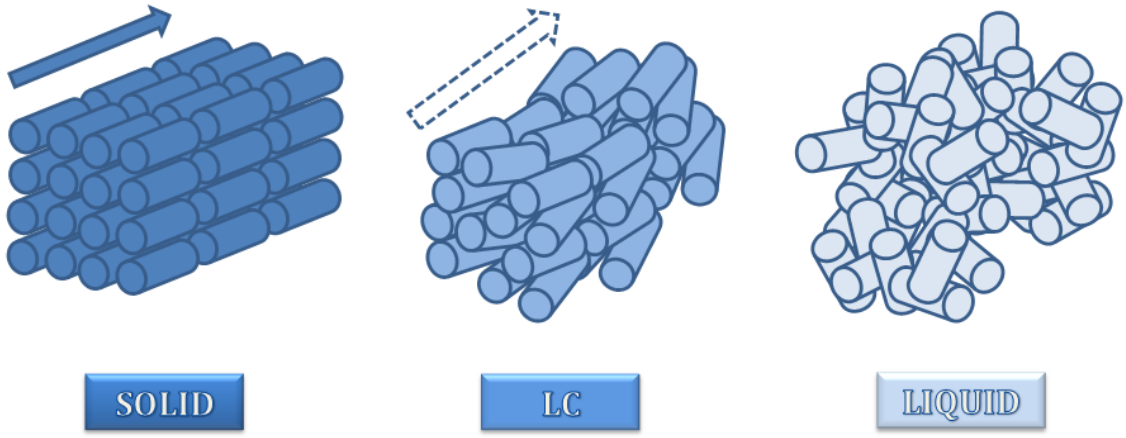

Figure 1.5. Representations of three different phases of matter- solid, liquid crystal, and liquid.

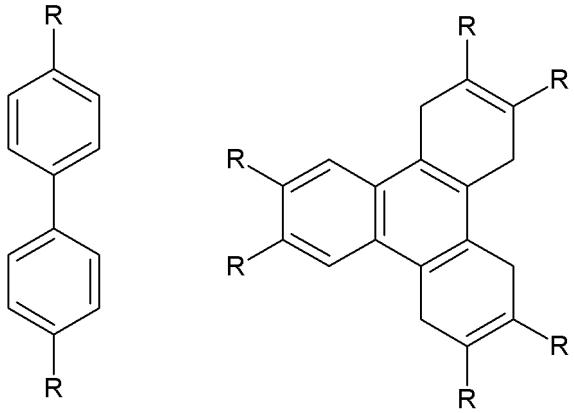

Figure 1.6. Examples of thermotropic liquid crystals, calamitic(left) and discotic(right).

The LLCs on the other hand are formed by at least two ingredients, a surfactant and a solvent. As compared to TLCs, in the LLCs, in addition to the temperature, there is one more degree of freedom, which is the concentration of the

ingredients. Therefore it is possible to observe a rich variety of different mesophases* in the LLCs.[12-16] The micellar phases are dominant at low surfactant concentrations. Increasing the surfactant concentration increases the number of micelles in the solution. In the solution phase, the intermicellar interactions are less significant and the structure of the micelles is determined by intramicellar forces[8,17]. At sufficiently high surfactant concentrations the number of micelles increases up to a point where intermicellar interactions become significant. Eventually the distances between micellar units decrease and micellar to LLC transition occurs. The structure of the micelles can change when intermicellar forces become important. For instance, spherical micelles may transform into hexagonal micellar domains of the LLC mesophase during such a transition.[11]

Figure 1.7 shows 4 different types of LLC mesostructures. The simple cubic phase is a close packing of spherical micelles either in body or face centered arrangements and labeled with $\mathbf{I_1}$. This structure is usually found between a micellar solution phase and hexagonal phase (at higher surfactant concentrations).

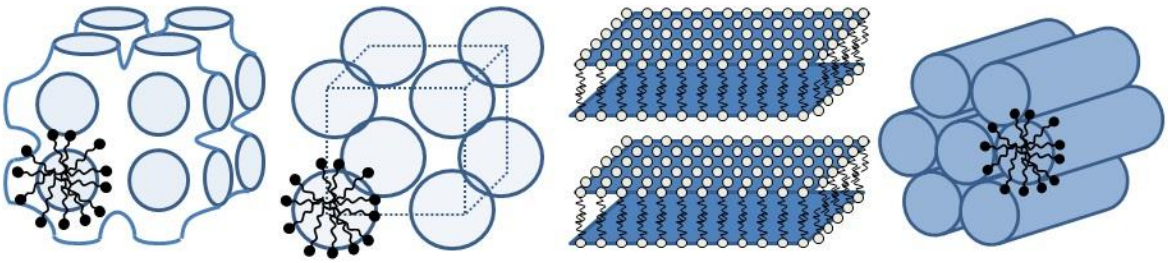

Figure 1.7. Schematical representation of bicontinuous cubic ($\mathbf{V_1}$), simple cubic ($\mathbf{I_1}$), lamellar ($\mathbf{L}_\alpha$), and 2D-hexagonal ($\mathbf{H_1}$) mesophases, from left to right.

The hexagonal phase, which is labeled as $\mathbf{H_1}$ – the subscript denotes if the phase is normal (1) or inverted (2)- is formed by rod-like micellar units, which are packed in a hexagonal arrangement. As the surfactant concentration is increased one may reach to a bicontinuous cubic phase, labeled with $\mathbf{V_1}$.The bicontinuous network has both positively and negatively curvatured regions. $\mathbf{V_1}$ phase is followed by the lamellar $\mathbf{L}_\alpha$ phase, where parallel surfactant bilayers are followed by water rich

* Meso- (*mesos* in Ancient Greek) meaning middle/intermediate. The LLC mesophases are thermodynamically stable phases, but they are build up by microstructural domains which may be mono- or polydisperse.11. Israelachvili, J.N. 20 - Soft and Biological Structures. in *Intermolecular and Surface Forces (Third Edition)* 535-576 (Academic Press, San Diego, 2011).

regions. To sum up, the transitions are as follows with increasing surfactant concentration: **L_1(micellar)→I_1→H_1→V_1→L_α**. In addition to surfactant concentration, the nature and the charge on the hydrophilic regions, the length, structure and the nature of the hydrophobic chains, electrolyte concentrations, and other thermodynamic variables such as pressure and temperature affect the structural preference.

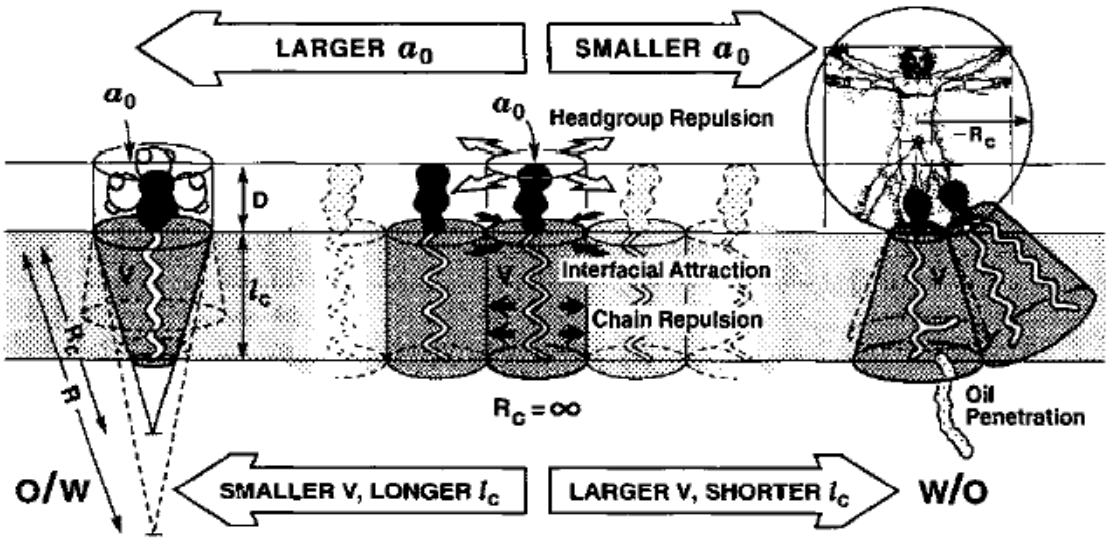

Figue 1.8.[*] Schematic representation of the core-shell interface where three main interactions are depicted; head group repulsion, interfacial attraction, and chain repulsion.[18]

The underlying mechanisms behind the phase transitions can be understood when the interplay of different forces acting on surfactant molecules are summarized, see **Figure 1.8**. In the figure, the cross sectional area of the surfactant at the interface is depicted with $\mathbf{a_o}$, the extended length of the alkyl chain – in near trans conformation- is depicted with $\mathbf{l_c}$ and the critical radius of curvature is given by $\mathbf{R_c}$. There are 3 major forces acting on each surfactant molecule. At the hydrophilic regions the interactions are repulsive, while at the core-shell interface hydrophobic moieties attract each other and tend to decrease their unfavorable

[*] Reprinted from Israelachvili, J. The Science And Applications Of Emulsions - An Overview. *Colloids and Surfaces a-Physicochemical and Engineering Aspects* 91, 1-8 (1994), with permission from Elsevier (1994).

interactions between the solvent molecules. [11,18]Finally, the interactions of alkyl chains in the core is considered repulsive because the need for a larger volume and higher degrees of freedom.[8] The interplay among these 3 forces will determine the as mentioned parameters $\mathbf{a_o}$, $\mathbf{l_c}$ and the effective hydrocarbon volume **v**. [11,18]These parameters in return determine the interfacial curvature, and the structure of the mesophase. As an example, one can consider a spherical micellar unit, the aggregation number (**N**) can be calculated by dividing the core volume of the micelle (**V**) to the volume of each hydrophobic chain, **v**. In general alkyl chains in the core are in a liquid phase, therefore they can be twisted and curled up. However at any time, there is at least one alkyl chain which is fully extended. This fully extended chain will determine the radius of the core. Therefore one can write:

$$N = \frac{V}{v} = \frac{4}{3}\pi\frac{R^3}{v} \qquad \text{(eqn. 1)}$$

We can also express the aggregation number by dividing the Area of the core-shell interface to the effective cross sectional area per molecule:

$$N = \frac{A}{a} = 4\pi\frac{R^2}{a} \qquad \text{(eqn. 2)}$$

Combining these two expression provides:

$$\frac{v}{Ra} = \frac{1}{3} \qquad \text{(eqn. 3)}$$

As mentioned before the maximum R_c can not be longer than the alkyl chain length, therefore it can be replaced by ***l***, to give the inequality.

$$\frac{v}{la} \leq \frac{1}{3} \qquad \text{(eqn. 4)}$$

where, *v*/*la* is defined as the critical packing parameter (CPP), which should be less than 1/3 for a spherical micellar unit. For lower curvatured phases, CPP should increase. For lamellar phase it has to be around 1, because the lamellar structure is almost flat. Values that are higher than 1 require inverted structures, where hydrophilic groups form the core and hydrophobic groups form the shell. **Figure 1.9** shows different structures with changing CPP.

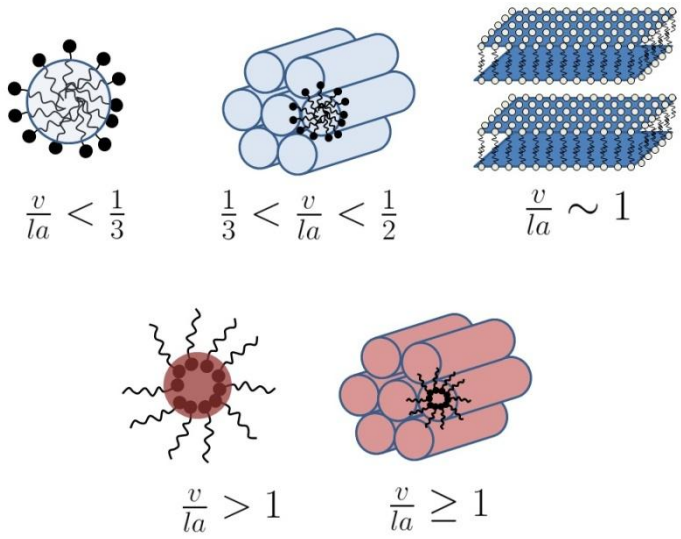

Figure 1.9. Mesostructures with different packing parameters, from left to right , top: spherical (micellar or cubic), rod-like (hexagonal), bilayers (lamellar) and- from left to right, bottom: inverted spherical (micellar or cubic) and inverted rod-like (hexagonal). The values were taken from ref 7.

1.2.2 Poly(ethylene oxide)- alkyl ether surfactant- water systems

1.2.2.1 Binary mesophases

The poly(ethylene oxide)monoalkylether surfactants are formed by a single alkyl chain attached to a hydrophilic ethylene oxide segment, see **Figure 1.1**. The shorthand representation of this surfactant is $\mathbf{C_nEO_m}$ where **n** represents the number of carbon atoms in the alkyl tail group and **m** is the number of ethylene oxide units on the head group.

Phase behavior of nonionic C_nEO_m surfactants has been extensively investigated in aqueous solutions,[19] room temperature ionic liquids,[20] supercritical carbon dioxide,[21,22]and other organic solvents.[23-25] Studying the phase behavior of C_nEO_m type surfactants are important because the alkyl and the ethylene oxide chain lengths can be varied and this provides specific control of the hydrophilic-lipophilic balance (HLB) of the molecule. Since they are also nonionic,

complications arising from electrostatic interactions are not a problem. **Figure 1.10** shows a typical phase diagram of $C_{12}EO_6$-water system, where different mesostructures follow the variations in the CPP with decreasing surfactant concentration, $\mathbf{L_\alpha \rightarrow V_1 \rightarrow H_1 \rightarrow L_1}$. The phase diagrams are constructed by combining several techniques, polarized optical microscopy (POM), differential scanning calorimetry (DSC), X-ray diffractometry (XRD), nuclear magnetic resonance (NMR) and Fourier transform infrared (FTIR) spectroscopy.

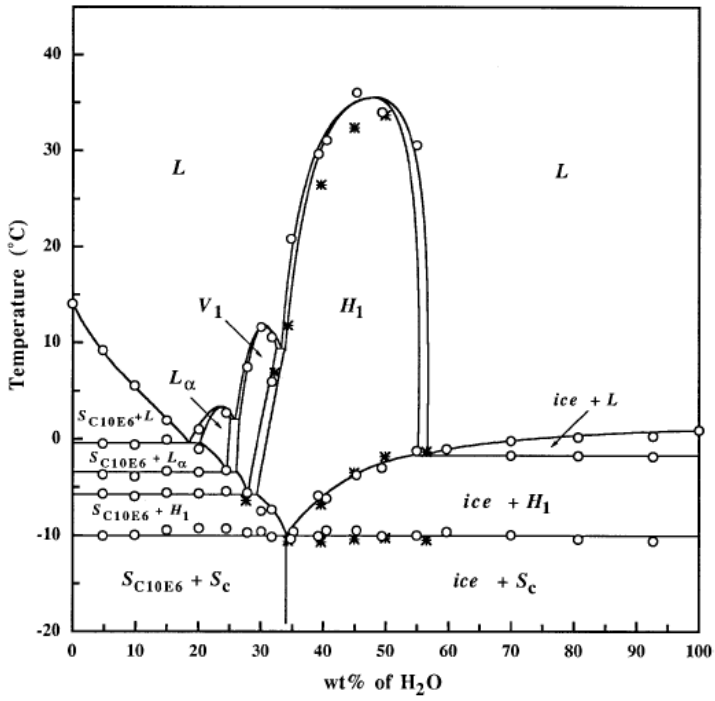

Figure 1.10.[*] Phase diagram of H_2O-$C_{10}EO_6$ at 1 atm.[28]

Tiddy and coworkers[8] constructed the phase diagrams of most of the binary H_2O-C_nEO_m systems. In order to monitor the effect of the length of both segments on the phase behavior, the alkyl and ethylene oxide chain lengths were varied between 8 to 16 and 3 to 12, respectively. They found that the $\mathbf{I_1}$ phases are observed for EO_m where m>8 and $\mathbf{L}_\alpha$ phases are dominant when m<5. This is mainly because the cross-sectional area increases with the ethylene oxide chain length and as a result structures, which have high interfacial curvature, are

[*] Reprinted from Nibu, Y. & Inoue, T. Phase behavior of aqueous mixtures of some polyethylene glycol decyl ethers revealed by DSC and FT-IR measurements. *Journal of Colloid and Interface Science* 205, 305-315 (1998), with permission from Elsevier (1998).

preferred. The sequence of the phases observed with increasing surfactant concentration was found to be in agreement with the ideas based on the geometrical considerations. Their theoretical predictions about the positions of $\mathbf{I_1 \rightarrow H_1}$, $\mathbf{H_1 \rightarrow V_1}$, and $\mathbf{V_1 \rightarrow L_\alpha}$ phase transitions on the phase diagram were in close agreement with their experimental results.[8] Increasing the temperature resulted in the following phase transitions $\mathbf{I_1 \rightarrow H_1 \rightarrow V_1 \rightarrow L_\alpha}$ which can be explained by a decrease in intramicellar repulsions with a decrease in the cross-sectional area. As the temperature is raised the statistical weight of **trans-gauche-trans** conformations of the ethylene oxide chains decreases. This conformation has a higher dipole moment than the **trans-trans-trans** conformations whose statistical weight increases at higher temperatures. The latter conformation interacts with the water molecules weakly and the ethylene oxide groups become more dehydrated. Therefore, the repulsions between the ethylene oxide chains are reduced and the cross sectional area is decreased.[26,27] There are also other explanations related to the dehydration of ethylene oxide chain with temperature which takes into account the disruption of water structuring around these

Table 1.2. * Critical micelle concentrations, cloud points and observed phases for different C_nEO_m surfactants[19]

surfactant	cmc[b] at 25 °C (10^{-5} mol·L^{-1})	cloud point (°C)	HLB	observed phases[d]	refs
$C_{10}EO_3$	60		9.1[c]	L_1,L_3,L_α,L_2	9, 25, 26
$C_{10}EO_4$	68	21	10.5[c]	L_1,L_2,L_3,L_α,H_1	2, 9, 25, 27
$C_{10}EO_5$	80	44	11.6[c]	L_1,L_α,V_1,H_1	2, 9, 25, 28
$C_{10}EO_6$	90	59	12.5[c]	L_1,L_α,V_1,H_1	2, 9, 28, 29
$C_{10}EO_7$	95		13.2[c]	L_1,H_1	30, 31
$C_{10}EO_8$	100	85	13.8[c]	L_1,H_1	25, 28, 32
$C_{12}EO_2$	3.3	32−35	6.4[c]	L_1,L_α,L_3,V_2,L_2,	25, 33, 34
$C_{12}EO_3$	5.2		7.5	L_1,L_3,L_α,L_2	2, 9, 25, 35, 36
$C_{12}EO_4$	4.3 (6.4)	6	9.0	L_1,L_3,L_α,L_2	2, 9, 25, 29, 32
$C_{12}EO_5$	6.4	30	10.0	$L_1,L_3,L_\alpha,H_1,V_1,L_2$	2, 9, 30, 35, 37
$C_{12}EO_6$	6.8	48	11.7[c]	L_1,L_α, H_1,V_1,L_2	2, 9, 37, 38
$C_{12}EO_7$	5.0	70	12.5[c]	L_1,L_α,H_1,V_1,L_2	2, 9, 30, 37, 39
$C_{12}EO_8$	7.1	77	13.1[c]	$L_1,L_\alpha,H_1,V_1,I_1,L_2$	2, 9, 37, 38
$C_{12}EO_9$	10	88	13.6[c]	L_1,H_1,I_1,L_2	25, 32, 37
$C_{12}EO_{10}$		96	14.1[c]	L_1,H_1,L_2	32, 37
$C_{12}EO_{12}$	14.0	98	14.8[c]	L_1,H_1,I_1	9, 38
$C_{12}EO_{23}$	17.5		16.9	L_1,I_1,L_2	37, 38, 40
$C_{14}EO_3$		<20	7.6[c]	L_1,L_3,L_α,V_2,L_2	2, 9
$C_{14}EO_6$	0.8	42	11.0[c]	L_1,L_α,H_1,V_1	2, 9, 29
$C_{14}EO_7$	0.95	58	11.8[c]		30, 41
$C_{14}EO_8$	0.99	70	12.4[c]	L_1,L_α,H_1,V_1,I_1	25, 32, 42
$C_{16}EO_3$		<20	7.0[c]	L_1, $L_3,L_\alpha,V_2,L_2,L_\beta$	9
$C_{16}EO_4$		<20	8.4[c]	L_1,L_3,L_α,V_2,L_2	2, 9
$C_{16}EO_6$	0.40	37	10.4[c]	$L_1,L_\alpha,L_\alpha{}^H,H_1,V_1,L_\beta{}^e,L_2$	9, 43−45
$C_{16}EO_7$	0.30	52	11.2[c]	L_1,L_α,H_1,V_1	41, 43, 46
$C_{16}EO_8$	0.12	63	11.9[c]	$L_1,L_\alpha,H_1,V_1,I_1,L_2$	2, 9, 25
$C_{16}EO_{12}$	0.23	92	13.7[c]	L_1,L_α,H_1,V_1,I_1	2, 9, 38
$C_{16}EO_{20}$	0.77		15.7[c]		47

[a] Expanded from ref 9. [b] The values of cmc's are approximate due to different experimental measurements. [c] HLB was calculated as HLB = wt % EO/5.[48] [d] Phase abbreviations are as described in the text. [e] L_β represents a gel phase.

* Reprinted from Dong, R. & Hao, J. Complex Fluids of Poly(oxyethylene) Monoalkyl Ether Nonionic Surfactants. *Chemical Reviews* 110, 4978-5022 (2010), with permission from American Chemical Society

regions.[19] The low temperature behavior of C_nEO_m-water systems was also investigated by Inoue and co-workers[28-30] by using FTIR, POM, and DSC techniques. It is observed that the LC phases exists only above -10^oC, see **Figure 1.10**. Below this temperature surfactant, ice and surfactant-ice complex crystals were observed. The phase diagram indicates a continuous curve in the temperature of ice crystallization with increasing surfactant concentration. Dong and Hao[19] summarized the work on poly(ethlene oxide) surfactant-water phase diagrams, **Table 1.2**.

1.2.2.2. Effect of electrolytes on C_nEO_m-water systems

The effect of electrolytes on the CMC and the phase behavior of ionic surfactants are dominated by the electrostatic interactions between the charged head groups and the ions in the solution. However, the electrolyte effects are quite different for nonionic surfactant systems. It is found that the electrolyte effects usually follow the Hofmeister series of ions.[31] In 1881, Hofmeister showed that ions affect the solubility of proteins differently and anions have stronger effects than the cations and with the following order:

$$SO_4^{2-} > HPO_4^{2-} > CO_3^{2-} > F^- > Cl^- > Br^- > NO_3^- > I^- > ClO_4^- > SCN^-$$

and for the cations:

$$K^+ > Na^+ > Li^+ > Ca^{2+} > \text{Guanidium}$$

The ions on the left side of the series tend to decrease the solubility of organic compounds in water (salting-out) and called as the *kosmotropes* because they tend to increase the hydrogen bonding network structure of water. [32] Hence the kosmotropes are also called as the structure-makers. The ions on the right side have an opposite effect (salting-in) and called as the *chaotropes* or structure-breakers. [32] The underlying mechanisms of Hofmeister series however is still not fully understood. According to one view kosmotropes tend to increase water structuring that is, the hydrogen bonding network of water.[33] This results in an increase in the hydrophobic force among organic moieties because the water solute interactions are diminished. Chaotropes on the other hand has the opposite effect. According to another view, ions do not affect the bulk water properties significantly and direct

ion-solute interactions plays a more important role. [34] The mysterious Hofmeister series is still a hot topic covering many different research fields in chemistry, biology and physics.[32-37]

The series is not limited to the solubility of proteins in water but the effects are ubiquitous for the solubility of many organic compounds including surfactants. For instance, the magnitude of the decrease in the cloud points* of C_nEO_m surfactants change in the following order: $F^->Cl^->Br^-$. There is even an increase of the cloud point in the presence of I^-.[38,39] Basically, when the water structure is preserved or increased, water molecules that are close to the hydrophilic shell tend to interact with each other rather than forming new hydrogen bonds with the ethylene oxide units. Therefore, the structure makers increase the extend of dehydration of ethylene oxide chain, which causes the cloud points to drop. Similar Hofmeister effects were also observed for the CMCs of poly(ethylene oxide) surfactants.[39,40] This time, the ions not only affect the ethylene oxide chain but the solubility of the change in the solubility of the alkyl chain becomes significant.

The salt effects on LLC mesophases of nonionic surfactants were studied only in a few cases. In one study, it was observed that NaSCN addition leads to an increase in the effective cross-sectional area of the surfactant molecules while NaCl behaves oppositely.[41] The behavior was attributed to the increasing hydration of ethylene oxide chain in the presence of SCN^- anions. Iwanaga et al.[42] showed that the isotropisation temperature drops with the addition of kosmotropes such as Cl^- and SO_4^{2-} and increases with the addition of chaotropic anion such as SCN^- in the hexagonal mesophases of H_2O-$C_{12}EO_7$ system. The differences on ion effects were again attributed to the hydration/dehydration of the ethylene oxide chains. With kosmotropic ions dehydration is increased and water-surfactant interactions are weaken. As a result, the isotropisation temperature is lowered. With chaotropic ions ethylene oxide chain is more hydrated that results in an increase in the isotropisation temperature. They also observed that in the presence of NaSCN the LLC mesophase dissappears around 20 wt. % NaSCN in aqueous solution. This concentration corresponds to about 18.5 water molecules per salt species. The

* temperatures at which ethylene oxide chain is significantly dehydrated and a phase separation occurs, forming surfactant rich and surfactant poor phases

importance of the amount of water per salt species will be discussed in detail in the following chapters.

Zheng et al.[43] studied the effect of Cl^- salts on the phase behaviour of H_2O-$C_{12}EO_7$ systems. 1.0 M solutions of NaCl, LiCl and CsCl were mixed with $C_{12}EO_7$ at different weight percent of salt solutions. The phase diagrams were plotted on one graph for comparison, see **Figure 1.11**. It is seen on the phase diagram that in the presence of Cl^- the $\mathbf{H_1}$ shrinks and $\mathbf{L}_\alpha$ phases expands. The authors interpreted the results in terms of the dehydration of the ethylene oxide units. [43] The dehydration of the ethylene oxide units decreases the effective cross sectional area of surfactant molecules and therefore increases the CPP of the surfactant molecules. Higher CPP values favor the $\mathbf{L}_\alpha$ phase and as a result its region expands in the phase diagram. For different cations, $\mathbf{L}_\alpha$ phase expands more with smaller cation. The effect of the cation was explained in terms of the hydration capability of the ions. The strongest hydration is expected for Li^+ and the weakest is expected for Cs^+. This means that the amount of water molecules necessary to hydrate the Li^+

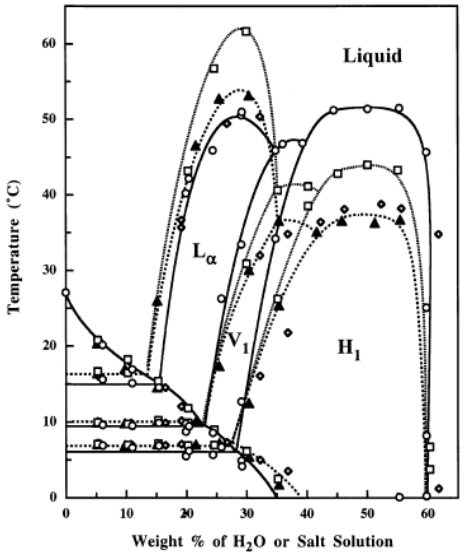

Figure 1.11.[*] Phase diagrams of the H_2O-$C_{12}EO_7$ (circles and straight line), LiCl(1.0 M)-$C_{12}EO_7$-(squares and dotted line), NaCl(1.0 M)-$C_{12}EO_7$ (triangles and dashed line), CsCl(1.0 M)$C_{12}EO_7$ (diamonds)[43]

[*] Reprinted from Zheng, L.Q., Minamikawa, H., Harada, K., Inoue, T. & Chernik, G.G. Effect of inorganic salts on the phase behavior of an aqueous mixture of heptaethylene glycol dodecyl ether. *Langmuir* 19, 10487-10494 (2003), with permission from American Chemical Society (2003).

ion is higher. Therefore, the extent of dehydration of the ethylene oxide chain increases with the following trend: $Cs^+ < Na^+ < Li^+$.

Inoue et al.[44]investigated the anion effect on the phase behaviour of $C_{12}EO_7$ system. A similar approach was taken to study the above and 1.0 M solutions of NaCl, NaI and $NaClO_4$ were mixed with the surfactant. **Figure 1.12** shows the phase changes encountered with different anions. It is seen that the Cl^- ion shrinks the $\mathbf{H_1}$ region, while ClO_4^- and I^- expands. The authors interpreted the results again in terms of the dehydration of the ethylene oxide chains. The cosmotropic ions cause the dehydration of the chains and reduces the effective cross sectional area per surfactant molecule. Which again results in the shrinkage of the H_1 phase. The chaotropic ions on the other hand, have an opposite effect.

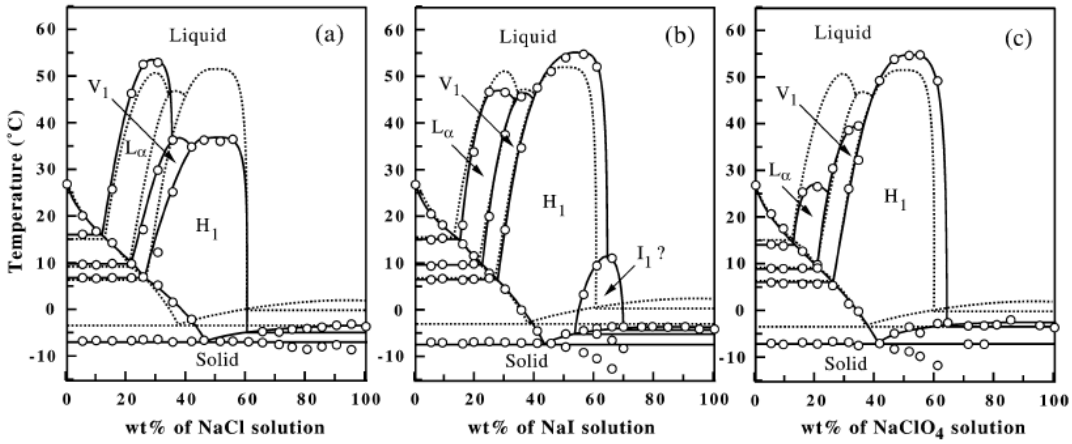

Figure 1.12.[*] Phase diagrams of 1.0 M aqueous solutions of different Na^+ salts with $C_{12}EO_7$. The dashed lines indicate the salt free phase diagram.[44]

The salts were usually regarded as additives in the study of the phase behavior of nonionic surfactants and their effects on cloud points and phase behavior were studied only at low salt concentrations. In addition to the cases listed above, Kahlweit and co-workers [45-48] investigated the ternary phase behavior of C_nEO_m -water-salt and C_nEO_m -water-salt-oil systems . They focused on the effects of chaotropic and kosmotropic ions on the immiscibility gap found in such ternary systems. The immiscibility gap is a triangle of 3 phase region on the ternary phase

[*] Reprinted from Inoue, T., Yokoyama, Y. & Zheng, L.Q. Hofmeister anion effect on aqueous phase behavior of heptaethylene glycol dodecyl ether. *Journal of Colloid and Interface Science* 274, 349-353 (2004), with permission from American Chemical Society (2004)

diagram and shows deviations with respect to temperature, pressure and type of the ions. They have also presented pseudobinary phase diagrams for ternary NaCl-H_2O- $C_{12}EO_6$ and $NaClO_4$-H_2O-$C_{12}EO_6$ systems by keeping water/salt weight ratio at 9, which corresponds to a H_2O/salt mole ratio of at least 29.[49] To the best of our knowledge, a detailed investigation of LLC mesophases at high salt concentrations have never been perfomed until 2001.[50] However, it is possible that the salt species can be the main constituent of surfactant self-assembly at high salt concentrations. We will investigate this issue on the forthcoming chapters.

1.2.3. Solvent choice in LLC systems

In a mixture of water and surfactant, water acts as the solvent. It forms the medium, where the surfactant molecules are dissolved and gather to form micellar or LLC mesostructures. So far, water is known as the best solvent in the self-assembly process of surfactants.[51] There are also other alternatives such as organics[52]or ionic liquids.[20,51] Surfactants can also form assemblies in oil-water mixtures where the oil interacts with the hydrophobic domains and water interacts with the hydrophilic domains. In the oil rich oil-water- surfactant systems very often reverse (or inverted) LC phases can be observed.[53-55]

The availability of different solvents plays an important role in surfactant science. The richness of the mesostructures obtained by surfactant assemblies provide a reaction media for organic and inorganic synthesis. Different solvents provide specific advantages, for instance, ionic liquids are non-volatile, less toxic and highly conductive as compared to other usual organic solvents. Therefore the self assembly of surfactants in ionic liquids has extensively been investigated.[20]

In general, solubility of the surfactant molecules should be low (either in a polar or nonpolar solvent) in order to form micellar and LLC mesophases, because if the surfactant is very soluble, the CMC becomes too high and less well defined. The cohesive energy of the solvent plays an important role in surfactant self-assembly. The *Gordon parameter* effectively reflects this cohesive energy density and defined as; γ/V_m^3, where γ is the surface tension of the solvent and V_m is the molar volume. [1,56] **Figure 1.13** shows the variation of the Gordon parameter with respect to the Gibbs free energy of transferring non-polar gases into solvents. The

lower the Gordon parameter, the less defined the micellisation is. In general liquids that have Gordon parameters over 1.3 tend to be suitable solvents for surfactant self-assembly. A solvent which has a higher Gordon parameter than water can be very interesting because some molecules which cannot self-assemble into micellar or LLC mesostructures in water, can be amphiphilic in such a solvent and exhibit micellar and LLC mesophases.

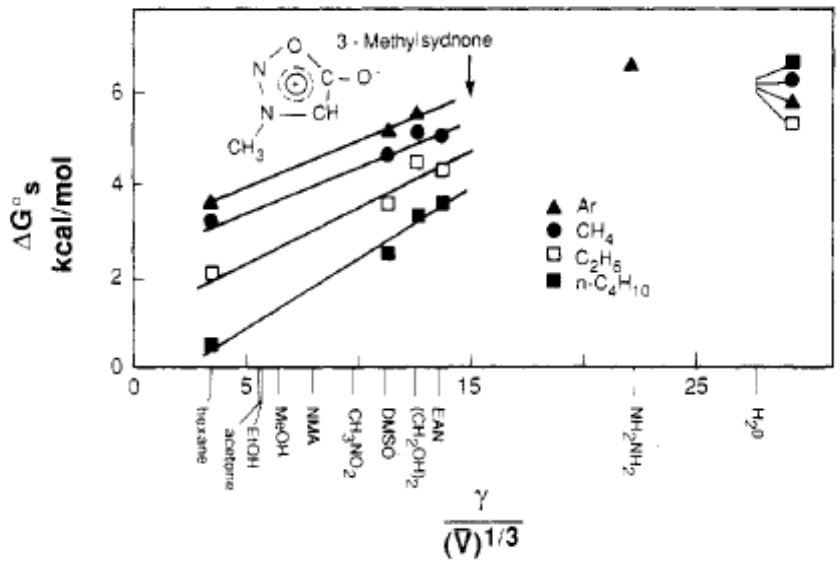

Figure 1.13.[*] Free energy change with respect to the transfer of argon, methane, ethane and n-butane from several liquids to the gas phase. Liquids that have Gordon parameters over 13 tend to be suitable solvents for the amphiphile self-assembly.[1]

1.3. Liquid Crystalline Mesophases in the Synthesis of Novel Materials

The phase behaviour of surfactants in water is examined in detail; since 1950s. They were mostly investigated as detergents and emulsion agents. In 1980s and 1990s, self-assembly of surfactants inspired some scientists who were interested in zeolite synthesis. The classical zeolite synthesis did not allow pore sizes larger than a few nanometers. At the same time, the synthesis of larger pore sized (either ordered or disordered) materials was required due to their better

[*] Reprinted from Evans, D.F. Self-Organization Of Amphiphiles. *Langmuir* 4, 3 (1988), with permission from American Chemical Society (1988).

transport properties and quantum size effects.[57] In 1992 Kresge et. al. synthesized mesoporous silica (mesoporous refers to the materials that have pore sizes crudely in between 2-50 nm) by using cetyltrimethylammonium bromide (CTAB) as a structure directing agent and tetraethylortosilicate (TEOS) as the polymerizing component.[58] In the synthesis, hydrophilic surface of the micelles provided a reaction media for the silica precursor. As the reaction continiues, silica particles surrounds the micelles and resulting composite structure starts to condense to form mesostructured particles. The surfactant-silica particles were calcined in order to remove the surfactant molecules and to form the porous structure, see **Figure 1.14A**. Calcination also provides more rigid walls for the resulting material. In 1995, Attard and co-workers tried a similar synthesis in an LLC mesophase and obtained porous silica films and monoliths.[59] From then, this field is extended towards on the synthesis of porous organic composites, metals, metal oxides, in addition to the developments in silica synthesis.[60-62]

Figure 1.14 summarizes two main approaches in the synthesis of mesostructured and mesoporous materials. The first approach (**Figure 1.14A**) is called the cooperative self-assembly method where the micelles and inorganic precursors cooperatively self-assemble into an ordered pseudo-LC phase. In liquid

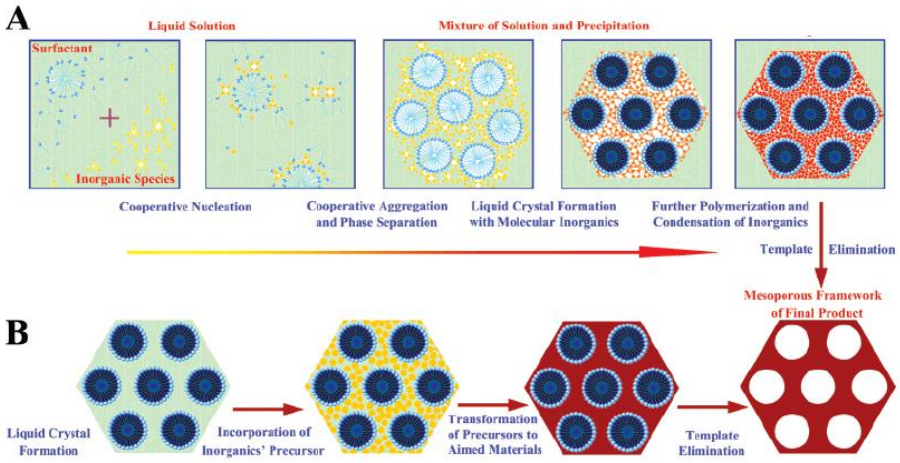

Figure 1.14.[*] Different routes in the synthesis of mesoporous materials A) Cooperative self-assembly B) True LC templating approach.[62]

[*] Reprinted from Wan, Y. & Zhao, D.Y. On the controllable soft-templating approach to mesoporous silicates. *Chemical Reviews* 107, 2821-2860 (2007), with permission from American Chemical Society.

crystalline templating approach (**B**) a solution (containing; surfactants, selective solvent, and inorganic precursors) is spun on a glass substrate and the evaporation of the solvent results in the formation of an LLC film. In LC templating method the resulting porous network mimics the LLC mesophase, however in cooperative self-assembly the final structure is established with an interplay of the initial precursors and cannot be guessed in a straightforward manner. The other main difference is that the synthesis was carried in a dilute micelle solution phase, while in the other method the reaction is guided by the LLC phase.

The synthesis of mesoporous silica has attracted a lot of attention not only because of its specific properties but also because sol-gel chemistry of silica is well known and the unique properties of silica allowed its controlled synthesis [62]. The synthesis of nonsilicaeous materials are much more difficult and is not well understood. For instance, the synthesis of metal sulfides requires a heterogeneous reaction, where H_2S gas is applied to a metal containing LLC film.[63,64] The reaction proceeds very fast by producing nanoparticles of metal sulfide rather than a continious network, which could mimic the LLC template. The conjugate acid of the counter anion of the metal precursor is produced, which can also attack the metal sulfide nanoparticles.[63,64] Moreover, even in the best optimized reaction conditions the concentration of the metal ions are not enough to produce a continious network of metal sulfide that could cover the hydrophilic regions of the LC bulding blocks.[64]Therefore, in order to synthesize a macroscopic film of metal containing mesoporous material, high metal ion concentrations in the LLC mesophase is a prerequisite. In conventional methods, the metal precursors are added as an additives and resulting materials are either supported by a silica or titania matrix or obtained as powders.

1.4. Salt-Surfactant LLCs

In 2001, Dag et. al. discovered a new class of LLCs, which are formed by transition metal aqua complex salts and C_nEO_m surfactants.[50] The transition metals were chosen from the first row of the periodic table; most noticeably, Co^{2+}, Ni^{2+}, Zn^{2+}, and Cd^{2+}. The metal precursors are in the form of hexa- or tetra-aqua complexes $[M(H_2O)_n]X_m$ with different counter-ions (X^-) such as nitrates,

perchlorates, and chlorides. The salt-surfactant LLCs have considerably higher metal ion content as compared to *water-salt-surfactant* systems. The difference is nearly 4 folds in terms of salt/surfactant mole ratio, where the salt-surfactant LC can be obtained with as much as 60 w/w% salt.[50]

The driving force for the formation of the salt-surfactant LLC is the strong hydrogen bonding between the hydrogens of the coordinated water molecules and oxygens of the ethylene oxide chain of the surfactant (hydrophilic region), see **Figure 1.15**. The hydrogen bonding between the coordinated water molecules and the ethylene oxide oxygens is significantly stronger than the one in water-surfactant mesophases[50]. This is due to the higher acidity of the coordinated water molecules as compared to pure water. Stronger hydrogen bonds results in higher isotropization temperatures for salt-surfactant systems, where hexagonal phases are observed up to 110^{o}C.[50]

Hexagonal and cubic mesophases were observed depending on the salt concentration and the counterion. In general, the LLC mesophases are hexagonal in nitrate systems and cubic in perchlorate systems. It is found that the solubility of the metal ion is 4 times higher in nitrate systems as compared to perchlorate systems. [50,65] The coordination of the nitrate to the metal center decreases the overall charge in

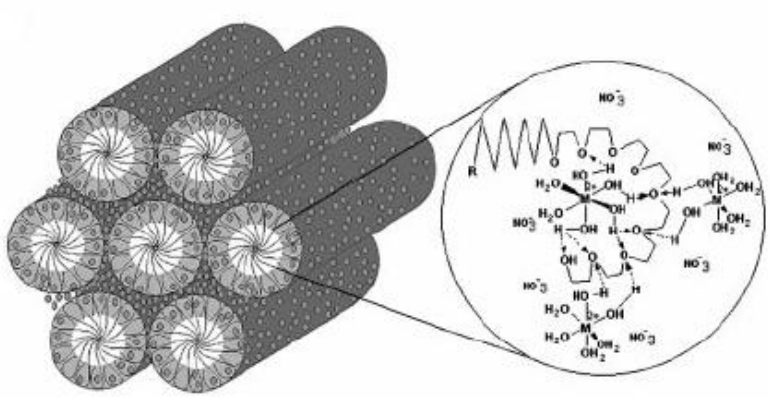

Figure 1.15.[*] Schematic representation of the hexagonal LLC phase and hydrogen bonding interactions among coordinated water molecules and the ethylene oxide chain.[50]

[*] Reprinted from Celik, O. & Dag, O. A new lyotropic liquid crystalline system: Oligo(ethylene oxide) surfactants with $[M(H_2O_n)]X_m$ transition metal complexes. *Angewandte Chemie-International Edition* 40, 3800 (2001), with permission from John Wiley and Sons (2001).

the mesophase and the solubility is increased.[66] In chloride systems, the LLC phases observed only when Co^{2+} used as the metal ion. Chlorides tend to coordinate to the metal center and form the tetrachlorocobaltate ion ($CoCl_4^{2-}$).[65] Lyotropic salts such as sulfates are found to be insoluble at all. The cation effects on the other hand has a less noticeable effect on the solubility, the above mentioned metal ions have more or less the same solubility.[66]

In 2005, the LLC mesophases were further extended to Pluronic type triblock copolymer amphiphiles ($OH(CH_2CH_2O)_n$-$(CH(CH_3)CH_2O)_m$-$(CH_2CH_2O)_n$-H).[67] Pluronic-salt systems show a richer variety of phases such as hexagonal, tetragonal, cubic and lamellar.[67] In Co^{2+} systems of Pluronics a phase separation is observed due to the catalytic oxidation of the surfactants.[68] Phase separation leads to salt rich and salt poor regions. It is also observed that different anions – nitrate and perchlorate- in a mixture will tend to occupy separate microdomains.[68] Both surfactant systems were used as templates in the synthesis of mesostructured materials.[64,69-71] Ternary mixtures of salt-surfactant-water has been used as template in the synthesis of mesostructured nanocomposite silica monoliths, while the salts were selected among noble metals; $AgNO_3$, $HAuCl_4$ and H_2PtCl_6.[72] Thermal or chemical reduction of the noble metals produces metal nanoparticles in the channels of silica network.[72] The salt-surfactant mesophases were further investigated as a rection media to produce mesostructured metal sulfide films.[63,64] Usually, the LLC samples were spin coated on glass slides and the resulting films are exposed to H_2S gas in order to produce metal sulfide films or nanoparticles.[63,64]

Dag and co-workers were interested in increasing the metal-uptake of the salt-surfactant system. The reason is that even 60 wt. % of salt was not enough to obtain stable films of resulting porous materials.[64] Addition of a charged surfactant (CTAB or SDS) to $C_{12}EO_{12}$-$[Zn(H_2O)_6](NO_3)_2$ system increased the salt uptake to 80 wt. %. [73,74] Charged surfactants make the core-shell interface charged, and interestingly, charged surfactants do not crystallize out in such a system that already has high ionic strength. The origin of the extension of LLC phase towards higher salt concentrations has been explained with the long-range coulumbic attraction of salt species towards the charged core-shell interface. Usually there is an unused volume of shell close to the core-corona interface. Presence of a charged group at the interface allows the salt species to accumulate in that region. As a

result higher salt-uptake is observed. Higher salt concentrations is found to be useful in synthesizing stable mesostructured/mesoporous metal sulfide films.[70]

1.5. On the confinement effects

The following chapters explain the basic concepts of hard and soft confinement of liquids since in the discussion part we will address some of our observations related to the soft confinement effect in the LLCs.

1.5.1. Hard Confinement

Capillary condensation of liquids from their unsaturated vapor is a well-known phenomenon. In a condensed liquid, the surface tension of solid-vapor and solid-liquid interfaces is related to the pore width with the Kelvin equation[75]:

$$H = -\frac{2v_m(\gamma_{sv}-\gamma_{sl})}{kTln[p/p_o]} \qquad \text{(eqn. 5)}$$

where H is the slit width of the pore**,** γ_{sl} is the solid-liquid surface tension, γ_{sv} is the solid-vapor surface tension, $\mathbf{p/p_o}$ is the relative vapor pressure, and $\mathbf{v_m}$ is the molecular volume of the liquid, **Figure 1.16**.

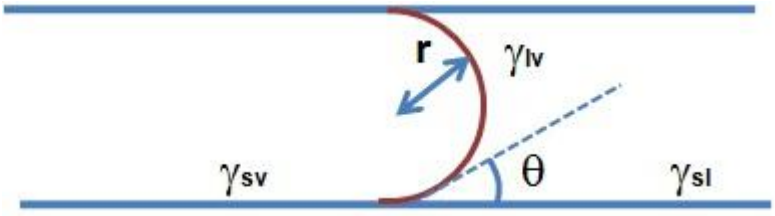

Figure 1.16. Side view of a cylindrical pore with a concave liquid inside.

Capillary condensation implies that if a solid is to melt in a pore, the liquid that wets the container walls can be thermodynamically stable. The result is the lowering of the melting point due to the confinement effect on the solid.[75]The Gibbs Thomson equation that can be derived from the Kelvin and Clasius-

Clapeyron equation expresses the melting point depression with respect to the pore radius.[75]

$$\triangle T = \frac{2T_m V_m \gamma_{sl}}{r \triangle H_f} \qquad \text{(eqn. 6)}$$

where, ΔT is the depression on the melting point, T_m is the melting point without confinement, V_m is the molar volume, γ_{sl} is the surface tension at the solid-liquid interface, r is the pore radius and H_f is the enthalpy of fusion.

The freezing point depression on the other hand always occurs with some degree of hysteresis and super cooling is inevitable in impurity free medium. When kinetic considerations are taken into account, freezing point depression is 3/2 times higher than the melting point depression.[75] Capillary melting and freezing has attracted a lot of attention from the scientific community, since many natural events such as frost heaving in the terrain and survival of organisms at subzero temperatures depend on the same phenomena.

Recent advances in the synthesis of uniformly porous materials with differing geometries allowed investigation of the freezing (melting) point depression of liquids in porous media.[76-79] Apart from the fundamental interest on the physical properties of liquids under confinement, the shift in the solid-liquid transition temperature is used in cryoporometry studies, since the melting point is related to the pore size and geometry, it gives information about the porosity of the material. In addition to the organic liquids[77] and water [76,79], Vargas et al studied the inorganic salt $[Zn(H_2O)_6](NO_3)_2$ as a cryoporometric probe material.[80] This salt has a melting point of 37^{o}C and high enthalpy of fusion. Hence the melting point shift is found to be more than twice as compared to water.

In addition to the freezing (melting) points, the effect of confinement of liquids in small geometries to the glass transition temperature has also been investigated on molecular liquids.[78] The glass transition is not a thermodynamic but a kinetic event and the Clasius-Clapeyron equation cannot be used directly. On the other hand the Ehrenfest relation[81] relates the glass transition with thermal expansion coefficient α and the heat capacity C_p.

$$\frac{\mathrm{d}T_g}{\mathrm{d}P} = T_g V \frac{\triangle \alpha}{\triangle C_p} \qquad \text{(eqn. 7)}$$

Combining eqn. 7 with the Kelvin equation (eqn. 5) gives the following relation.[82]

$$\triangle T = T_g V \frac{\triangle \alpha 2 \gamma_{sl}}{\triangle C_p R} \qquad \text{(eqn. 8)}$$

Zhang et al[82] notes the depression of glass transition in porous media , $\Delta T/T_g$, is less significant (15%) as compared to the freezing point depression ratio $\Delta T/T_f$ (20%) for some molecular organics. The observed shifts in glass transition however can be contradictory and varies between -18 to +15 K for different molecular liquids.[83] Christiansen et al. notes also that the freezing point can be elevated due to confinement at very low pore radii.[75] Therefore, while the physical properties of liquids under confinement can be altered significantly, the direction of the alteration may be different for different liquids depending on the characteristic of the liquid, pore material, pore size and geometry.

1.5.2. Soft- confinement effects

Soft confinement may refer to two different phenomena: i) The effect of confinement on the structural or physical properties of a soft materials such as polymers[84,85], thermotropic LCs[86,87], and other macromolecules[88] and ii) The confinement of liquids in between rapidly fluctuating soft walls. Here, we will only consider the 2nd case. In general, the most widely used systems for the investigation of soft confinement effects are inverse micelles and microemulsions systems (from nanometers to micron sized droplets).[89-91] In these systems, the walls are constructed by rapidly fluctuating surfactant molecules which may significantly alter the physical properties of the liquid in consideration. For instance, propylene glycol encapsulated in dioctyl sodium sulfosuccinate (AOT) reversed micelles exhibit a glass transition shift of -7K.[91] For liquids that have boiling point to melting point ratio higher than 2.0 , $T_b/T_m<2.0$, a glass transition is almost never observed, [92] while theoretically every pure liquid may show a glass transition, very fast cooling rates and small sample sizes are required. Macfarlene et al. showed that for liquids that have $T_b/T_m< 2.0$ glass transitions become observable if the liquids are encapsulated in microemulsions.[93]

To the best of our knowledge the low temperature stability of nonionic surfactant-water LLC systems, see **Figure 1.11-1.12**, has never been attributed to soft confinement effects. In the phase diagrams given in **Figure 1.12**, it is seen that the phases are stable down to -10^{o}C. Since water molecules are entrapped in between the hexagonal LLC domains a freezing point depression can be expected. The state of water is usually considered on a molecular level by commenting the presence of surfactant-water complexes.[28,30]At low temperatures such complexes has been detected and is also depicted in the phase diagrams. However the state of water in LLC mesophases was not taken into account from a thermodynamical point of view.

1.6. Concentrated Electrolyte Solutions and Deliquescence of Salts

Electrolyte solutions of some inorganic salts are known to be supercooled very easily,[94] which makes them potential candidates in the investigation of glass forming materials. **Figure 1.17** and **1.18** shows phase diagrams of various salts with water.[95] The eutectic compositions show aqueous solutions which can be stable down to -80^{o}C (in LiCl systems), see **Figure 1.17**. The top curves on the water rich regions in the phase diagrams are the equilibrium liquidius lines below which ice + electrolyte solution is in a thermodynamic equilibrium. This line can represents the freezing point depression of water with added salt. The top curve in the salt rich regions depicts the solubility or the melting point of the salt depending on the salt concentration.

In divalent non-transition and transition metal salt systems, the interaction of the metal ion with the hydration sphere is much stronger and water molecules are better be regarded as coordinated ligands. In the unhydrated form, when exposed to ambient conditions, these divalent or transition metal salts are usually hygroscopic.

While the top line at high salt concentrations can be regarded as the solubility line with respect to temperature, at some points of the line it is better to define it as the melting temperature of the salt. For instance, in the $Zn(NO_3)_2$ system the 14.2 mole percent of the salt refers to 6 water molecules per metal ion, which is the correct number of water molecules that is sufficient to form the octahedral $Zn(H_2O)_6^{2+}$ complex, **Figure 1.18**. Indeed when cooled down, the salt crystallizes

with 6 water molecules which are coordinated to the metal center and nitrates as free counterions. The vertical lines in the phase diagrams represent such critical concentrations, and their melting points.

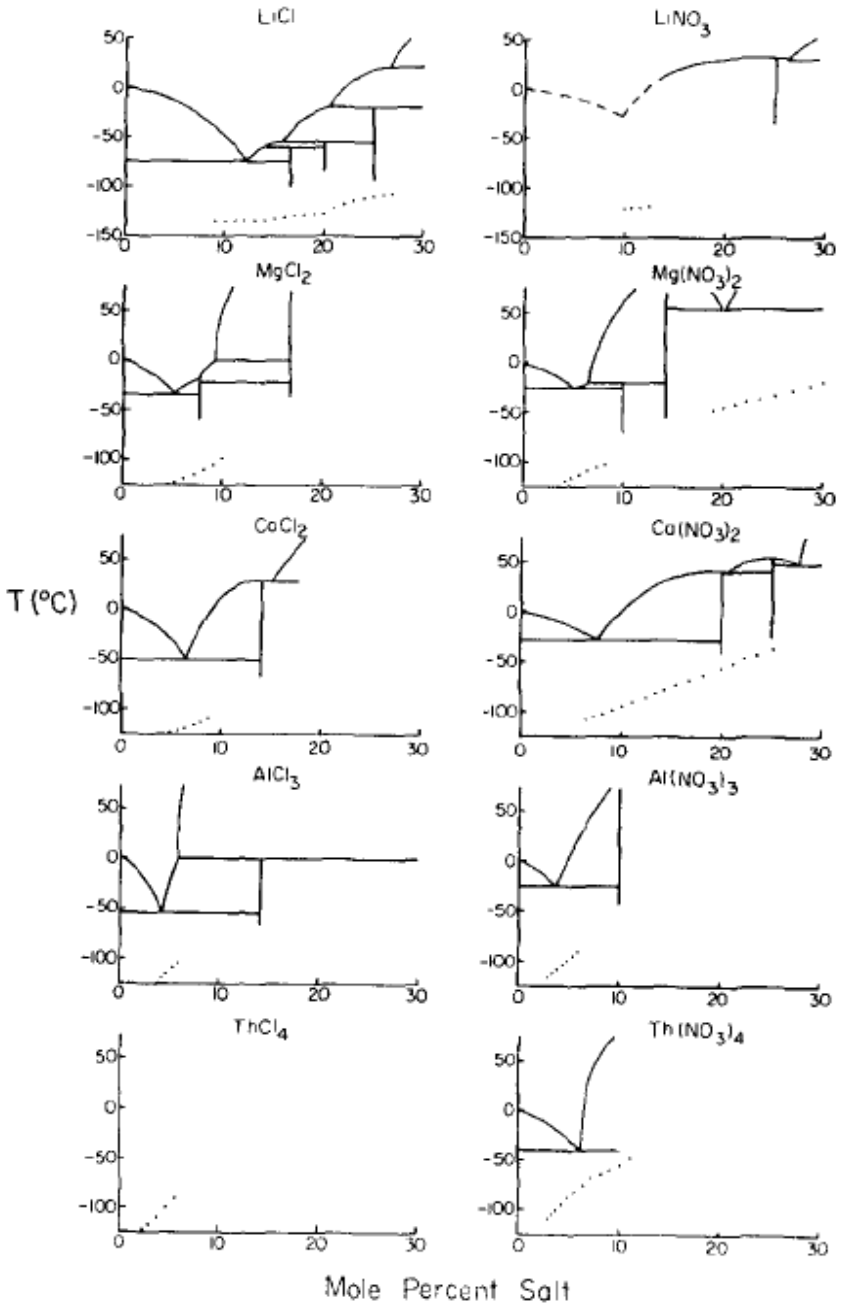

Figure 1.17.[*] Phase diagrams of various salts with water. (Reprinted from ref. 95, with permission from American Institute of Physics) [95]

[*] Reprinted from Angell, C.A. Angell, C.A. Glass-Forming Composition Regions and Glass Transition Temperatures for Aqueous Electrolyte Solutions. *J. Chem. Phys.* 52, 1058 (1970), with permission from American Institute of Physics (1970)

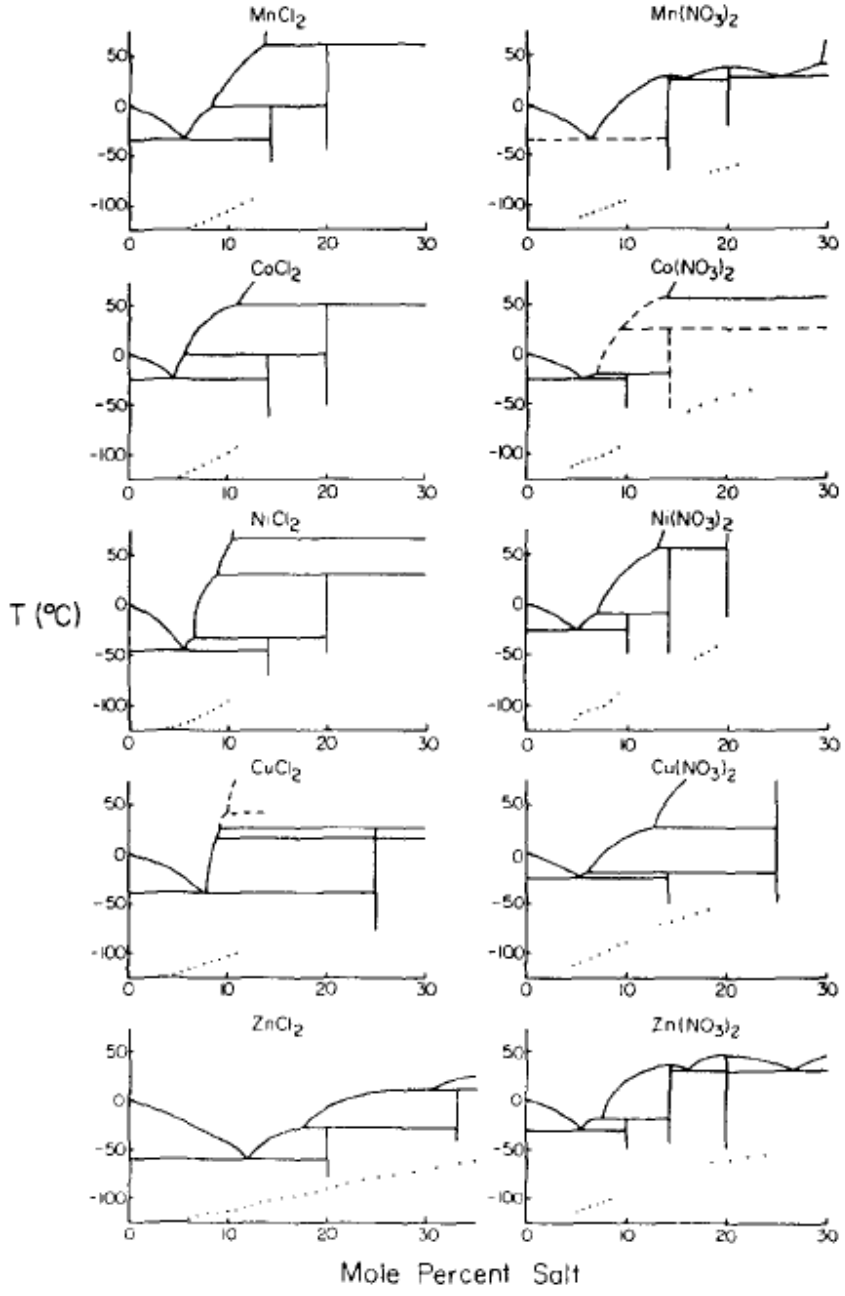

Figure 1.18.[*] Phase diagrams of various salts with water, continued. [95]

In a broad range of concentrations, depending on the cooling rate and the sample size, all the concentrated electrolyte solutions shown in the phase diagrams exhibit glass transition - the glass transitions are depicted with dot-lines in the bottom of the diagrams. For determination of the glass transitions, usually, the

[*] Reprinted from Angell, C.A. Angell, C.A. Glass-Forming Composition Regions and Glass Transition Temperatures for Aqueous Electrolyte Solutions. *J. Chem. Phys.* 52, 1058 (1970), with permission from American Institute of Physics (1970).

samples are quenched to temperatures below the glass transition in order to avoid any nucleation. [95]Once it is understood that there is no nucleation, the samples are heated and glass transitions are recorded by a DSC or DTA instrument.

At the glass transition, the viscosity of the material changes so fast that in the life time of the observer it seems to be a phase transition.[96] That is, the glass transition is purely a kinetic phenomenon and the glassy material have tendency to be a crystalline solid.[96] Basically, the expectation time for a nucleation to occur is infinity at the melting point, and decreases with temperatures below the melting point. If the experimental time scale of observation is shorter than the expectation time for the nucleation, a glass can be formed. In a typical DSC thermogram, glass transition is observed as in **Figure 1.19**. The heat capacity of the material decreases drastically with liquid-solid transition.

In concentrated electrolyte solutions the glass transition decreases with decreasing metal ion concentration. **Figure 1.19** shows that for each additional

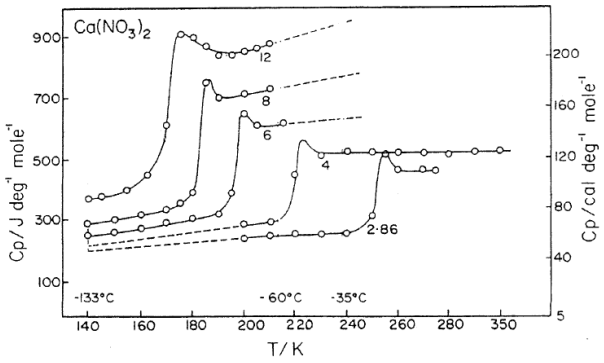

Figure 1.19.[*] The effect of the number molecules on the glass transition temperature. (Reprinted from ref. 96, with permission from American Chemical Society)

water molecule, there is a 10K shift in T_g of the $Co(NO_3)_2$ solution.[96] Tg is also affected by the basicity of the counter anion. More basic counterions form stronger hydrogen bonds with the water and increase the glass transition more. [95]

Salt-Surfactant-Water mesophases have been investigated in order to understand the effect of different salts on the phase behaviour of Water-Surfactant LLC mesophases. In these studies salt concentrations are kept at low levels,

[*] Reprinted from Angell, C.A. Liquid Fragility and the Glass Transition in Water and Aqueous Solutions. *Chemical Reviews* 102, 2627-2650 (2002), with permission from American Chemical Society (2002)

because they are considered to be additives. As it is seen in the phase diagrams of Salt-Water systems can be very stable at very low temperatures and if sufficiently cooled glass transitions can be observed. To the best of our knowledge, there is no report on the glass transition of the solvent in the LLC media. As in the microemulsions and inverted micelles, the spacing in LC domains are in the nanometer scale (2-10 nm). Therefore investigation of such unexplored domains in LLC phases will be illuminative for the colloid chemistry of surfactants.

For a water soluble solid, there exists a critical value of relative humidity (RH) above which the solid starts to dissolve with the water from the air.[97] This critical point in RH is called as the deliquescence relative humidity. Basically, if the equilibrium vapour pressure of a saturated solution is below the vapour pressure of water in air, the salt spontaneously absorbs water from the air until a thermodynamic equilibrium is achieved. **Table 3.4** (p.100) gives a list of different salts in terms of their deliquiescence relative humidities. It can be seen that saturated solutions of some Li and Ca^{2+} salts have low vapour pressures. At an ambient humidity, the saturated solutions of these salts are expected to be stable under open atmosphere. We will see that low DRH values are critical in LLC formation for salt-surfactant systems.

1.7. Scope of the Thesis

This thesis work shows that molten hydrated salts which have low melting points close to room temperature can be used as solvents in surfactant self-assembly. Analogous to molten hydrated salts, concentrated solutions of some alkali and alkaline earth metal salts which have low deliquescence relative humidity form stable LLC mesophases under ambient conditions. These mesophases are obtained at very low water/salt mole ratios, and therefore the ion effects play a significant role in the assembly process. Therefore salt-water couple should be considered as the solvent in the mesophase.

2. Experimental

2.1. Materials

Tap water was distilled and deionised using a Millipore Synergy 185 water purifier and used without further treatment. Other chemicals were obtained from the following companies and used without further treatment:

Sigma Aldrich: LiBr, LiCl, $LiNO_3$, $LiClO_4$, KSCN, KCl, $KClO_4$, KNO_3, NaI, NaCl, $NaNO_3$, NaSCN, $NaClO_4$, $Zn(NO_3)_2.6H_2O$, $Ca(NO_3)_2.4H_2O$, $C_{12}EO_{18}$, $C_{12}EO_{10}$, CH_3COONa.

Merck: NaBr, $MgNO_3.6H_2O$, KI, $CaCl_2.6H_2O$.

Riedel- de Haen: $MgCl_2.6H_2O$

2.2. Instrumentation

The X-ray diffraction (XRD) patterns were recorded on a Rigaku Miniflex Diffractometer using a high power Cu-K_α source operating at 30kV/15mA and a wavelength of 1.5405 Å. **The Polarized Optical Microscopy (POM)** images were obtained in transmittance mode using a ZEISS Axio Scope.A1 Microscope with a Linkam LTS350 temperature controlling stage attached to the microscope. Temperature control is done with a Linkam T95-LinkPad temperature programmer attached to the stage. **The Fourier Transform - Infrared (FT-IR)** spectra were recorded using Bruker Tensor 27 model FTIR spectrometer. A Digi Tect TM DLATGS detector was used with a resolution of 4.0 cm^{-1} in the 400-4000 cm^{-1} range. The spectra were recorded by spreading or spin coating the samples on silicon wafers. **The Differential Scanning Calorimetry (DSC)** measurements were carried out using a Perkin-Elmer Diamond differential scanning calorimeter.

AC Impedance conductivity measurements were carried out using a Gamry G750 potentiostat/galvanostat. **The micro-Raman** spectra were recorded on a LabRam confocal Raman microscope with a 300 mm focal length. The spectrometer is equipped with a Ventus LP 532 50 mW, diodepumped solid-state laser operated at 20 mW, with a polarization ratio of 100:1, awavelength of 532.1 nm, and a 1024x256 element CCD camera. The signal collected was transmitted via a fiber optic cable into a spectrometer with a 600 g/mm grating.

2.3. Sample Preparation and Methods

2.3.1. Preparation of the LC gel samples without evaporation

LC gel samples were directly prepared by mixing the required weight of the ingredients without further treatment. This procedure was applied only for $[Zn(H_2O)_6](NO_3)_2$-$C_{12}EO_{10}$ and for $LiNO_3$-H_2O-$C_{12}EO_{10}$ systems in construction of the phase diagrams. This procedure allows definite control and knowledge of the amount of the ingredients. Some samples for LiCl-H_2O-$C_{12}EO_{10}$, $LiClO_4$-H_2O-$C_{12}EO_{10}$ and H_2O-$C_{12}EO_{10}$ were also prepared in this way.

2.3.1.1. Preparation of the $[Zn(H_2O)_6](NO_3)_2$-$C_{12}EO_{10}$ gel samples

The samples were prepared at different compositions by keeping the amount of the surfactant weight constant at 1.0 g. If one wants to scale up the preparation, further treatments are necessary. These procedures were optimized only for 1.0g $C_{12}EO_{10}$. For instance, when we used 2.0 g of $C_{12}EO_{10}$ we observed some salt crystallization because of the insufficient homogeneity.

In preparation of $2.0[Zn(H_2O)_6](NO_3)_2$- $1.0C_{12}EO_{10}$ sample (numbers indicate the mole ratios), 0.950 g of $[Zn(H_2O)_6](NO_3)_2$ and 1.0g of molten $C_{12}EO_{10}$ was weighted and mixed in a 20 ml glass vial. The cap of the vial was then tightly sealed with a Teflon band. The sample was constantly shaken in a heat bath above the melting point of the composition for 24 hours in order to complete the homogenization. The homogenized samples may be slightly turbid in appearance because of the micro structured nature of the LLC phase. However a homogeneous

single phase sample should never be opaque or contain salt crystals. The samples that have melting points above 80-90^{o}C were not kept above these temperatures for a long time to avoid the reduction of the nitrates. These samples were kept at higher temperatures only at short time periods, typically 1-2 hour. Complete homogenization was achieved by constantly shaking these samples around 80^{o}C at least for 24 hours.

2.3.1.2. Preparation of the LiX.xH_2O-$C_{12}EO_{10}$ gel samples

The samples were prepared at different compositions by keeping the amount of the surfactant weight constant at 1.0 g. For example, in preparation of 3.0$LiNO_3$-3.0H_2O-1.0$C_{12}EO_{10}$ sample (numbers depict the mole ratios), 0.330 g of $LiNO_3$, 0.258 g of H_2O and 1.000 g of molten $C_{12}EO_{10}$ was weighted and mixed in a 20 ml glass vial. The cap of the vial was then tightly sealed with a Teflon band. The sample was constantly shaken in a heat bath above the melting point of the composition for 24 hours in order to complete the homogenization. The homogenized samples may be slightly turbid in appearance because of the micro structured nature of the LLC phase. However a homogeneous single phase sample should never be opaque or contain salt crystals.

2.3.2. Preparation of the samples in solution phase

The solution phase preparation does not require heating. The required weights of the ingredients were weighted and mixed in glass vials with a stirrer for 6 hours. For instance, in preparation of 2.0$CaCl_2$-1.0$C_{12}EO_{10}$-excess H_2O, 0.700 g of $CaCl_2.6H_2O$, 1.0 g of $C_{12}EO_{10}$ and 5 ml of H_2O were mixed and stirred 6 hours for homogenization. The homogeneous solutions became ready for further treatment.

2.3.2.1. Preparation of small scale gel samples and thin LLC films

The LLC thin films were prepared by spin coating the homogenized solutions on glass slides or silicon wafers. The spin coater speed was kept between 1000 and 750 rpm depending on the purpose. Some small scale LLC samples were prepared

by dropping 1-2 drops of the homogenized solution on a suitable substrate – glass slide or silicon wafer. The evaporation of the excess water creates the LLC samples. Note that, LLC samples which are prepared in this way are not homogeneous and the composition may vary along the sample. The spin coated samples are more homogeneous in this respect because of the rapid evaporation of the excess water. The slow evaporation of water in drop casted samples creates a concentration gradient. Additionally, if the samples are not stable under open atmosphere the dropped samples will equilibrate more slowly. For instance, instant crystallisation of salt can be detected for spin coated samples, while for dropped samples the crystallisation may take several hours or even days.

2.3.2.2. Preparation of mesostructured crystalline thin LLC films

The preparation of these samples require the steps mentioned in section 2.3.2 and spin coating on suitable substrates- such as glass slides or silicon wafers. These spin coated samples were aged at a suitable temperature and humidity for 2-3 hours. The mesocrystals starts to appear in time. The temperature and humidity conditions are specified in related chapters.

2.4. Methods

2.4.1. XRD Measurements

The samples were either spin coated over glass slides from the homogeneous solutions at 1000 rpm or spread over a glass sample holders. Care was taken to align the surface of the samples at 0 degrees. For low temperature measurements, a a holder, which is in contact with liquid N_2, was placed under the glass slides. The temperature of the sample was monitored with a thermocouple. For samples which have high diffraction intensities a copper plate was placed before the detector to avoid the saturation of the detector from the intense light. The copper plate reduces the light intensity by 10 times. The measurements were made with 0.01-0.02 degree intervals and 0.1-5 degree/minute scan speed.

2.4.2. POM measurements

The samples were investigated on glass slides, as substrates. For heating and cooling measurements the samples were sandwiched between two glass slides to avoid water evaporation. The cooling is achieved by computer controlled pumping of the chamber with liquid N_2, therefore the atmosphere of the chamber was practically 100% N_2. The heating and cooling rates were varied between 1-5 degrees/minute. The images were captured/monitored using a camera attached on top of the microscope.

2.4.2. FT-IR spectroscopy

The samples were either spin coated on IR transparent Si substrates, from homogeneous solutions at 750 rpm, or spread as a thin layer from a gel sample. The samples were sandwiched between silicon wafers if the water content is to be analyzed. During the measurements the temperature and humidity of the atmosphere was noted because the water content of the samples may vary with these parameters. The resolution of the instrument was kept at 4 cm^{-1} for all measurements and the number of scans were varied between 8 and 512.

2.4.2. DSC measurements

The DSC measurements were performed under N_2 atmosphere using uncapped aluminium holders. The heating and cooling scans were performed at 5-10 degrees/minute. 2-4 mg of gel samples was required for an efficient DSC analysis.

2.4.3. AC Impedance conductivity measurements

Ionic conductivity measurements were carried out in a conductivity cell which allows direct insertion of the electrodes to the vial in which the sample was prepared, see **Figure 2.1**. The conductivity cell has a cell constant of 0.59 cm^{-1}, which was determined using a standard solution of 0.1 M KCl at RT. In a usual procedure, the sample was never taken out of the vial and the O-ring system avoids leakages therefore the loss of water during heating was prevented. The cap system was placed on top of the glass vial that contains the sample. The insertion of the electrodes into the sample creates air bubbles that can affect the conductivity. Therefore, after the insertion of the electrodes the sample was melted and bubbles were allowed to migrate to the sample surface.

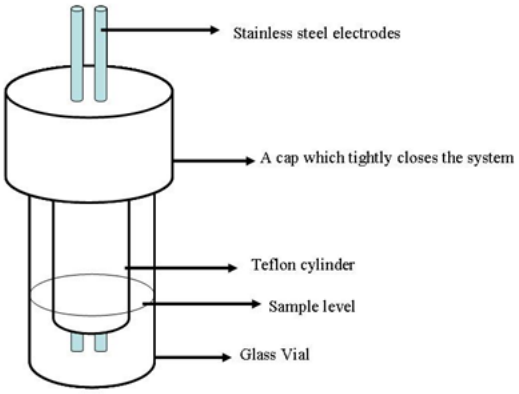

Figure 2.1.[*] Schematic representation of the conductivity cell.[103]

The counter and reference electrodes (short-cut) were attached to one electrode and working electrode was attached the other one. A Nyquist Plot was

[*] Reprinted from Albayrak, C., Cihaner, A. & Dag, Ö. A New, Highly Conductive, Lithium Salt/Nonionic Surfactant, Lyotropic Liquid-Crystalline Mesophase and Its Application. *Chemistry – A European Journal* 18, 4190-4194 (2012), with permission from John Wiley and Sons (2012).

obtained by applying 10mV AC voltage and varying the frequency between 0.1Hz to 300kHz. Typical Nyquist plots are shown in **Figure 2.2**. On the plot the point where the $Z_{imaginary}$ equals to 0 is the total ionic conductivity of the the sample.[98]

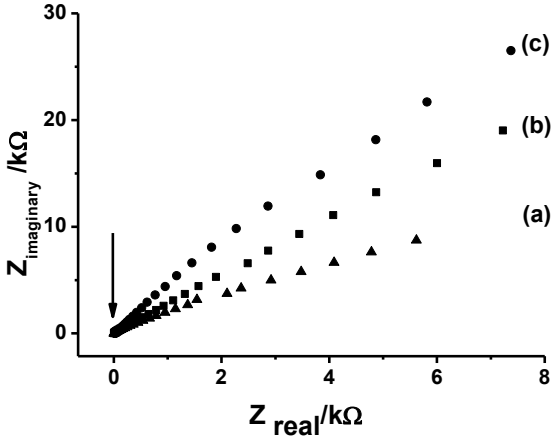

Figure 2.2.[*] Nyquist plots of samples between $1.0x10^4$Hz and 0.2Hz, (a) $3.0LiNO_3.6H_2O$-$C_{12}EO_{10}$, (b) $3.0LiNO_3.4H_2O$-$C_{12}EO_{10}$, and (c) $3.0LiNO_3.9H_2O$-$C_{12}EO_{10}$.[103]

The conductivity measurements at low temperatures were done by immersing the conductivity cell in an ethanol bath, which was temperature controlled with a Thermo HAAKE EK 45/90 cryostat. The measurements at or above RT were performed by immersing the conductivity cell in a hot water bath. In all conductivity measurements, resistance data were recorded after the equilibration of the sample temperature with the bath temperature.

2.4.3. Micro-raman spectroscopy

The samples were spread over or spin coated on silicon wafers in order to obtain a smooth background. Measurements which require the control of the water content was performed by putting a thin glass slide on top of the sample. Cooling measurements were also performed during micro-Raman measurements by using the same Linkam heating-cooling stage.

[*] Reprinted from Albayrak, C., Cihaner, A. & Dag, Ö. A New, Highly Conductive, Lithium Salt/Nonionic Surfactant, Lyotropic Liquid-Crystalline Mesophase and Its Application. *Chemistry – A European Journal* 18, 4190-4194 (2012), with permission from John Wiley and Sons (2012).

2.5. Sample Preparation and Methods on an Electrochromic Device

Experiments related to electrochromic device application were performed in Prof. Atilla Cihaner's laboratory with his help at Atılım University. An electrochromic device were prepared in the following way: Poly(4,7-di-2,3-dihydrothieno[3,4-b][1,4]dioxin-5-yl-2,1,3-benzoselenadiazole)[99], exhibiting green color when neutralized and transmissive sky blue when oxidized, and poly (3,4-diethleyedioxythiophene), showing dark blue and transmissive sky blue upon oxidation, were coated separately on ITO electrodes in 0.1 M $LiClO_4$ dissolved CH_2Cl_2 and acetonitrile solutions, respectively. The electrochromic device was constructed using these electrodes separated by gel electrolyte from each other, see **Figure 2.3**. The device was allowed to stay at room temperature for 1 h under ambient conditions. The electronic and optical properties of the device were recorded by switching between the two colored states (reference and counter electrodes shorted together) *via* square wave potential method. Under a square potential input of −1.0 and +1.2 V with a residence time of 4 s at each potential, the electrical response of the device were recorded simultaneously.[100]

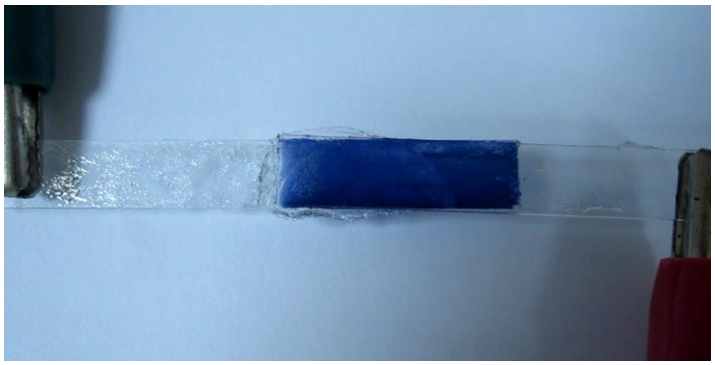

Figure 2.3.[*] The image of the electrochromic device showing the gel phase entrapped between two ITO electrodes, which were also coated with electrochromic polymers. [103]

[*] Reprinted from Albayrak, C., Cihaner, A. & Dag, Ö. A New, Highly Conductive, Lithium Salt/Nonionic Surfactant, Lyotropic Liquid-Crystalline Mesophase and Its Application. *Chemistry – A European Journal* 18, 4190-4194 (2012), with permission from John Wiley and Sons (2012).

3. Results and Discussion

3.1. $[Zn(H_2O)_6](NO_3)_2$-$C_{12}EO_{10}$ System

The liquid crystalline properties of transition metal aqua complex salt-surfactant mixtures were discovered by Dag et al. in 2001.[50] Since then, the investigations on this field are mainly lead by his research group.[50,65,67,73,74,101,102]There are many questions in the $[M(H_2O)_a](X)_b$-Surfactant systems that waits to be answered. For instance, the nature of the salt in the system has not been elucidated until this thesis.[103,104]Again, the origin of the LLC formation and the phase behavior was substantially unknown.[50,65,67,73,74,101,102] The boundaries related to the type of the surfactants and the salts that can self-assemble into LLC mesophases were not well defined. These mesophases are potential candidates as a reaction medium for the chemistry in a confined space. The distances between the micellar surfactant domains are in the range of 2-10 nm and a considerable part of this space is filled by the salt species (in contrast to water-surfactant LC systems). The $[M(H_2O)_a](X)_b$-surfactant systems have been used as templates for the synthesis of metal containing mesoporous or mesostructured films.[64,70] However, currently $[M(H_2O)_a](X)_b$-surfactant systems role in the synthesis and their potentiality as novel materials strictly depends on the fundamental research in this area. Our aim in this thesis, is to shine more light onto this anomalous LLC mesophases.

In order to clarify our perspective on the $[M(H_2O)_a](X)_b$-C_mEO_n systems, we have constructed a phase diagram, **Figure 3.1**, of $[Zn(H_2O)_6](NO_3)_2$-C_mEO_n mixtures. The selection of the transition metal salt is arbitrary since the first row transition metals behave more or less the same. The surfactant has been chosen as $C_{12}EO_{10}$ because it was the most widely used one in these systems. The mixtures of $[Zn(H_2O)_6](NO_3)_2$-$C_{12}EO_{10}$ system have been investigated using POM, DSC, FT-IR, micro-Raman, XRD and AC-Impedance Spectroscopy.

The high temperature boundaries of the hexagonal region 30-70 wt % $[Zn(H_2O)_6](NO_3)_2$ had previously been investigated by Çelik et al. [50,66] We also prepared our samples in this region and checked their validity under POM. **H_1**

regions showed the classical fan texture under POM, and $\mathbf{I_1}$ phases were isotropic and gave a dark image. The high temperature boundary for the $\mathbf{H_1}$ phase was also checked with our heating stage attached to the microscope. Additionally, we had noticed the presence of a two phase region ($\mathbf{H_1}$+ $\mathbf{I_1}$), between the $\mathbf{H_1}$ and $\mathbf{I_1}$ phases. $\mathbf{L_1}$ and $\mathbf{I_1}$+**SSa** boundary was determined using POM and DSC. In this region several measurements were performed (5 trials) and we presented the average value at this region because of the high tendency of the $[Zn(H_2O)_6](NO_3)_2$ species to supercool. The 0-30 wt % $[Zn(H_2O)_6](NO_3)_2$ and all other low temperature regions were also constructed mainly using the DSC, POM and XRD, Raman and FT-IR spectroscopy were performed when needed. The measurements were performed at heating and cooling rates of both 1^oC/min and 5^oC/min under POM and 5^oC/min in DSC. In a typical sample run in DSC analysis, the maxima of the exo/endo signals were assigned as the temperature of the event and shown in the phase diagram as points. Later on, these points were combined according to our results from the other

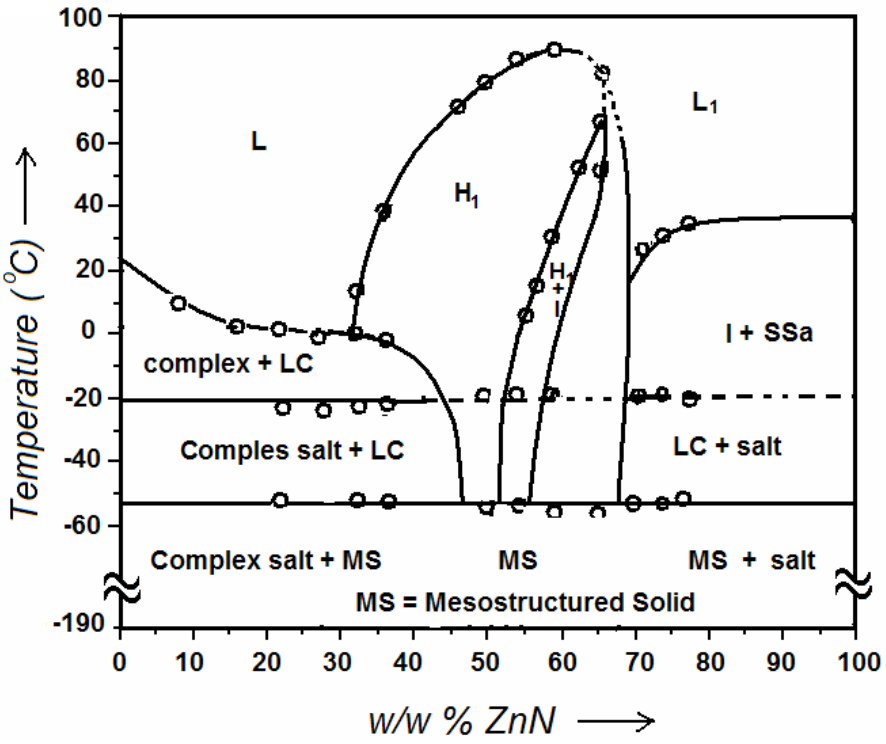

Figure 3.1.[*] The phase diagram of the ZnN-$C_{12}EO_{10}$ binary system (ZnN is $[Zn(H_2O)_6](NO_3)_2$).[104]

[*] Reprinted from Albayrak, C., Özkan, N. & Dag, O. Origin of Lyotropic Liquid Crystalline Mesophase Formation and Liquid Crystalline to Mesostructured Solid Transformation in the Metal Nitrate Salt−Surfactant Systems. *Langmuir* 27, 870-873 (2010), with permission from American Chemical Society (2010)

complementary tecniques. The $\mathbf{L_1}$ phase have been assigned as the micellar phase without further characterisation of the micelles in this region. The presence of LLC phases ipso facto indicates the presence of a micellar region at high solvent concentrations, or high temperatures.[8]

Notice that the phase diagram of $[Zn(H_2O)_6](NO_3)_2$-$C_{12}EO_{10}$ closely resembles the phase diagrams of H_2O-C_mEO_n systems (see **Figure 1.11** and **1.12**) at and above the room temperature.[28-30] The transitions from $\mathbf{V_1}$ to $\mathbf{H_1}$, and from $\mathbf{H_1}$ to $\mathbf{I_1}$ are evidences for the increase of the surface curvature with increasing metal salt concentration. Note that this behavior is universal for other surfactant-water systems, too. On the other hand, the low temperature behavior of the $[Zn(H_2O)_6](NO_3)_2$-$C_{12}EO_{10}$ system is quite different as compared to the water-surfactant systems. The DSC thermographs of all samples show two main events at around -20 and -52^{o}C, **Figure 3.2**. Former exothermic event is related to a leach out of some surfactant entities (will be discussed later). The magnitude of this event decreases with increasing salt concentration, and it becomes invisible in thermographs at 60 wt. % $[Zn(H_2O)_6](NO_3)_2$. The latter event is related to a glass transition (T_g), see **Figure 3.2**. Glass transition phenomenon is common for transition metal aqua-complex salts- usually determined with rapid quenching and reheating-[95] and it is likely that the molten $[Zn(H_2O)_6](NO_3)_2$ forms solid walls in the mesostructure below T_g. The temperatures, at which these two major events occur, are loosely dependent on the composition and shown in the phase diagram as two straight lines. Note also that, below -10^{o}C, the typical phase diagrams of surfactant-water mesophases undergo a complete phase separation to surfactant and water or a complexation between them.[28-30] However, the $[Zn(H_2O)_6](NO_3)_2$-$C_{12}EO_{10}$ mesophases are more stable and the mesostructured salt form is stable down to -190^{o}C, as evident from the POM images, recorded down to -190^{o}C and XRD data below -52^{o}C (see further discussions).

The molten $[Zn(H_2O)_6](NO_3)_2$ has a freezing point close to 37^{o}C. Upon addition of surfactant, the freezing point gradually decreases down to 20^{o}C. However, when the $\mathbf{I_1}$ region is reached at 68 wt % $[Zn(H_2O)_6](NO_3)_2$, the molten $[Zn(H_2O)_6](NO_3)_2$ does not crystallize but freezes as an amorphous solid at -52^{o}C. It means that confinement of the $[Zn(H_2O)_6](NO_3)_2$ in the LLC domains avoids its

crystallisation. The stability of the $[Zn(H_2O)_6](NO_3)_2$ species as compared to water is related to the differences between the strength of the interactions between *$[Zn(H_2O)_6](NO_3)_2$ and $C_{12}EO_{10}$* and the *H_2O and $C_{12}EO_{10}$*. The FTIR investigations of both systems show stronger hydrogen bonding in the $[Zn(H_2O)_6](NO_3)_2$-$C_{12}EO_{10}$ system.[50] **Figure 3.3** shows the FT-IR spectra of $3.0[Zn(H_2O)_6](NO_3)_2$-$1.0C_{12}EO_{10}$ and $35.0H_2O$-$1.0C_{12}EO_{10}$. Both samples exhibit LLC mesophases at these compositions. It is seen that the ν-CO stretching frequency of the ethylene oxide chains shift to lower energy (1085 cm^{-1}) due its interaction with the salt species. The $[Zn(H_2O)_6]^{2+}$ ions form hydrogen bonds[50] with the ethylene oxide oxygens through the coordinated water molecules. The higher acidity of the coordinated water molecules is also reflected on the ν-OH stretching band of water around 3000-3700 cm^{-1}. It is seen that the water band shifts to lower energy in the $[Zn(H_2O)_6](NO_3)_2$-$C_{12}EO_{10}$ system. In addition, the isotropization temperatures of this $[Zn(H_2O)_6](NO_3)_2$-$C_{12}EO_{10}$ system can be ~50°C higher than H_2O-C_mEO_n systems. However, the relation between the isotropization and the degree of hydrogen bonding in these systems has not yet been elucidated.

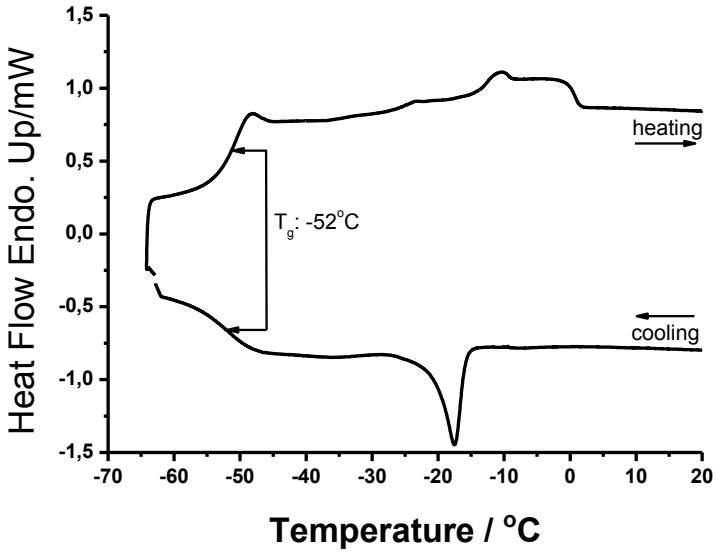

Figure 3.2. A typical DSC thermograph of $[Zn(H_2O)_6](NO_3)_2$-$C_{12}EO_{10}$ showing two main events (See appendix for all the DSC data used in the phase diagram)

The two phase region $\mathbf{H_1}$+$\mathbf{I_1}$ has been constructed using POM. **Figure 3.4** shows the captured images during a cooling experiment for the 50 wt % $[Zn(H_2O)_6](NO_3)_2$ sample. The images display a typical fan-like texture for a 2D-Hexagonal LC phase. During cooling the texture remains substantially the same. For samples having high surfactant concentration (salt/surfactant ratio below 50 wt % $[Zn(H_2O)_6](NO_3)_2$), surfactant entities can be observed at around -20^{o}C, nonetheless the texture was also preserved in those samples too (not shown). It is seen in Figure 3.4 that, below the glass transition, the texture still remains the same, which indicates a transition from LLC to a mesostructured solid that cracks usually below -100^{o}C, characteristic for thick solid films. Upon heating back to room temperature, these crack patterns were healed and the sample had exactly the same texture. The cooling measurements were repeated at least 5-10 times and we did not notice any change in the behaviour of the sample(s).

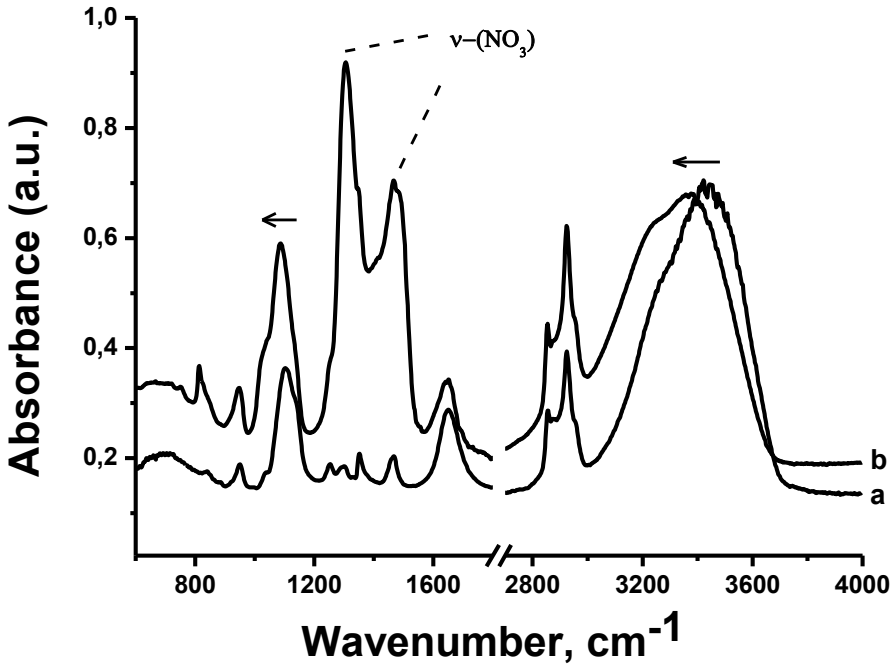

Figure 3.3. FT-IR spectra comparison of $[Zn(H_2O)_6](NO_3)_2$-$C_{12}EO_{10}$ and H_2O-$C_{12}EO_{10}$ mesophases. Note that the spectra were not normalized.

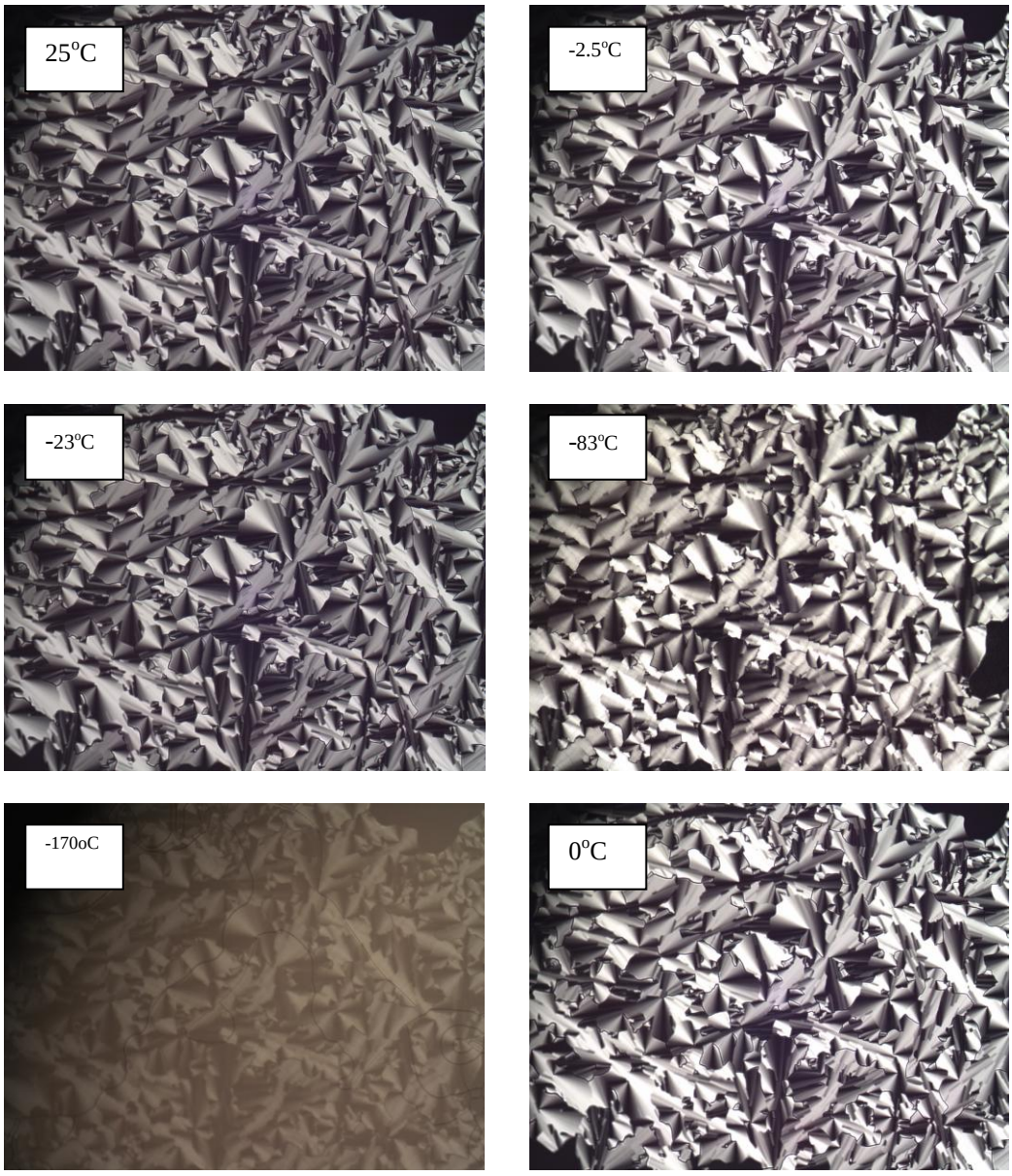

Figure 3.4.[*] The POM images of a sample having 50 wt % $[Zn(H_2O)_6](NO_3)_2$ at various temperatures (cooled from 25 °C to -170°C and heated to 0°C) as indicated in the images.[104]

[*] Reprinted from Albayrak, C., Özkan, N. & Dag, O.m. Origin of Lyotropic Liquid Crystalline Mesophase Formation and Liquid Crystalline to Mesostructured Solid Transformation in the Metal Nitrate Salt−Surfactant Systems. *Langmuir* 27, 870-873 (2010), with permission from American Chemical Society (2010).

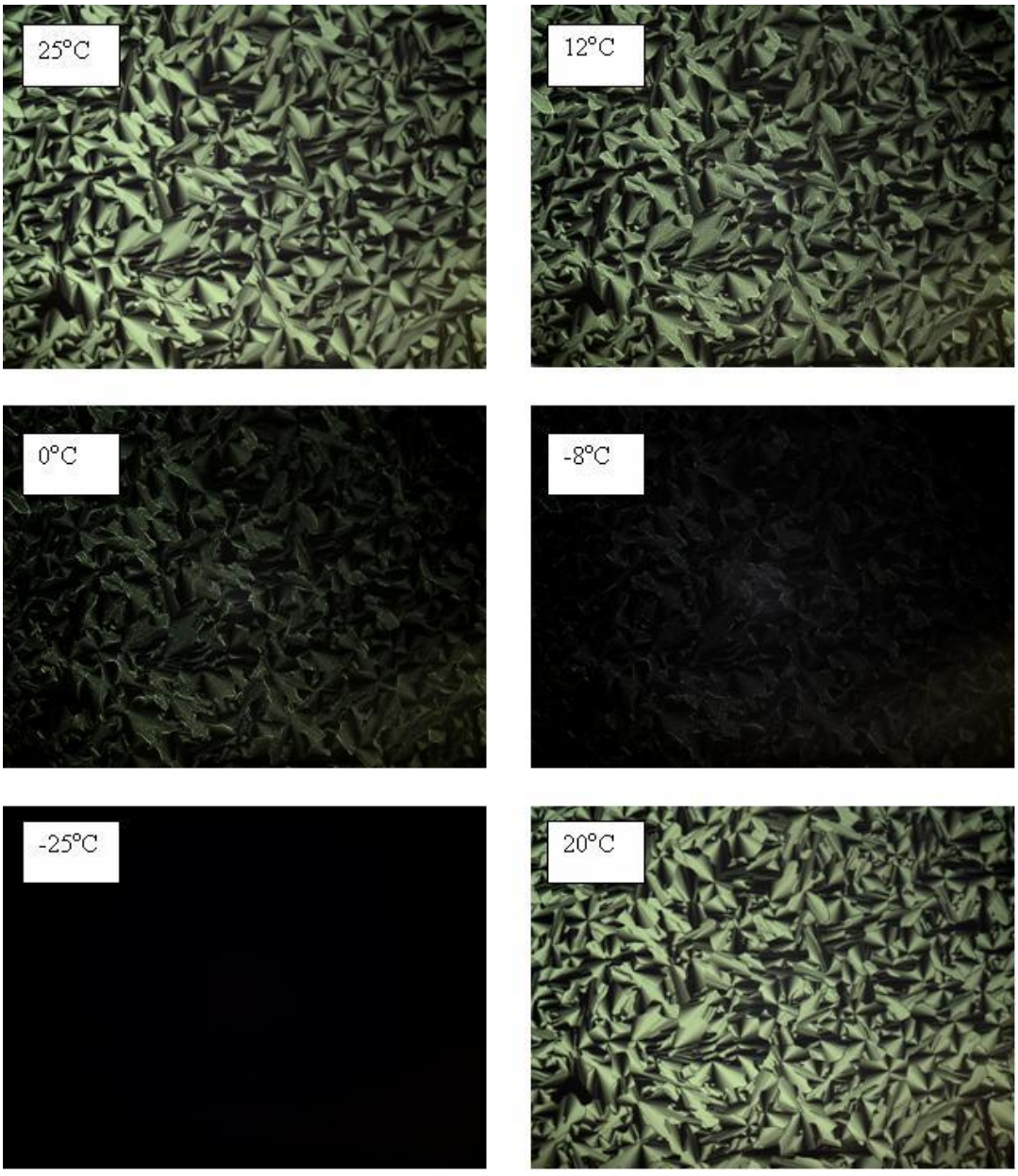

Figure 3.5. The POM images of a sample having 57 wt % $[Zn(H_2O)_6](NO_3)_2$ at various temperatures as indicated in the images. (cooled from 25 ^oC to -25^oC and heated to 0^oC)

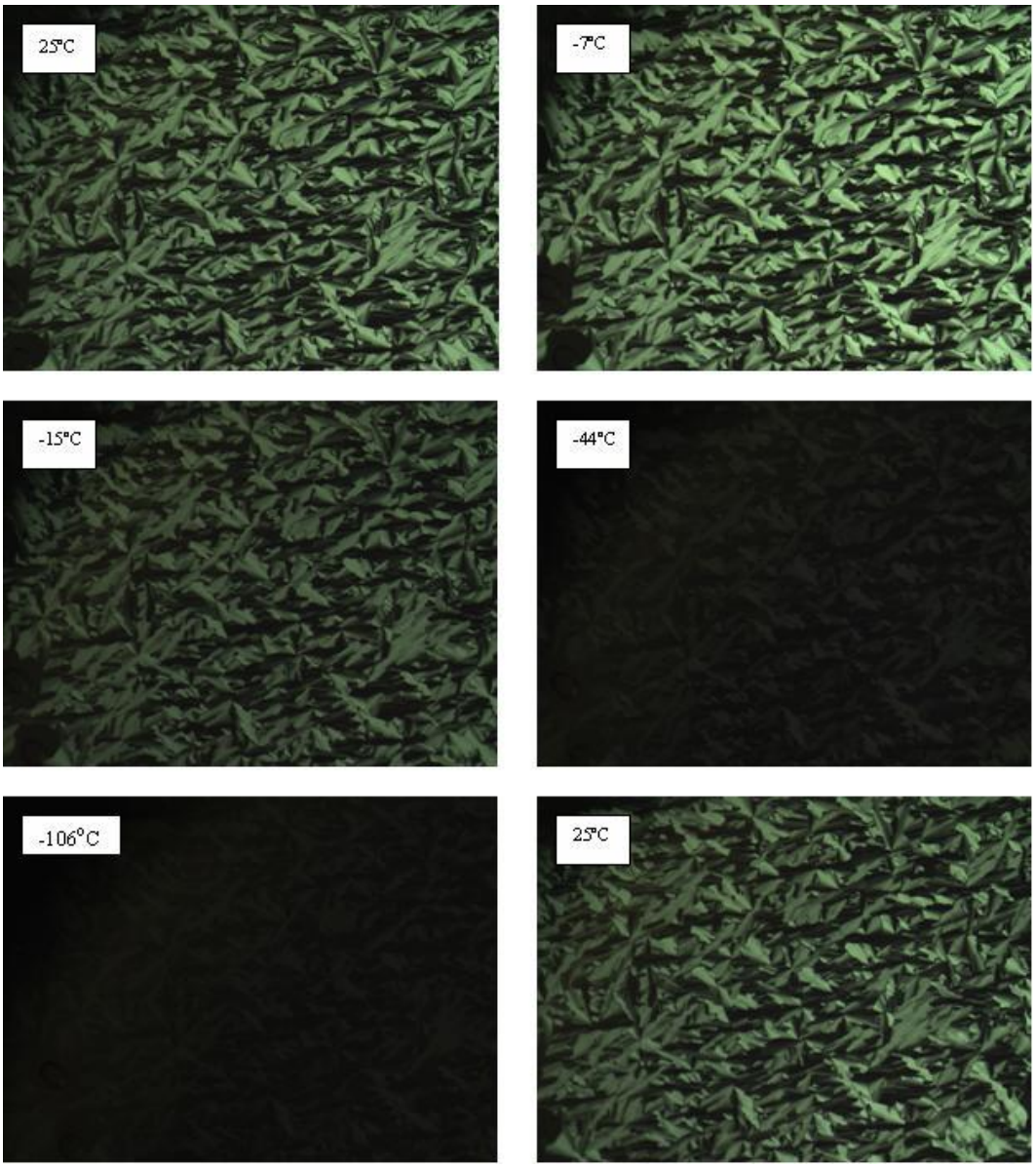

Figure 3.6. POM images of a sample having 53 wt % $[Zn(H_2O)_6](NO_3)_2$ at various temperatures as indicated in the images. (cooled from 25 ^oC to -106^oC and heated to 25^oC)

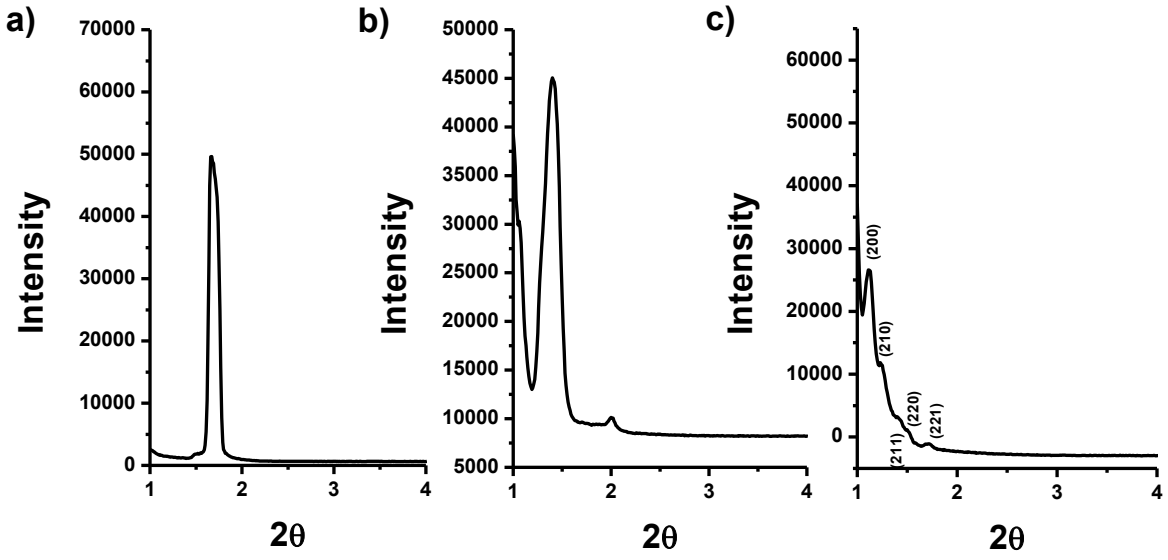

Figure 3.7.[*] The XRD patterns of a sample having 57 wt % $[Zn(H_2O)_6](NO_3)_2$ a) hexagonal phase at room temperature, b) hexagonal+cubic phase somewhere between room temperature and -20°C and c) cubic phase below -20°C.[104]

The samples between 53 and 68 wt % $[Zn(H_2O)_6](NO_3)_2$ show hexagonal to cubic transition with the presence of an extensive two phase region (H+I). **Figure 3.5** shows the selected POM images recorded during the cooling-heating processes in this region. At around 20°C black dots starts to appear, indicating the emergence of the isotropic cubic phase, (see **Figure 3.7** for the XRD pattern of this composition). At around -20°C, the sample completely transforms into a cubic phase; the dark image also correlates with the XRD pattern of the sample below -20°C. Below glass transition, the sample again cracks (not shown) like the hexagonal phase and upon heating back to room temperature, the sample provided exactly the same texture.

[*] Adapted from Albayrak, C., Özkan, N. & Dag, O.m. Origin of Lyotropic Liquid Crystalline Mesophase Formation and Liquid Crystalline to Mesostructured Solid Transformation in the Metal Nitrate Salt−Surfactant Systems. *Langmuir* 27, 870-873 (2010), with permission from American Chemical Society (2010).

There is also a composition range, where the samples freeze into two different mesostructured solid domains between 52 and 56 wt % $[Zn(H_2O)_6](NO_3)_2$. The POM images of the two-phase region is shown in **Figure 3.6**. The presence of a texture with a significant darkening can be seen in the image of these samples collected at -106^oC.

It is evident from the phase diagram of the $[Zn(H_2O)_6](NO_3)_2$-$C_{12}EO_{12}$ that $[Zn(H_2O)_6](NO_3)_2$ acts as the solvent in the mesophase as in most other surfactant-solvent phases. The $[Zn(H_2O)_6](NO_3)_2$ species induce self-assembly of surfactant molecules, which is universal in many other solvents. The phase diagram may also open a new area of research in colloid and surfactant science. Such as the presence of vesicles, inverted mesophases, cloud points and many other soft-matter phenomena can be investigated in these type of molten hydrated salts.

FT-IR spectra of the samples with different concentrations elucidate the state of the $[Zn(H_2O)_6](NO_3)_2$ further. **Figure 3.8** shows the FT-IR spectra of various compositions. At around 36 wt % $[Zn(H_2O)_6](NO_3)_2$ where the transition to $\mathbf{H_1}$ phase takes place, major changes are observed in the spectra, the most important one being the ν-CO stretching of the ethylene oxide groups of the surfactant molecule. The ν-CO signal gradually shifts from 1110 cm^{-1} to 1087 cm^{-1} as the salt concentration is increased. The ν-CO stretching is responsive to the degree of hydrogen bonding between the oxygens of the ethoxy groups and the hydrogens of the coordinated water molecules.[50] At around 60 wt % $[Zn(H_2O)_6](NO_3)_2$, which corresponds to $\mathbf{H_1}$ to $\mathbf{I_1}$ transition at room temperature, the changes stop in that region, which means above 60 wt. % $[Zn(H_2O)_6](NO_3)_2$ additional salt does not affect the extend of hydrogen bonding. At the same time, the intensity of the asymmetric stretching mode of the free nitrate ion[50] at around 1400 cm^{-1} starts to increase. The signals at around 1420 cm^{-1} and 1270 cm^{-1} correspond to coordinated nitrate ions. [50]In the molten $[Zn(H_2O)_6](NO_3)_2$, some of the nitrates are coordinated to the metal centre. In the LC mesophase up to 60 wt % $[Zn(H_2O)_6](NO_3)_2$ the extend of the coordination is significant, however above 60 wt % $[Zn(H_2O)_6](NO_3)_2$ intensity of the free nitrate signal increases and eventually the spectra at higher compositions of $[Zn(H_2O)_6](NO_3)_2$ closely resembles the spectrum of pure molten phase of the salt. The coincidence of these two events at 60 wt % $[Zn(H_2O)_6](NO_3)_2$– cease in the shift of ν-CO stretching and intensifying free

nitrate signal- indicate a different salt species, which does not interact with surfactant head groups as strongly as before and resembles the molten $[Zn(H_2O)_6](NO_3)_2$ more, starts to form around 60 wt % $[Zn(H_2O)_6](NO_3)_2$. At around 70 wt % $[Zn(H_2O)_6](NO_3)_2$, there is no way to keep micellar units ordered and a transition from $\mathbf{I_1}$ to $\mathbf{L_1}$ phase (micellar solution phase) occurs. Above 70 wt % $[Zn(H_2O)_6](NO_3)_2$ confinement effect diminishes and the system behaves like a micella solution.

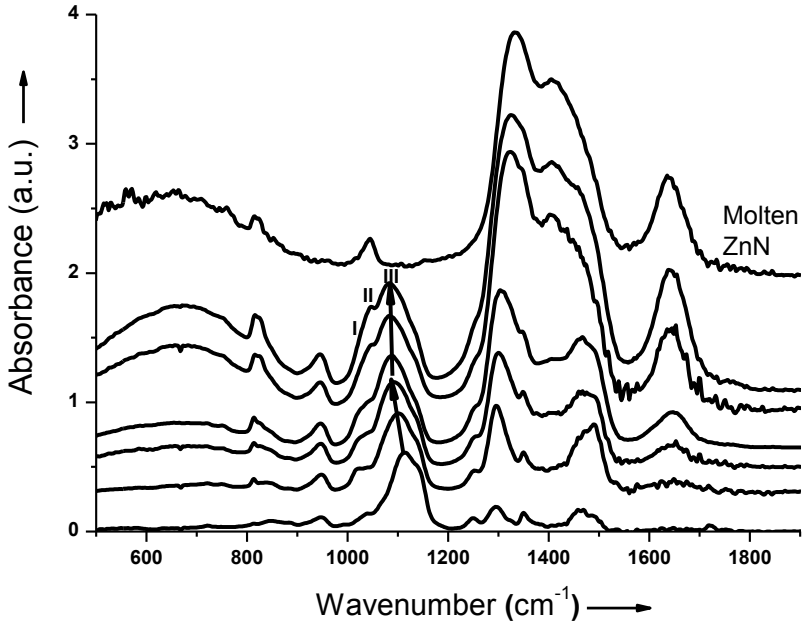

Figure 3.8.[*] FT-IR spectra of samples from top to bottom; 100 , 74, 60, 57, 50, 40, and 0 wt % $[Zn(H_2O)_6](NO_3)_2$-$C_{12}EO_{10}$.[104]

The Raman spectra of some samples were also recorded in order to enlighten the low temperature regions in the phase diagram and also the glass transition. A cooling stage was attached under the micro-Raman instrument and the samples were sandwiched between two glass slides. Upon cooling the molten surfactant – $C_{12}EO_{10}$- , many of the peaks sharpen, most notably the signal in the ν-CH stretching region at 2880 cm^{-1}, **Figure 3.9**, due to the crystallisation of the

[*] Adapted from Albayrak, C., Özkan, N. & Dag, O. Origin of Lyotropic Liquid Crystalline Mesophase Formation and Liquid Crystalline to Mesostructured Solid Transformation in the Metal Nitrate Salt−Surfactant Systems. *Langmuir* 27, 870-873 (2010), with permission from American Chemical Society (2010).

surfactant species. For the remaining samples we have monitored this peak because it gives the best response with decreasing temperature. The surfactant peak again arises with decreasing temperature of the sample having a 27.5 wt % $[Zn(H_2O)_6](NO_3)_2$, see **Figure 3.10**, because of the leach out of some surfactant entities. For the sample having a 65.5 wt % $[Zn(H_2O)_6](NO_3)_2$–corresponding to the cubic region- there are no observable events between room temperature and glass transition in the DSC thermographs (see Appendix for DSC data). However, in the Raman spectra, **Figure 3.10**, the intensity of the signal at 2880 cm^{-1} starts to increase close to -20°C. This is correlated with the exothermic event at -20°C, but the DSC instrument is incapable of detecting this event. The magnitude of the surfactant signal decreases and becomes insignificant with increasing salt concentration and starts to appears just around -20°C for all samples.

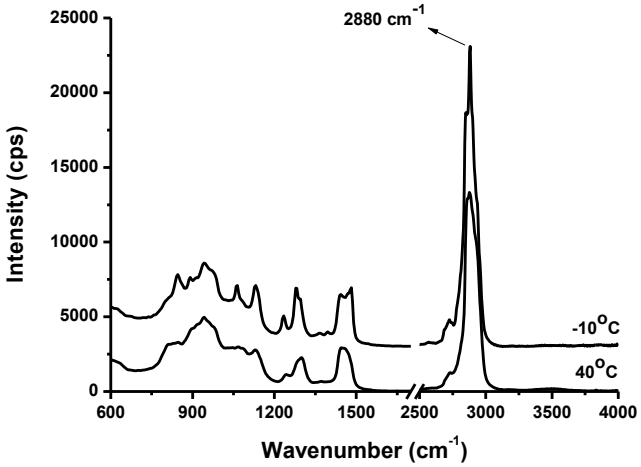

Figure 3.9. The Raman spectra of $C_{12}EO_{10}$ at -10°C and 40°C

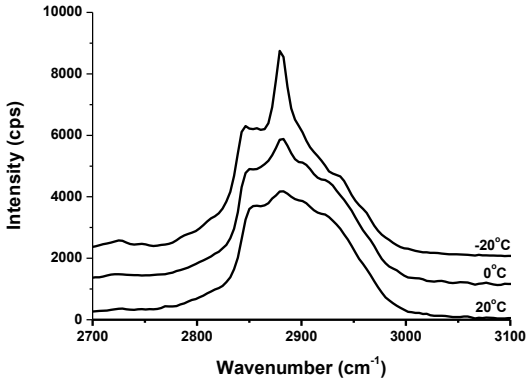

Figure 3.10. The Raman spectra of 27.5 wt % $[Zn(H_2O)_6](NO_3)_2$ during cooling from 20°C to -20°C, the temperatures are indicated on the spectra

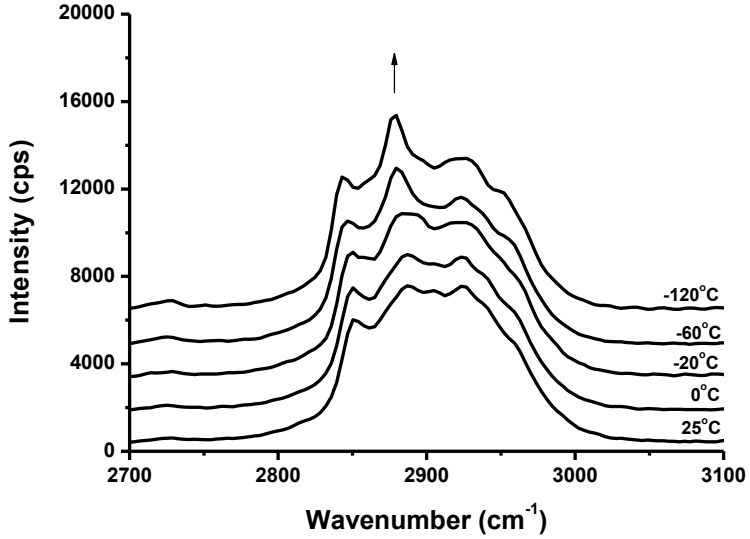

Figure 3.11. The Raman spectra of 65.5 wt % $[Zn(H_2O)_6](NO_3)_2$ during cooling from 25 to -120^{o}C.

which accompanies the observable exothermic event (during cooling) in DSC thermographs at the same temperature. This indicates that the exothermic event at -20^{o}C is related to the crystallisation of some surfactant molecules leached out of the mesophase.

To further insight on the nature of the salts species in the mesophase, we have also recorded the conductivity of a series of samples using AC impedance spectroscopy method. The conductivity values change between $7.0x10^{-5}$ and $2.13x10^{-3}$ Scm^{-1} depending on the salt content of the mesophase. The conductivities recorded for the $[Zn(H_2O)_6](NO_3)_2$-$C_{12}EO_{10}$ mesophase at RT get closer to the molten phase of $[Zn(H_2O)_6](NO_3)_2$ at higher salt content.

3.1.1. On the confinement of $[Zn(H_2O)_6](NO_3)_2$ in the LLC mesophase

Pure $[Zn(H_2O)_6](NO_3)_2$ has a glass transition temperature at around -75^{o}C. [95] The T_g of the molten salts and electrolyte solutions can be monitored by using DSC measurements. In measuring the T_g of pure molten salts, the crystallization of the

salts were prevented by quenching the samples below their glass transition temperatures.[95] The T_g's then determined by monitoring the DSC thermographs during the heating step. In the $[Zn(H_2O)_6](NO_3)_2$-$C_{12}EO_{10}$ system, the cooling rates in DSC and POM measurements were carried out as low as 1^oC/min and we have never observed any indication of crystallisation at the LC region during these measurements. As discussed before, freezing point of the $[Zn(H_2O)_6](NO_3)_2$ species, is altered significantly when the **I_1** cubic phase is formed. The $[Zn(H_2O)_6](NO_3)_2$ species does not crystallize out but exhibits a glass transition inside the LC domains at -52^oC.

The confinement of $[Zn(H_2O)_6](NO_3)_2$ in between liquid-like soft walls of the hydrophilic segments avoids its crystallization. On the molecular level, this corresponds to the hydrogen bonding interactions. In addition to the hydrogen bonding, the difference between the T_g of pure $[Zn(H_2O)_6](NO_3)_2$ and confined $[Zn(H_2O)_6](NO_3)_2$ may also be related to the differences in the coordination sphere of the metal centers. In the LLC mesophases, the extend of the coordination of nitrate ion to the metal center is significantly higher as compared to pure molten $[Zn(H_2O)_6](NO_3)_2$, **Figure 3.8**. The mechanisms behind increasing coordination in LLC systems have not yet been investigated, but it is plausibly related to the hydrogen bonding interactions between hydrophilic segments and the $[Zn(H_2O)_6](NO_3)_2$ species.

To further enlighten the state of $[Zn(H_2O)_6](NO_3)_2$ in LLC mesophases we have performed ionic conductivity measurements at different compositions. Since the physical property of the salt has changed drastically with confinement, the changes might also be reflected on the conductivity of the LLC system. The experiments were performed at 40^oC in order to prevent crystallization of $[Zn(H_2O)_6](NO_3)_2$ at high $[Zn(H_2O)_6](NO_3)_2$ weight ratios. **Figure 3.12** shows the conductivity profile of the mixtures with respect to the mole fraction of the salt. At **L_1** region, conductivity decreases with surfactant addition. However the decrease in the conductivity is significanly lower in the LLC region with decreasing mole fraction of the salt. From here, it may be deduced that the molar conductivity of salt increases with the confinement. However, further studies are required to reach this conclusion. For instance, the surface coverage of the electrodes with micellar domains is not known. It may be possible that the surface coverage increases until

the LLC mesophase is reached. Therefore the electrode surface area would be reduced with additional micelles which may result in a sharp decrease in the conductivity until the LLC phase is reached. Definitely more work is required to elucidate conductivity behaviour of the $[Zn(H_2O)_6](NO_3)_2$-$C_{12}EO_{10}$ LLC mesophases.

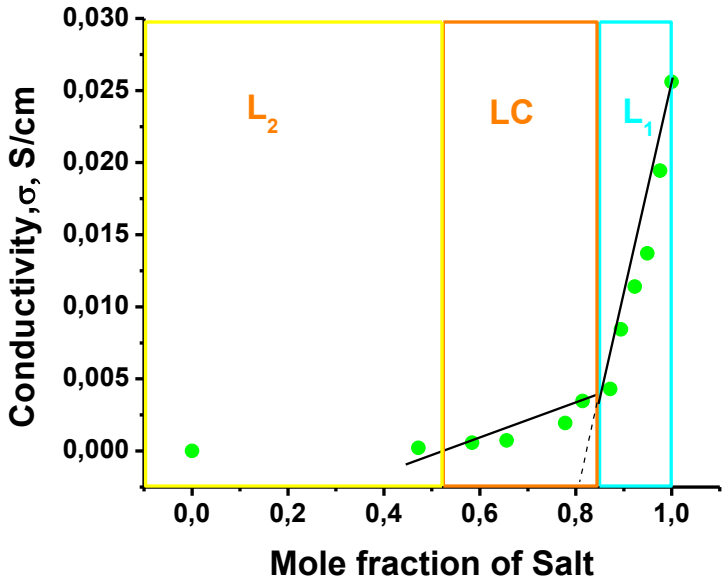

Figure 3.12. Total ionic conductivity of samples with varying mole fraction of the salt $[Zn(H_2O)_6](NO_3)_2$

3.2. LiX-$C_{12}EO_{10}$-nH_2O Systems

Previously, alkali and alkaline earth metal salts were considered as additives in the self assembly of non-ionic amphiphiles and usually the effect of additives on the phase boundaries were investigated at low salt concentrations.[41,42,44] The studies in this field were limited to a few cases. On the other hand, the origin of the self-assembly in the transition metal salt-surfactant systems were unknown. In section 3.1, we showed that the transition metal salt species acts as the solvent component in the self-assembly of the amphiphiles. In this chapter, we will demonstrate that the concentrated solutions of alkali metal salts can also organize the surfactant molecules into LLC mesophases. The concentrated aqueous solutions of alkaline or alkaline earth metal salts are also analogous to transition metal molten salts. Early studies on the physical chemistry of aqueous solutions and molten salts show that highly concentrated electrolyte solutions can exhibit similar properties to molten salts, when the amount of water is sufficiently low, so that only the first hydration sphere of the cation is satisfied.[105] In addition, at high salt concentrations, the bulk properties of water are significantly altered and the salt-water interactions start to dominate. At high salt concentrations, the salt effects become significant and these mesophases should be distinguished from the dilute salt-surfactant systems.

We will use the abbreviation LiX.xH_2O-$C_{12}EO_{10}$ for alkali metal salt-surfactant systems for samples which are open to atmosphere. However, we do not imply that all the water molecules in the mesophases are in the hydration sphere of the ions. Five different Li^+ salts were used in this study, namely: $LiNO_3$, LiCl, LiBr, LiI and $LiClO_4$ (LiF is practically insoluble and were not studied). The LLC mesophases were prepared either as gels by mixing necessary amounts of salt, surfactant and water or as solutions by mixing salt and surfactant in excess water. The LLC thin films can then be obtained by spin-coating, dip-coating or drop casting the homogenized solutions on desired substrates. The hexagonal mesophases exhibit typical fan textures under the POM and diffract at small angles with a typically observed unit cell parameter around 4-6 nm with $C_{12}EO_{10}$ surfactant, see **Figure 3.13**.

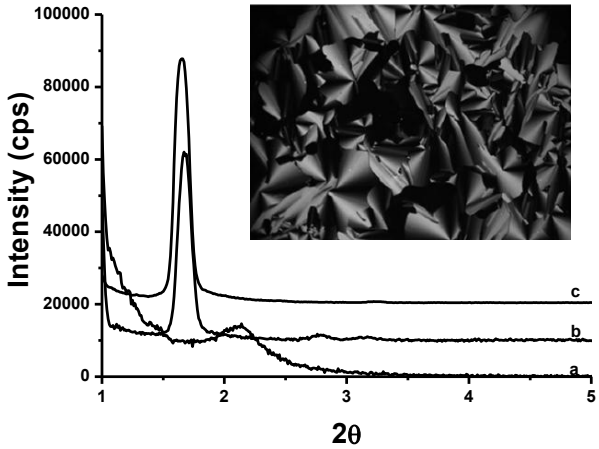

Figure 3.13.[*] Typical XRD patterns at small angles (a) $LiClO_4$-H_2O-$C_{12}EO_{10}$, (b) LiCl-H_2O-$C_{12}EO_{10}$, and (c) $LiNO_3$-H_2O-$C_{12}EO_{10}$ systems and a POM image in the inset.[103]

3.2.1. $LiNO_3$-H_2O-$C_{12}EO_{10}$ phase diagram

A ternary phase diagram of the $LiNO_3$-H_2O-$C_{12}EO_{10}$ system, **Figure 3.14**, has been constructed using XRD patterns and POM images, over 60 samples with a broad range of composition. A considerable region in the phase diagram belongs to a hexagonal LLC mesophase (marked as **H**). The two phase regions that contain salt or surfactant crystals together with the **H** phase were not studied in detail; these regions are marked with **2** and **4** in the phase diagram, respectively. At high water contents, micellar solution phases are observed (region **1** and towards higher water compositions). The samples were followed for months to monitor any sign of super saturation. Further investigations are necessary for the characterisation of the **H** phase in detail, and the clarification of two phase regions such as **H**+H_2O, if there are any. In general, the XRD patterns provide 2 or 3 diffraction lines at most, which make a detailed characterisation of the **H** phase difficult. The boundaries at the high salt (**2)** and low water concentrations were determined by using a POM, and by monitoring the presence of anisotropic $LiNO_3$ crystals. These boundaries can also be identified further. The boundary at the high water concentration (**1)** was

[*] Reprinted from Albayrak, C., Cihaner, A. & Dag, Ö. A New, Highly Conductive, Lithium Salt/Nonionic Surfactant, Lyotropic Liquid-Crystalline Mesophase and Its Application. *Chemistry – A European Journal* 18, 4190-4194 (2012), with permission from John Wiley and Sons (2012).

determined by controlling the fluidity of the samples with naked eye and also by checking the birefringence under the POM. Note that the hexagonal mesophase forms between 37 and 65 wt % $C_{12}EO_{10}$ in the water-surfactnat LLC without salt. The highest amount of $LiNO_3$ can be 33 wt % that corresponds to around 7 mole ratio of $LiNO_3/C_{12}EO_{10}$ and the amount of water can be as low as 12 wt %, which corresponds to 2 $H_2O/LiNO_3$ mole ratio. Along the broken line, the $LiNO_3/H_2O$ ratio is constant at 47 wt %, which is the highest amount of salt that can be dissolved in pure water at RT. Notice that, a considerable hexagonal region exists above this line. The higher intake of $LiNO_3$ in the **H** phase as compared to the pure H_2O is related to the confinement of the salt and water species in the hydrophilic domains of the hexagonal mesophase.[12] The interaction of Li^+ (or Li^+---H_2O) with the surfactant head groups (will be discussed further) prevents $LiNO_3$ crystallisation above the solubility limit.

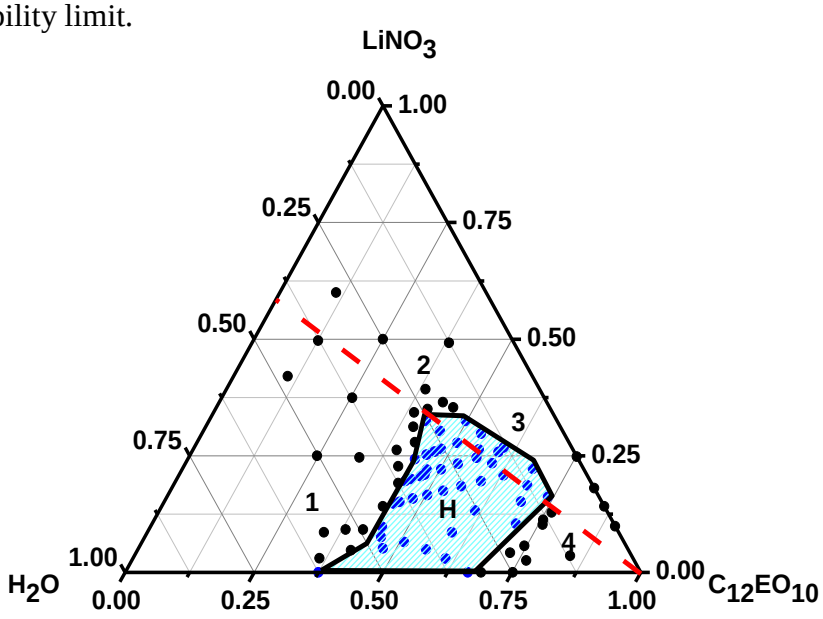

Figure 3.14.* Ternary phase diagram of $LiNO_3$-H_2O-$C_{12}EO_{10}$ system. The red-line that divides the phase diagram into two corresponds to the weight ratio of $LiNO_3$ to water in saturated $LiNO_3$ solution at RT. Blue and black dots represent the prepared samples.[103]

At such high concentrations of salt, the salt species become a primary constituent of the mesophase rather than being an additive. That is, the salt-water

* Reprinted from Albayrak, C., Cihaner, A. & Dag, Ö. A New, Highly Conductive, Lithium Salt/Nonionic Surfactant, Lyotropic Liquid-Crystalline Mesophase and Its Application. *Chemistry – A European Journal* 18, 4190-4194 (2012), with permission from John Wiley and Sons (2012).

couple acts collaboratively to constitute a solvent species, which can organize the surfactant molecules into micellar and/or liquid crystalline mesophases.

3.2.2. Effect of different anions on the phase behavior

In order to have an idea on the effect of different anions on the phase behaviour of $LiNO_3$-H_2O-$C_{12}EO_{10}$ systems, the LLC mesophases of $LiNO_3$, LiCl, LiBr, LiI and $LiClO_4$ systems were investigated under ambient conditions. The samples were prepared by mixing 5 ml of water, 1g of surfactant and required weight of the salt. Before the XRD measurements the samples were spin coated on glass slides at 1000 rpm and allowed to equilibrate a few minutes under open atmosphere at RT and 20-25% RH. The samples that were kept under open atmosphere were affected by the humidity in the laboratory, therefore the measurements had to be carried out at constant humidity. **Figure 3.15** shows the POM images of $LiNO_3$ and LiCl containing samples under two different humidities. The images were captured after 1 day at a specified humidity at RT. Note that, the crystals of $LiNO_3$ are visible at 10% RH meaning that the samples undego water exchange with the air. **Figure 3.16** shows the Raman spectra of the $LiNO_3xH_2O$-$C_{12}EO_{10}$ system at 3.0

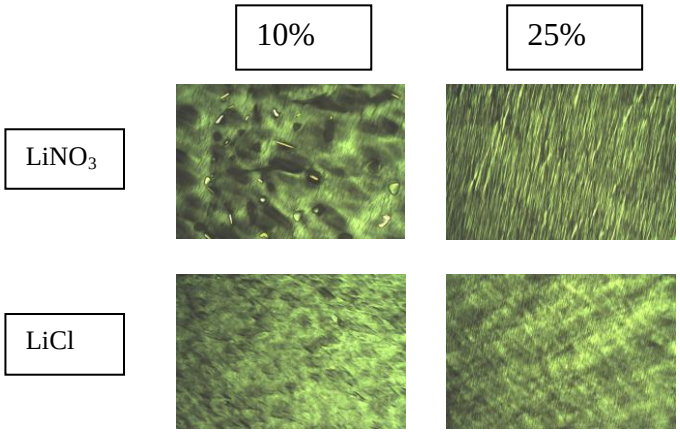

Figure 3.15.* POM images of the samples with a Salt/$C_{12}EO_{10}$ mole ratio of 3.0 at two different humidity levels (as marked on the images).

* Reprinted from Albayrak, C., Cihaner, A. & Dag, Ö. A New, Highly Conductive, Lithium Salt/Nonionic Surfactant, Lyotropic Liquid-Crystalline Mesophase and Its Application. *Chemistry – A European Journal* 18, 4190-4194 (2012), with permission from John Wiley and Sons (2012).

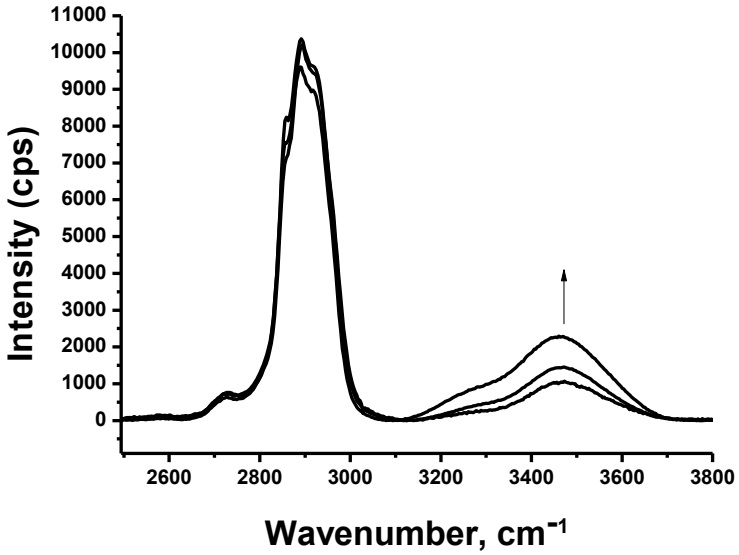

Figure 3.16. Raman spectra of $3.0LiNO_3.xH_2O$-$C_{12}EO_{10}$ at 25, 40 and 65% RH levels and RT.

$LiNO_3/C_{12}EO_{10}$ mole ratio at three different %RH levels. The intensity of the ν-OH stretching band around 3000-3500 cm^{-1} indicates that the amount of water in the sample increases with the increasing %RH in the atmosphere.

The open atmospheric measurements are advantageous because it gives an idea about the strength of the Salt-Water interactions in the mesophase and the air stability of the samples. Furthermore, it is important for the mesophases to be air stable if these phases are going to be considered for their material properties. For instance, most of the time, the mesostrucutured/mesoporous material synthesis requires open atmospheres. These mesophases can also be important as conductive gel materials where non-volatile behaviour is also highly important (see Chapter 7). The construction of the ternary phase diagram of each salt is necessary but requires tedious effort and out of the scope of this thesis.

Figure 3.17, **3.18**, **3.19**, **3.20** and **3.21** shows the XRD patterns of LiCl, $LiNO_3$, LiBr, LiI and $LiClO_4$ systems at different $Salt/C_{12}EO_{10}$ mole ratios, respectively. The water content of the samples is dependent on the amount and type of the salt and can be different. Each salt has a different tendency to keep water in the mesophase – see FTIR section for details. As can be seen in the figures, a general trend is that the first diffraction line shifts to smaller angles with increasing

salt concentration in all of the salt systems. This means that the intermicellar spacing increase with increasing salt concentration. This observation is also in accord with the $[Zn(H_2O)](NO_3)_2$-CTAB-$C_{12}EO_{10}$ systems,[73] where increasing the concentration of the salt species increases the d-spacing values. Basically, more volume is needed for additional ions in the mesophase, therefore expansion of the domains is expected. In some of the measurements the detector was blocked with a copper plate between 1.2 and 2.0 degrees to avoid saturation from the intense light. The copper plate reduces the X-ray intensity 10 times, therefore between 1.2 and 2.0 degrees some of the diffraction data should be multiplied by 10. A discontinuity at 2.0 degrees implies that the detector was blocked before 2.0 degrees.

It can be deduced from the XRD patterns that the LiCl and LiBr systems work in a broadest range of salt/surfactant mole ratios, 2-12. These salts also show no sign of crystallisation under the specified experimental conditions. However, the $LiNO_3$ system leaches out some salt crystals above 6.0 Salt/$C_{12}EO_{10}$ mole ratio and $LiClO_4$ system does not have a significant LLC behaviour even at 1.0 salt/surfactant mole ratio and crystallizes, see **Figure 3.21**. The LiCl, LiBr and LiI systems loose mesostructure at around 10.0-12.0 mole ratio. The $LiClO_4.xH_2O$-$C_{12}EO_{10}$ system does not have a noticeable liquid crystallinity. However $LiClO_4.xH_2O$-$C_{18}EO_{10}$ (note that the surfactant has a longer alkyl chain) samples do have up to 3 salt/surfactant mole ratio. In general, most of the XRD patterns include 2 or 3 diffraction lines, see Figures **3.17**, **3.18**, **3.19**, **3.20** and **3.21**. The diffraction lines between 1.0 and 2.0 degrees are very close to each other, with a d-spacing ratio of 1.03, where d-spacings vary between 47 and 64 Å. The third diffraction line is found at a multiple of the first diffraction line and does not provide any additional information. 3 diffraction lines can be indexed to a rectangular columnar phase with **a** and **b** parameters very close to each other. However the second diffraction line may also arise from an inhomogenity along the sample thickness. Since the samples are open to the atmosphere water concentration along the sample may vary. The topmost layers may include lower water content and therefore diffract at a higher angle. Because of the difficulties in characterization of the mesostructures directly from XRD, POM images were used to assign hexagonal to isotropic phase transitions. The isotropic phases give a dark image under the POM and theoretically should be a $\mathbf{I_1}$ phase, since $\mathbf{H_1}$ phase is usually transforms to a $\mathbf{I_1}$ phase at higher

solvent concentrations. **Table 3.2** gives our assignements of the type of the mesophases based on the XRD and POM tecniques at RT and 23-25% RH. The POM images can be found in the related Appendix.

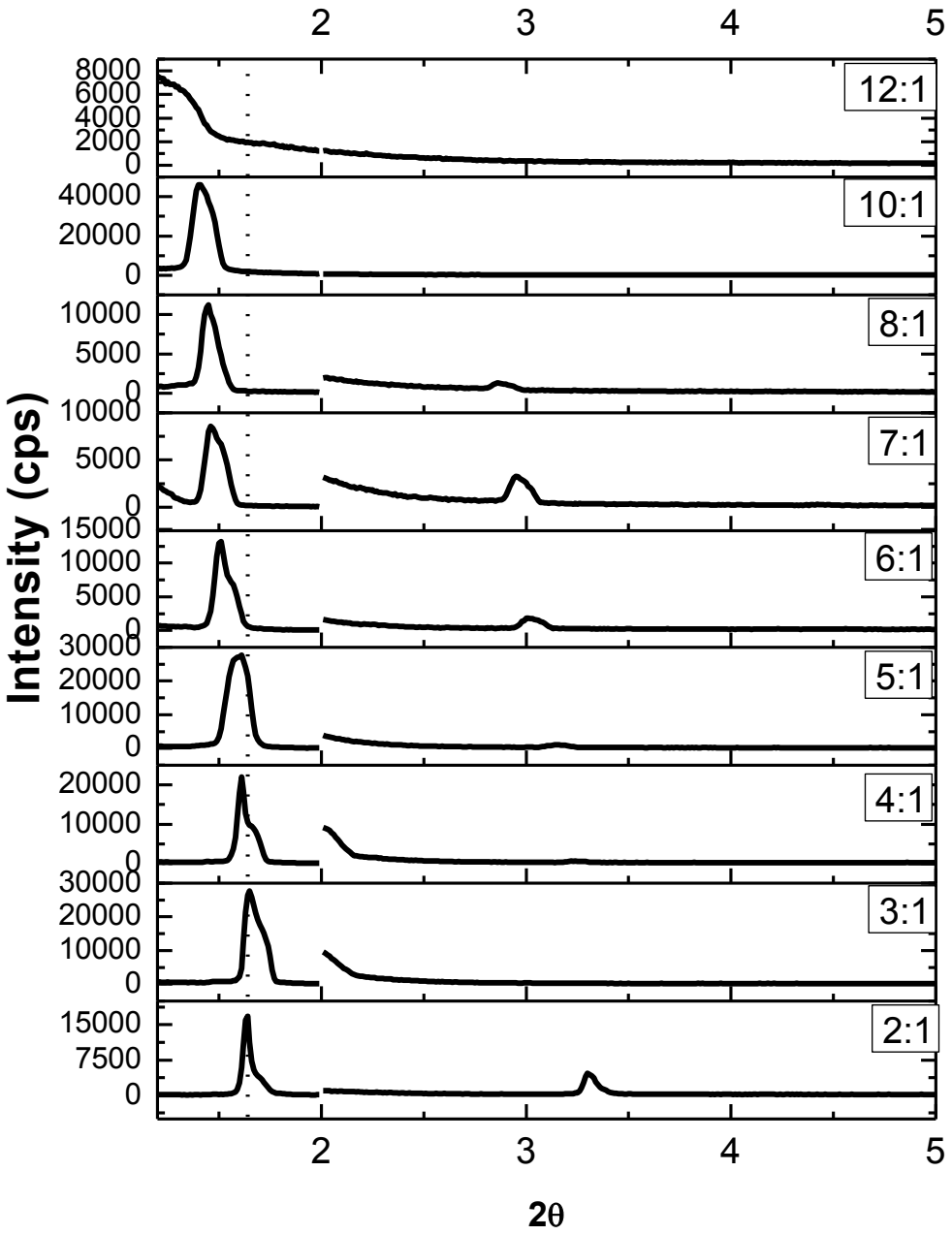

Figure 3.17. XRD patterns of $LiCl.xH_2O$ -$C_{12}EO_{10}$ at 24^{o}C, 23% RH

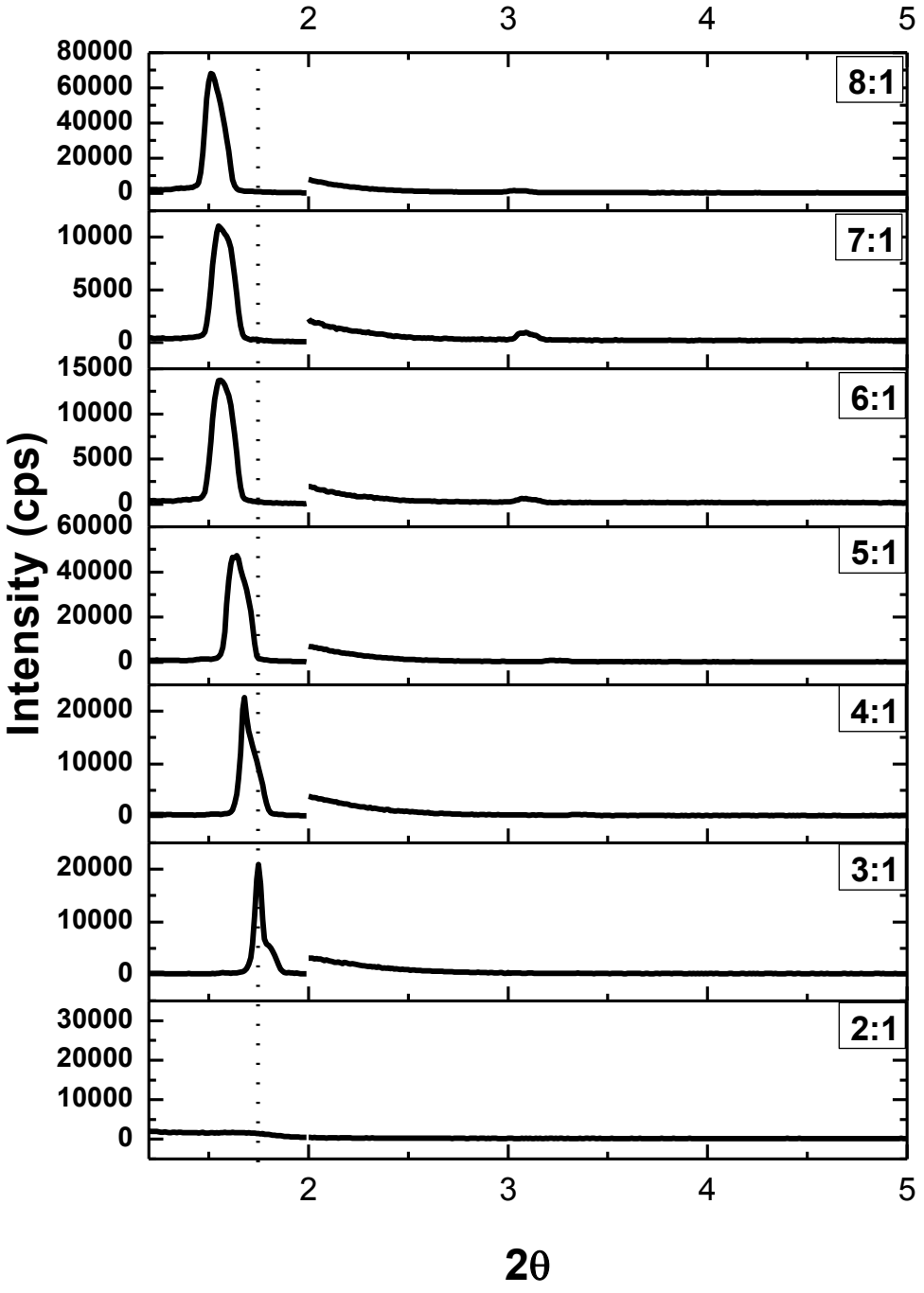

Figure 3.18. XRD patterns of $LiNO_3.xH_2O$ -$C_{12}EO_{10}$ at 24^{o}C, 23% RH

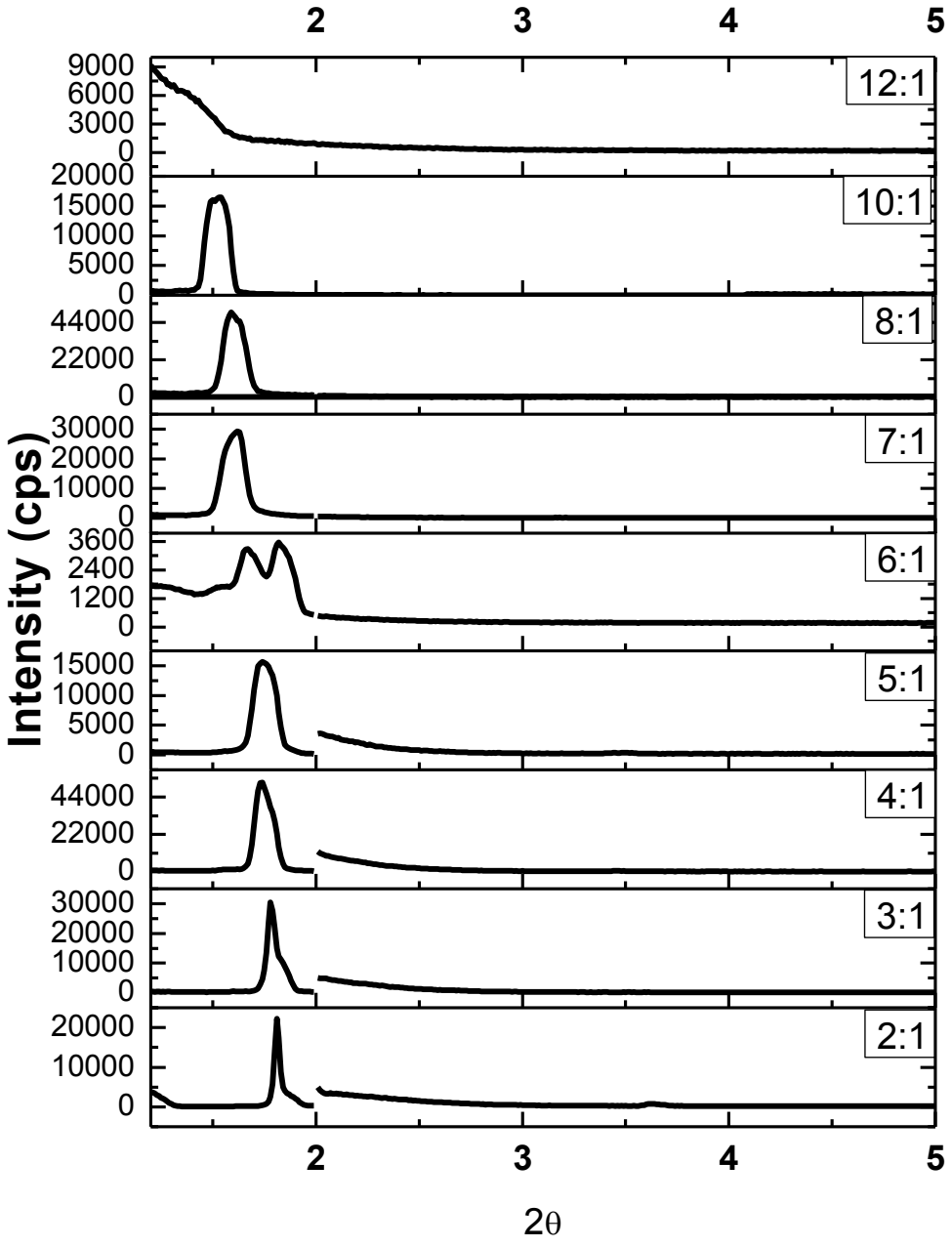

Figure 3.19. XRD patterns of LiBr-$C_{12}EO_{10}$-xH_2O at 24^{o}C, 23% RH

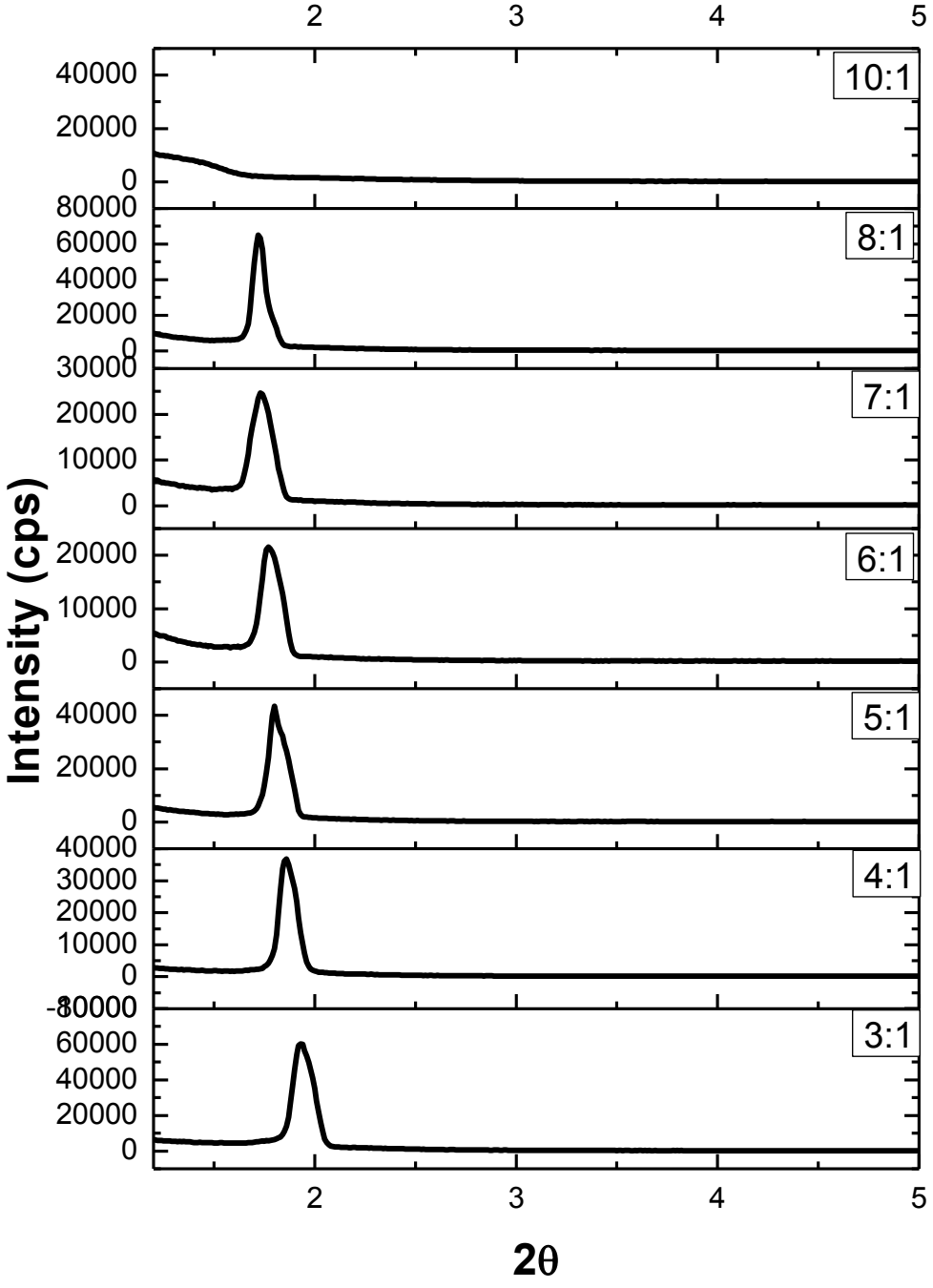

Figure 3.20. XRD patterns of LiI. xH_2O -$C_{12}EO_{10}$ at 24^{o}C, 23% RH

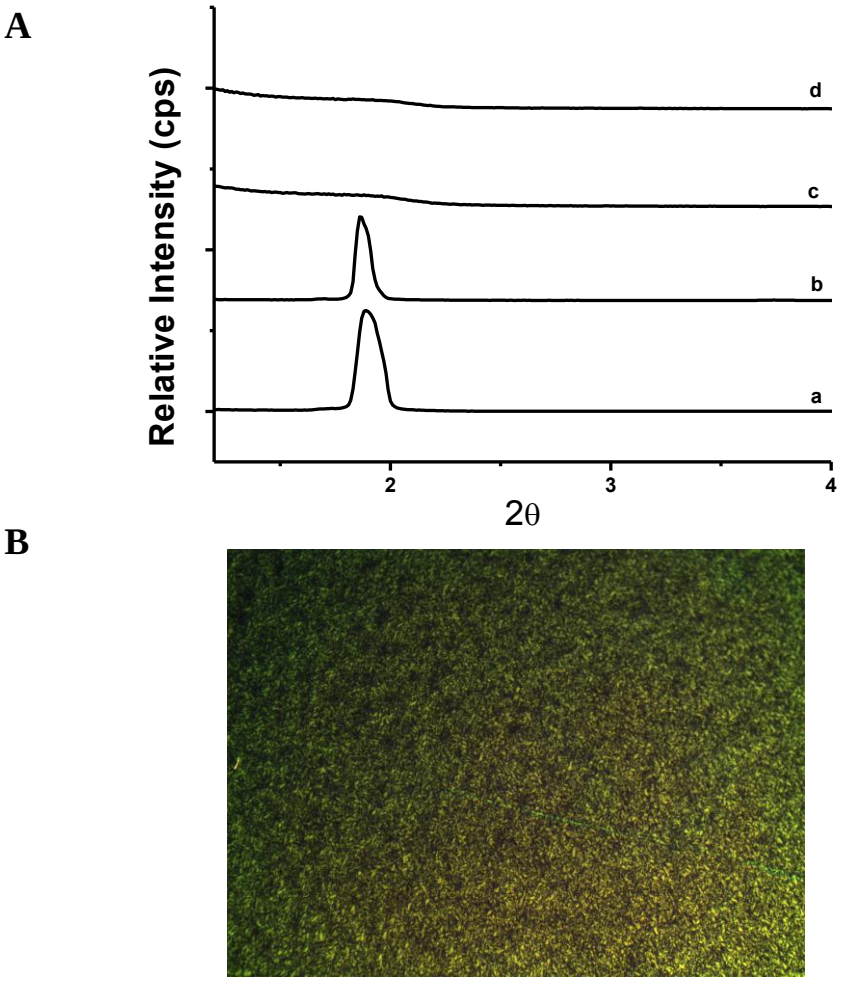

Figure 3.21. (A) XRD patterns of **a)** $1.0LiClO_4$. xH_2O -$C_{18}EO_{10}$ **b)** $2.0LiClO_4$. xH_2O -$C_{18}EO_{10}$ **c)** $1.0LiClO_4$. xH_2O -$C_{12}EO_{10}$ **d)** $2.0LiClO_4.xH_2O$-$C_{12}EO_{10}$ at 24^oC, 23% RH **(B)** POM image of the sample $2.0LiClO_4.xH_2O$-$C_{18}EO_{10}$.

As shown on the **Table 3.1,** the system has a tendency for a $\mathbf{H_1}$ to $\mathbf{I_1}$ phase transition following a Hofmeister series. It is known that the structure breakers are usually loosely hydrated and can penetrate in the vicinity of hydrophobic moieties more as compared to the structure makers, these ions therefore tend to increase the interfacial curvature. From another point of view, the structure breaker ions can also increase the hydration of the ethylene oxide chains, which again results in an increase in the cross sectional area of surfactant molecules and so the interfacial curvature. [42-44]

Table 3.1. Phase behaviour of $LiX.xH_2O$-$C_{12}EO_{10}$ systems at RT and 23-25% RH

Mole ratios →	**2.0**	**3.0**	**4.0**	**5.0**	**6.0**	**7.0**	**8.0**	**10.0**	**12.0**
$LiNO_3$	-	**H**	**H**	**H**	**H**	**H**	-	-	-
LiCl	**H**	**H**	**H**	**H**	**H**	**H**	**H**	**H**	-
LiBr	**H**	**H**	**H+I**	**I**	**I**	**I**	-	-	-
LiI	**H**	**H+I**	**I**	**I**	**I**	-	-	-	-
$LiClO_4$	-	**Cryst.**	-	-	-	-	-	-	-

When the concentration of a structure breaker ion is increased, the repulsive forces between the hydrophilic chains increase and eventually a phase transition to a phase with higher curvature is observed. In this study, the $\mathbf{H_1}$ to $\mathbf{I_1}$ phase transition is observed with the following order of ions $I^->Br^->NO_3^->Cl^-$ - which is the Hofmeister series. In this system, it seems that the Hofmeister series works except for the $LiClO_4$ system. There may be two limitations for the $LiClO_4$ salt. First, it is not as hygroscopic as the other salts, that is, the salt-water interactions are weaker (see FTIR section for more detail). Second, it is possible that the ClO_4^- ion is disrupting the mesophase by making the surfactant molecules too hydrophilic. We therefore used a more hydrophobic surfactant $C_{18}EO_{10}$, in order to balance the higher hydrophilicity in the presence of ClO_4^-. Expectedly, $C_{18}EO_{10}$ surfactant exhibit stable $\mathbf{H_1}$ mesophase with $LiClO_4$ up to 3 salt/surfactant mole ratio, see **Figure 3.21** for the XRD patterns and POM images. The samples crystallize at 3.0 $LiClO_4/C_{18}EO_{10}$ mole ratio.

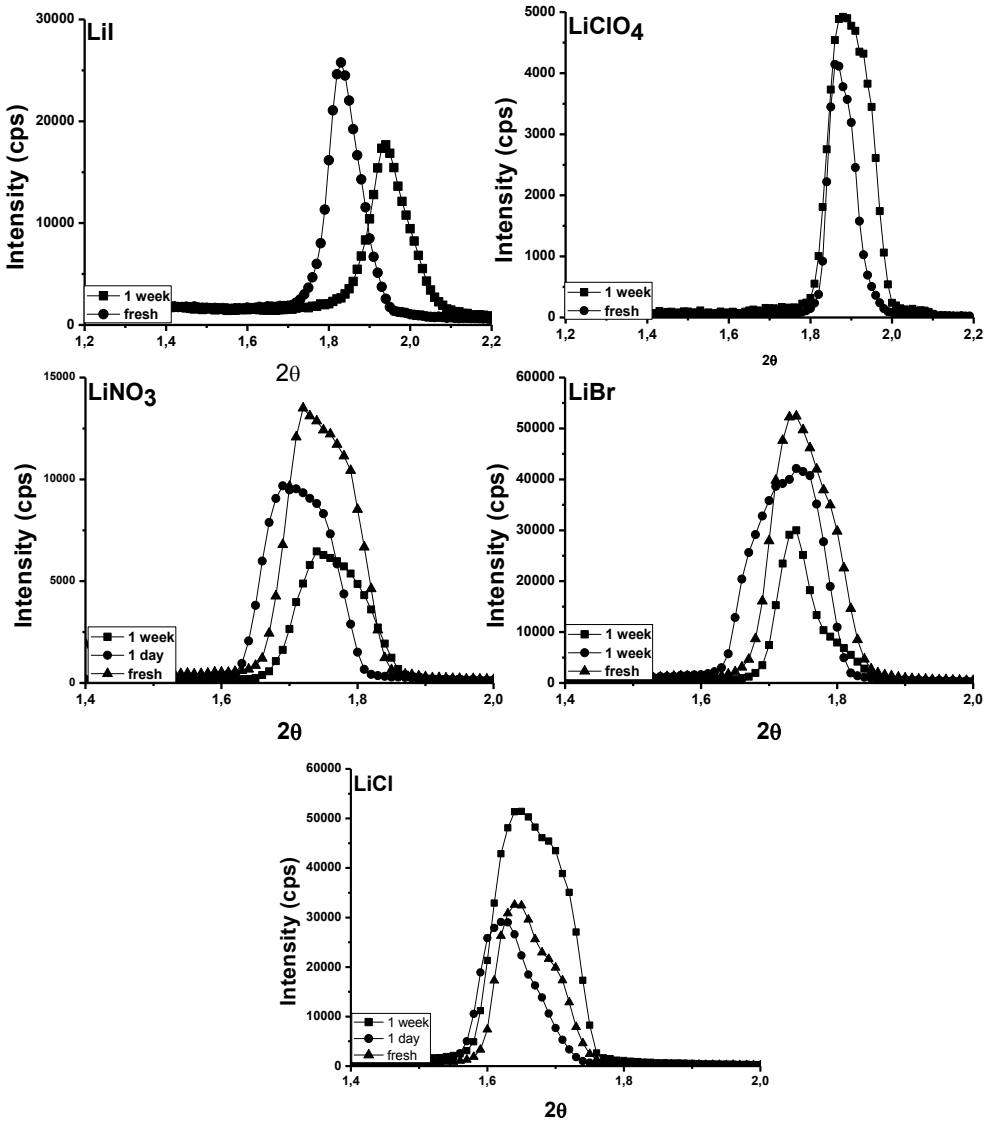

Figure 3.22. XRD patterns of different salt systems at 4.0 salt/surfactant mole ratio except for $LiClO_4$ which is at 2.0 salt/surfactant mole ratio. The measurements were done at 23-25^{o}C and 21-25% RH.

We have also monitored the stability of the samples under open atmosphere. **Figure 3.22** shows the XRD patterns of the fresh and aged salt systems. It is seen on the graphs that the most intense diffractions are maintained in time meaning that the samples are stable. The intensity and the position of the diffraction lines may change in time. The intensity of the line is related to the orientation and the order of the samples. The LLC materials are not rigid oriented materials, therefore fluctuations in orientation and order in time can be expected. The position of the

diffraction lines however is related to the spacing between micellar surfactant domains. The d-spacings can deviate with the salt and water content of the sample. Therefore positions of the diffraction lines may also change with the variations of the temperature and humidity in the atmosphere.

3.2.3. Salt–water-surfactant interactions, IR and Raman spectroscopic studies

In order to have an understanding of the effect of anions on the phase behaviour at the molecular level, FTIR spectra was collected at different salt/$C_{12}EO_{10}$ mole ratios. The experiments were performed at the exact temperature and humidity conditions for all spectra (at 27^{o}C and 22% RH). **Figure 3.23** represents the spectra for increasing mole ratios. Increase in the mole ratio of salt species is acompannied by the increase in the intensity of ν-OH band of water around 3100-3700cm^{-1}. This obviously means that, the amount of water kept in the mesophase is directly related to the salt concentration. In the LLC mesophases, ions are hydrated with the water molecules and excess water evaporates. Therefore, the water species is kept in the mesophase due to its interaction with the salt. The amount of water in the mesophase, is therefore determined by the salt concentration. In addition, this means that most of the water molecules in the mesophase is in the form of hydration waters. Since, other than nitrate and perchlorate anions, the salt species cannot be monitored directly in IR spectra, we will comment mostly on the indirect effect of these salts on the signals of surfactant and water. It is seen that increasing the mole ratio of the salt does not affect the position of the maxima for the ν-OH band. On the other hand, the ν-CO stretching -around 1100 cm^{-1}-of the surfactant head groups is red-shifted in all spectra (except ClO_4^-) due to the increase in the extent of salt-surfactant interactions. Other than these two regions, there is no noticeable difference with increasing salt concentration for all salt systems except $LiClO_4$. At 3.0 salt/surfactant mole ratio, the crystallisation of $LiClO_4$ salt leads to well defined sharp peaks for the ν-OH band and intensification of the ν-CO peak. Note that, the surfactant peaks do not sharpen meaning that the only crystallized species is the salt together with some hydrated water molecules.

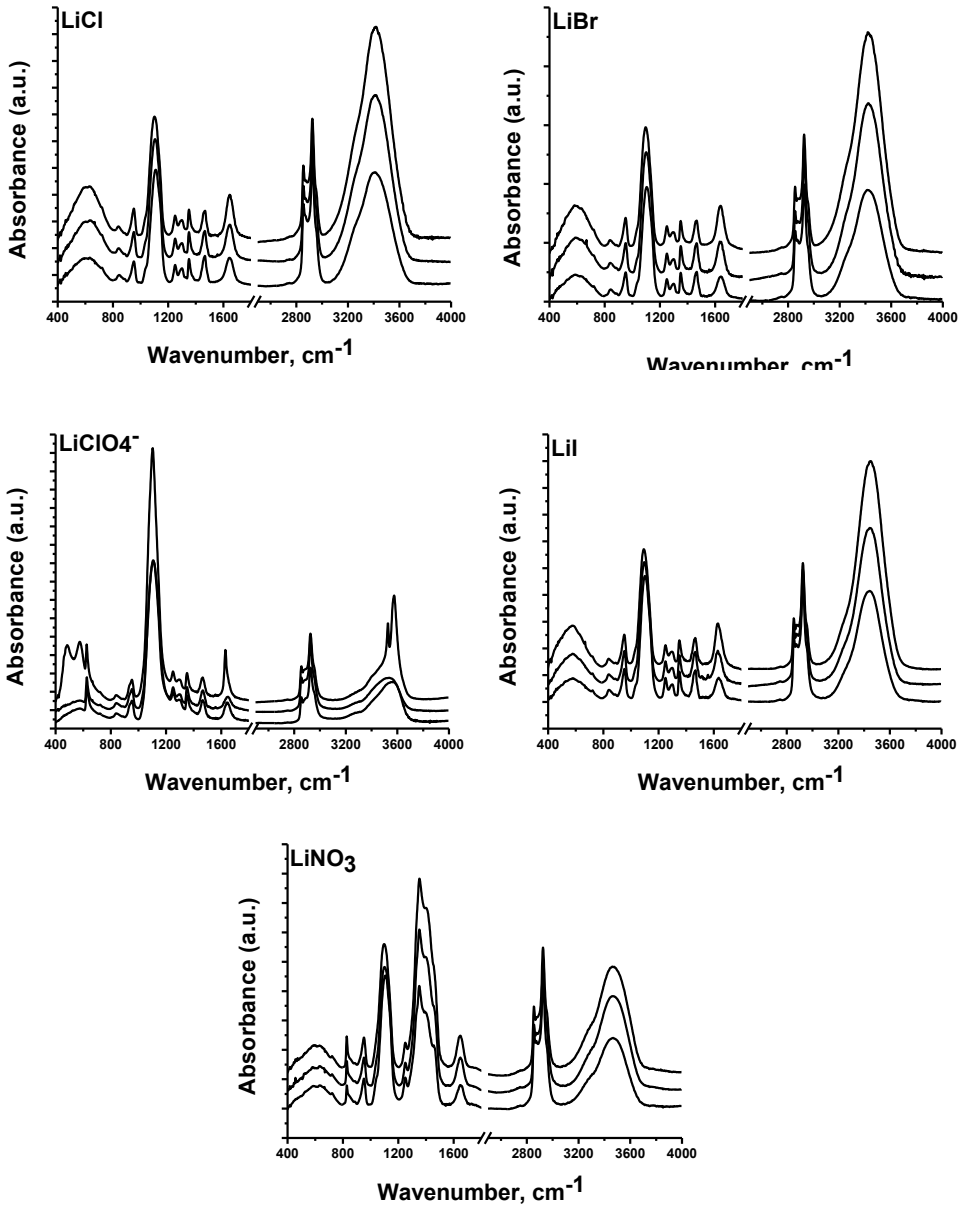

Figure 3.23. FT-IR Spectra of different salt systems at various salt/surfactant mole ratios, from bottom to top 2.0, 3.0, 4.0.

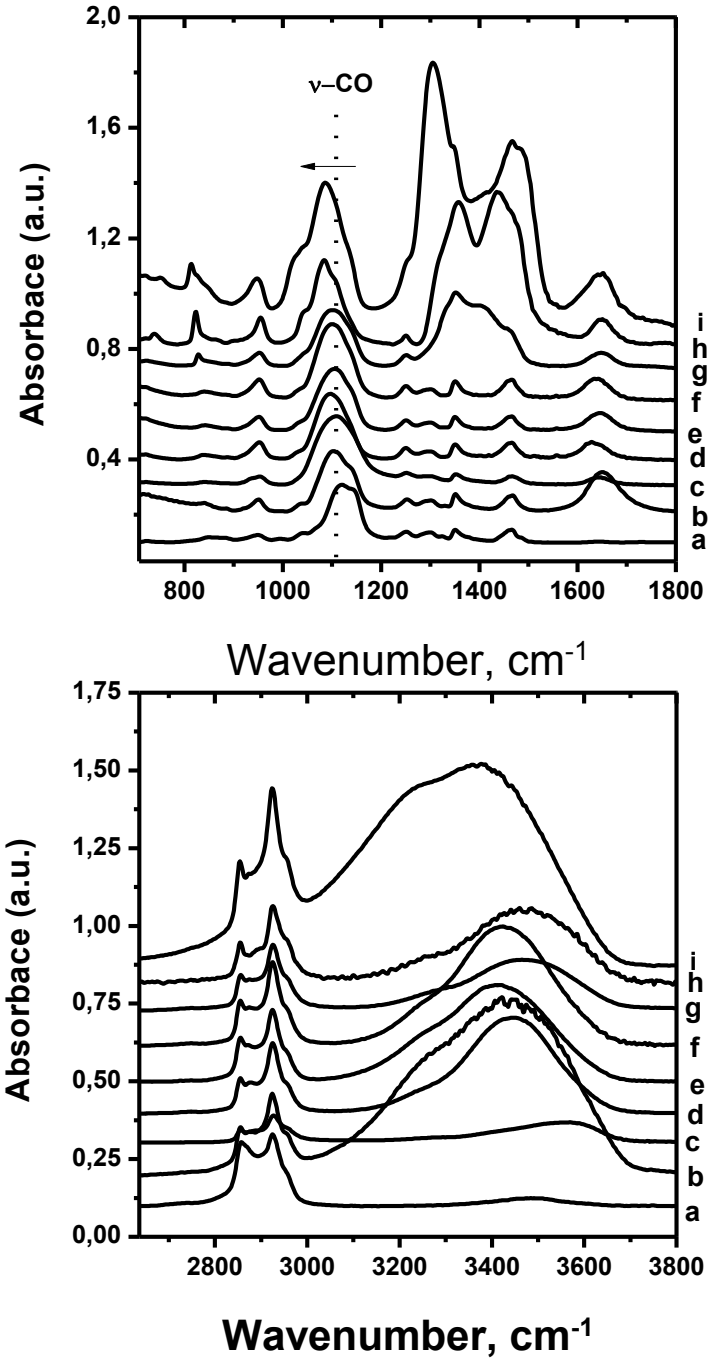

Figure 3.24. FT-IR spectra of **a**) molten $C_{12}EO_{10}$ **b)** $35.0H_2O$-$1.0C_{12}EO_{10}$ **c)** $2.0LiClO_4xH_2O$-$1.0C_{12}EO_{10}$ **d)** $2.0LiI.xH_2O$-$1.0C_{12}EO_{10}$ **e)** $2.0LiCl.xH_2O$-$1.0C_{12}EO_{10}$ **f)** $2.0LiBr.xH_2O$-$1.0C_{12}EO_{10}$ **g)** $2.0LiNO_3.xH_2O$-$1.0C_{12}EO_{10}$ **h)** $2.0Ca(NO_3)_2.xH_2O$-$1.0C_{12}EO_{10}$ and **i)** $2.0[Zn(H_2O)_6](NO_3)_2$-$1.0C_{12}EO_{10}$

We have combined the IR spectra of all Li^+ systems under study, H_2O-$C_{12}EO_{10}$ system, molten $C_{12}EO_{10}$, Zn^{2+} system and Ca^{2+} system (see next chapter for details) in one graph for comparison, see **Figure 3.24**. In the 800-1800 cm^{-1} region, the free nitrate signal at 1400 cm^{-1} splits into two because of the reduction of its symmetry from D_{3h} [50,106] to C_{2v} with its coordination to the metal ion(s). The magnitude of the splitting shows the strength of this interaction. In the Zn^{2+} system, the nitrate ions undergo ligand exchange with the coordinated water molecules and coordinate to the metal center,[50,106] while in the $Ca^{2+}$and Li^+ systems such a strong covalency is not expected. As a result, the antisymmetric ν-(NO_3) stretching at 1400 cm^{-1} splits weakly in these systems. It is also seen in the spectra that the higher charge on the metal ion, red shifts the ν-CO stretching frequency more –as compared to pure $C_{12}EO_{10}$ and H_2O-$C_{12}EO_{10}$ system- indicating that in salt-surfactant systems surfactant-solvent interactions are stronger. The maxima of the ν-CO stretching band of the molten surfactant is around 1200 cm^{-1}. This band shifts to 1103 cm^{-1} in the presence of water (1/1 wt. ratio of $H_2O/C_{12}EO_{10}$) and to 1085 cm^{-1} in divalent metal salt systems. The position of this band does not change significantly in the presence of monovalent salts. It is observed at 1104 cm^{-1}, 1100 cm^{-1}, 1098 cm^{-1}, 1095 cm^{-1} in LiCl, $LiNO_3$, LiBr and LiI systems, respectively. This can be explained by the increasing hydration of the ethylene oxide chains with the addition of more chaotropic ions. Basically, chaotropic ions such as I^- breaks the water structure more and they are also able to penetrate more to the vicinity of core-shell interface. In addition, it shows that the Li^+ ion interacts with the ethylene oxide units mostly through the interaction of hydrated water molecules. The FT-IR data also correlates with the observed phase transitions from $\mathbf{H_1}$ to $\mathbf{I_1}$. The ions which increase the solvent-surfactant interactions make the surfactant more hydrophilic and decrease the onset of $\mathbf{H_1}$ to $\mathbf{I_1}$ transition.

The high energy region of the spectra originates from the ν-CH and ν-OH stretching vibrations of surfactant and water species, respectively. While there is no significant change in the surfactant signals in this region among the samples, the ν-OH stretching bands show differences. In the Zn^{2+} system, due to the presense of coordinated water molecules, the ν-OH stretching band red-shifts significantly as compared to all other systems. The water band in this region can be deconvoluted to four different signals, **Figure 3.25**. The deconvolution was made on the basis of

the shape of the water streching band in mesocrystalline samples, see the next section for details. The low energy signals are related to hydrogen bonded water molecules and coordinated water molecules. The high energy signals are related to ‘’free’’ water molecules.[107,108] In aqueous solutions of structure breaker ions, the intensity of the low energy region decreases due to the disruption of the hydrogen bonding network of water molecules. Similarly in the Li^+ systems, it is seen that the low energy portion of the ν-OH band disappears and the band width gets narrower. In order to compare the effect of different anions on the ν-OH band, one also needs to consider the salt/water mole ratios. It is seen that ClO_4^- system cannot hold much water and NO_3^- system also have lower water content as compared to halide systems. The halide systems however are more or less similar in this respect and the ν-OH band exhibits a similar trend, which can also be found in concentrated electroylte solutions.[107,108] Lastly, it is seen that Ca^{2+} and Li^+ systems almost have the same ν-OH band structure indicating the insignificant effect of the cation on water structuring. This is consistent with the current understanding of the Hofmeister effect that the cations have much less effect than the anions. [33]

The Raman spectra of water, concentrated LiBr solution and LiBr LLC system gives a clearer picture of the above discussion and is shown in **Figure 3.26**. The water band at 3250 cm^{-1} vanishes due to the breakage of hydrogen bonded water structure. Note the similarity between the concentrated solution and LiBr system.

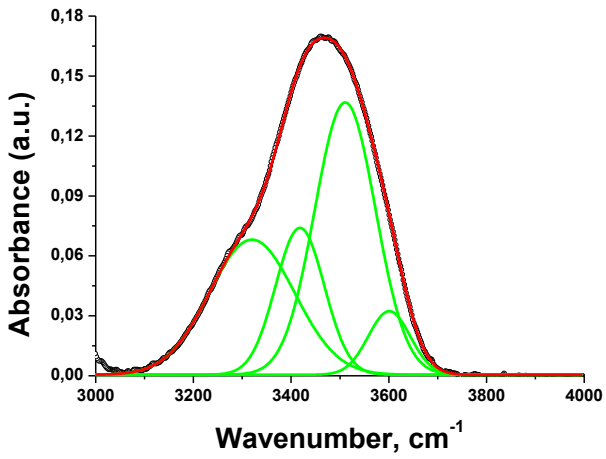

Figure 3.25. Example of the deconvolution of water bands

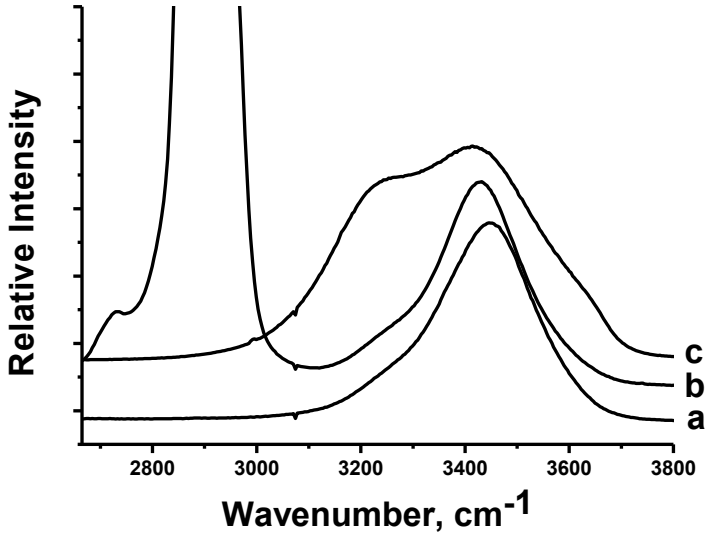

Figure 3.26. Raman spectra of **a)** saturated LiBr solution **b)** LiBr-$C_{12}EO_{10}$-xH_2O at 3.0 salt/ $C_{12}EO_{10}$ mole ratio, and **c)** H_2O.

The lower energy band at 3250 cm^{-1} is related to the ν-OH stretching of hydrogen bonded water molecules. In saturated LiBr solution the water band at 3250 cm^{-1} almost vanishes mostly because of the structure breaker Br^- ion breaks the hydrogen bonding network of water.

The water content of the spin coated samples were investigated using FT-IR spectroscopy. **Figure 3.27A** shows the FT-IR spectra of 3.0$LiNO_3$.x$H_2$0-$C_{12}EO_{10}$, 35.0H_2O-$C_{12}EO_{10}$ and 3.0$LiNO_3$-15.0H_2O-1.0$C_{12}EO_{10}$ samples (numbers indicate the mole ratio of each species). The spectra were normalized by taking the surfactant signals as the reference. The FT-IR spectra of the 35.0H_2O-$C_{12}EO_{10}$ and 3.0$LiNO_3$-15.0H_2O-1.0$C_{12}EO_{10}$ samples were collected by sandwiching them in between Si wafers to avoid water evaporation. The compositions were prepared by mixing required weight for each ingredient and homogenizing in air tight vials. The ν-OH stretching of the water band 3000-3700 cm^{-1} gives a qualitative idea about the water content of the samples. It is seen in **Figure 3.27A** that the amount of water in the sample 3.0$LiNO_3$.xH_2O-$C_{12}EO_{10}$ is lower than 15.0, which means the water/salt mole ratio below 5.0. We avoid making a quantitative determination of the water

content of the mesophases since the extinction coefficients may vary and there may be deviations from the Beer's Law.

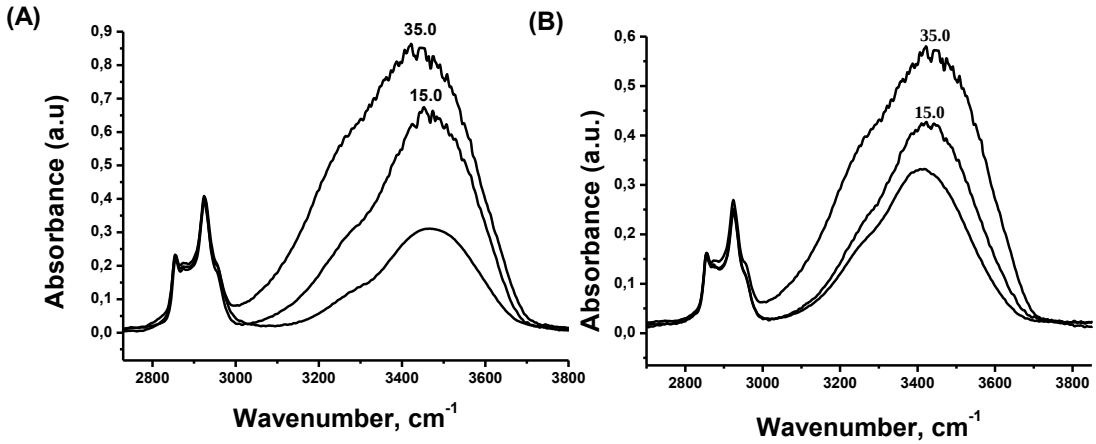

Figure 3.27. FT-IR spectra of **(A)** $3.0LiNO_3.xH_20\text{-}C_{12}EO_{10}$, $35.0H_2O\text{-}C_{12}EO_{10}$ and $3.0LiNO_3\text{-}15.0H_2O\text{-}1.0C_{12}EO_{10}$, from bottom to top and **(B)** $3.0LiCl.xH_2O\text{-}C_{12}EO_{10}$, $35.0H_2O\text{-}C_{12}EO_{10}$ and $3.0LiCl\text{-}15.0H_2O\text{-}1.0C_{12}EO_{10}$ from bottom to top. For both $3.0LiNO_3.xH_2O\text{-}C_{12}EO_{10}$ and $3.0LiCl.xH_2O\text{-}C_{12}EO_{10}$ the atmospheric conditions were 27^oC and 24% RH

The same experiment was also performed for the LiCl system. **Figure 3.27B** shows the FT-IR spectra of $3.0LiCl.xH_20\text{-}C_{12}EO_{10}$, $35.0H_2O\text{-}C_{12}EO_{10}$ and $3.0LiCl\text{-}15.0H_2O\text{-}1.0C_{12}EO_{10}$ samples. It is again seen that the water content of the $3.0LiCl.xH_20\text{-}C_{12}EO_{10}$ system is lower than 15.0. However, it is a little bit higher than the $LiNO_3$ system. Overall these experiments indicate that the spin coated samples which are left open to atmosphere are highly concentrated in terms of water/salt mole ratio.

3.2.4. A new phase in the $LiI.xH_2O\text{-}C_{12}EO_{10}$ system.

In the $LiI.xH_2O\text{-}C_{12}EO_{10}$ system, we have observed an interesting phase transition from LLC mesophase to a mesocrystalline complex phase, which gives diffractions at both small and high angles – similar to XRD patterns of zeolites. The FTIR spectrum of the sample with 4.0 salt/surfactant mole ratio shows significant differences after transforming into a mesocrystalline phase, **Figure 3.28A**, **B** and **C**.

Some of the surfactant signals split into its components and new peaks arise and on overall all of the peaks get sharper. In **Figure 3.28A**, it is seen that two new peaks arise at 1274 and 1339 cm^{-1}. The former is previously assigned as the CH_2 twisting mode of trans C-O bond and the latter is assigned as CH_2 rocking mode of trans C-C bond[66] (in the ethylene oxide chain), see Chapter 4 for more detail. This means that, upon phase transformation the surfactant molecules extend. This extension also corralates with the change in the XRD patterns, see below.

The changes in the surfactant signals cannot be attributed to surfactant crystals, which has a very different spectrum, see **Figure 3.28D**. Note that, in the crystalline surfactant, the peaks related to the ν-CO stretching of the ethoxy groups (1000-1200 cm^{-1}) are significantly blue-shifted.

Upon the mesocrystalline phase transformation, the sample does not loose water molecules. The broad ν-OH stretching band also gets sharper and four different water peaks becomes visible upon phase transformation, **Figure 3.28B**. In the case of a salt crystallisation, salt-water-surfactant systems does not show such drastics chages related to surfactant signals. For instance, **Figure 3.11** shows the FTIR spectrum of the $3.0LiClO_4.xH_2O$-$C_{12}EO_{10}$ sample where the $LiClO_4$ salt has crystallized out. Notice that, in the $LiClO_4$ sample, crystallization of the salt does not affect the surfactant signals. Moreover, the water amount in the samples, where $LiClO_4$ crystallization occurs is very low and the sharp signals on top of the ν-OH stretching band (related to the cocrystallized water molecules) emerge.

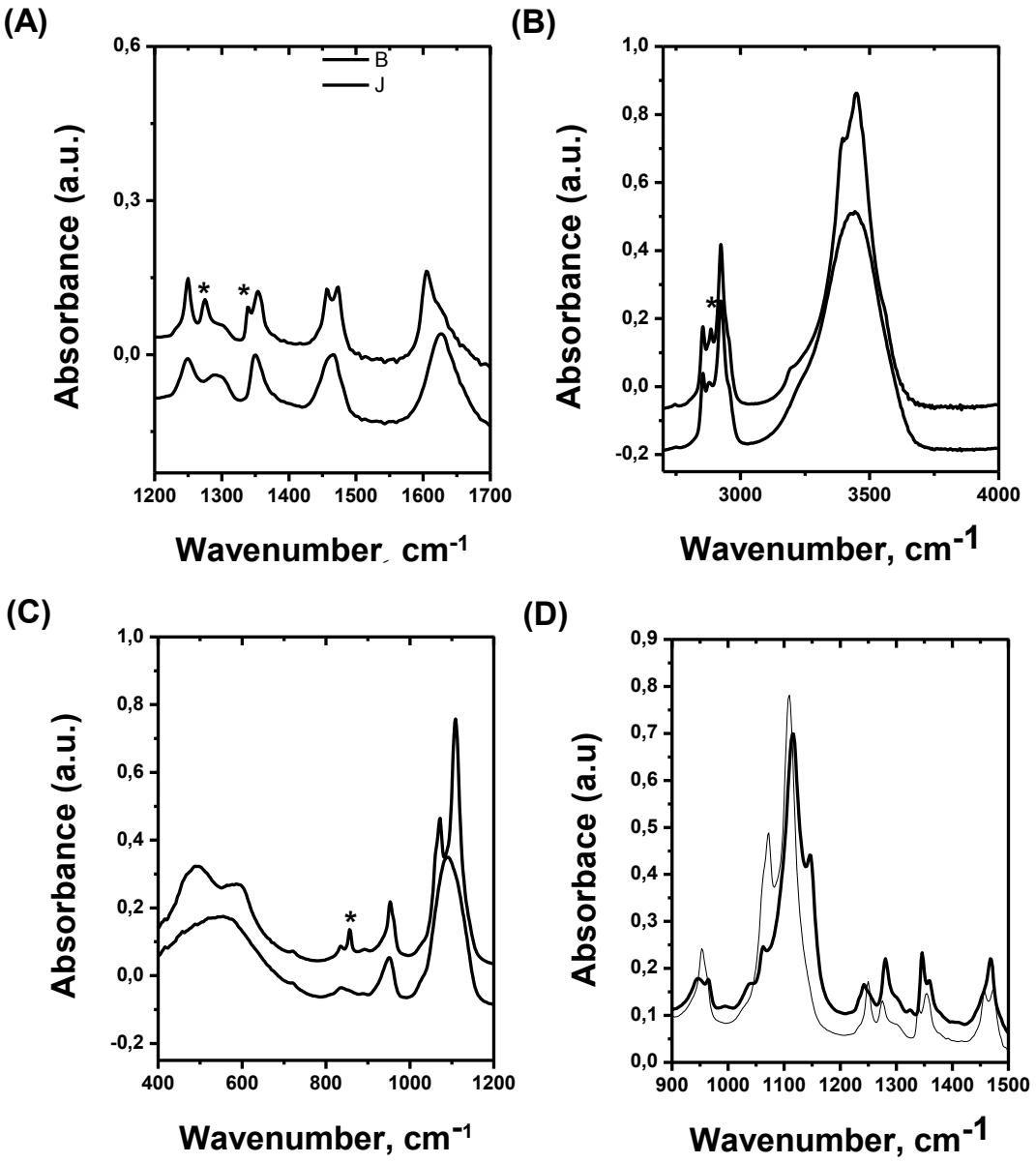

Figure 3.28. The **(A)**, **(B)** and **(C)** shows the FT-IR spectra of LC phase (**bottom**) and mesostructured complex phase (**top**) The sample has 4.0 LiI/$C_{12}EO_{10}$ mole ratio. The spectra in **(D)** belongs to the crystalline $C_{12}EO_{10}$ (thick line) and the mesocrystalline phase (thin line)

There is also another peak arising at 851cm^{-1},which we were not able to assing yet. Overall the FT-IR spectra indicate that the surfactant, water and salt species form a complex together.

Figure 3.29 shows the XRD pattens of the 4.0LiI.xH_2O-1.0$C_{12}EO_{10}$ sample with aging. The patterns show a phase transition from a cubic LLC phase to a mesocrystalline complex phase (from botttom to top). The fresh sample has two

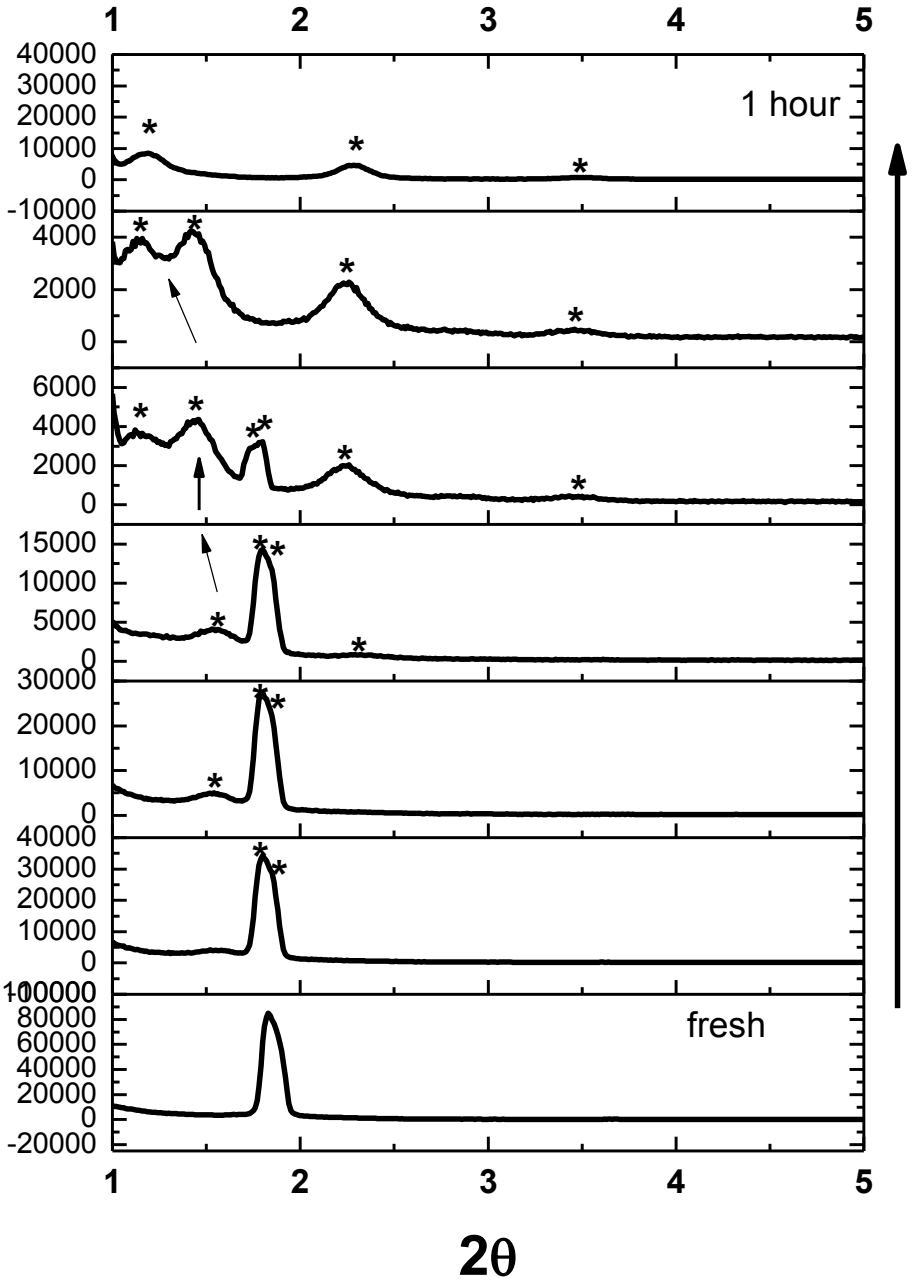

Figure 3.29. XRD pattern indicating the transiton from LLC mesophase to mesocrystalline phase. The sample has 4.0 LiI/$C_{12}EO_{10}$ mole ratio.

diffraction lines around 1.8 degree. However, after a few minutes, a broad diffraction line starts to emerge at 1.55 degree while the intensity of the previous diffraction lines decrease. The phase transition to the mesostructured complex phase, with an interlayer spacing of 74.77 Å, is almost complete in an hour, see the top diffraction pattern in **Figure 3.29**. The structure of the mesocrystalline phase may be lamellar because the d-spacing increases drastically and FT-IR data indicate an increase in the trans population for both C-O and C-C bonds.

The mesostructured complex phase also has broader and weaker diffraction as compared to the cubic phase. The high angle region of mesocrystalline phase is shown in **Figure 3.30**. At high angles there are four diffraction lines (as depicted in the image), which are broad and cannot be assigned to any LiI or $LiI.xH_2O$ salt crystals. These lines can originate from the distances between the solid-like surfactant entities in mesocrystals.

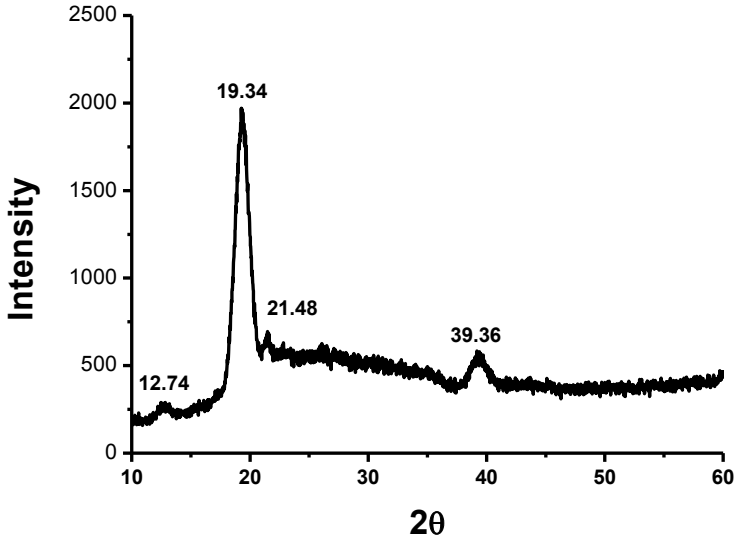

Figure 3.30. XRD pattern indicating the transiton from LLC mesophase to mesocrystalline phase at high angles. The sample has 4.0 $LiI/C_{12}EO_{10}$ mole ratio.

Figure 3.31 displays POM images of the same sample upon phase transformation. The sample is birefringent and the POM images show sharp edged textures, which are unusual for the LLC mesophases. However, inside these crystal shaped birefringent domains, there is a sponge like texture (not characteristic for normal crystals), which rules out the possibility that the domains originate from the

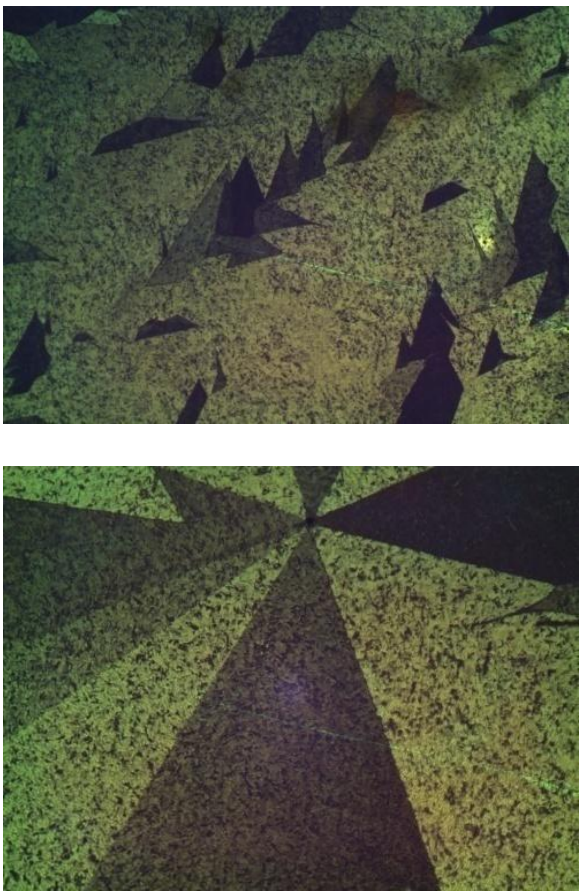

Figure 3.31. POM images of $LiI.xH_2O$-$C_{12}EO_{10}$ system at 4.0 salt/$C_{12}EO_{10}$ mole ratio.

salt crystals. **Figure 3.31** also shows another POM image in which some well defined polygons stepped out of the sample leaving their holes behind. Such cracking is also indicative of a solid-like behavior, rather than a gel phase. Overall our observations indicate that the mesocrystals have intermediate properties in between a solid and LC.

The formation of mesocrystalline phase is strongly dependent on the temperature and relative humidity in the air. The mesocrystals reconstruct to a LLC phase above 25 % RH at RT. The samples, which have higher salt concentration have a higher tendency to form the complex phase. For instance, among 3.0 and 8.0 salt/surfactant mole ratio, the complex phase is observed in the 5.0-8.0 mole ratios at 20% RH, and 3.0-5.0 at 15 % RH both at RT. We also inspected the presence of

a similar behavior by changing the counter-ion by Cl^-, Br^-, and NO_3^-. In the light of the information that low humidity is a prerequest for the mesocrystal formation, we investigated other salt systems under POM in a drybox, between 0^o to 50^oC. However, we did not observe any indication of such a transition in other salt systems. On the other hand, detailed investigations under varying humidities and temperatures should be carried out in order to reach a valid conclusion. Further investigations are needed to improve the understanding of this novel phase at the molecular level. The samples that response to humidity by changing the birefringence may also be interesting for their application as humidity sensors. We believe that this new phase is another indication of the richness and potentiality of the concentrated salt-surfactant LLC mesophases which are almost unexplored, and is another proof of the effect of salt in concentrated systems.

3.3. $CaX_2.xH_2O$-$C_{12}EO_{10}$ Systems

We extended our studies to include the alkaline earth family. As example systems, the LLC properties of the $CaCl_2$ and $Ca(NO_3)_2$ salts with the $C_{12}EO_{10}$ surfactant were investigated. The Ca^{2+} salts are especially important in the synthesis of bioactive and biocompatible materials such as hydroxyapatite, $Ca_{10}(PO)_4)_6(OH)_2$, and bioactive glass, CaO-P_2O_5-SiO_2-MO. Hydroxyapatite is the major component of natural bone and is used in bone cavity fillings and implants.[109-111] Bioactive glasses can chemically bind to the inorganic part of the natural bone, hydroxycarbonate apatite.[112] In addition, the porosity in these materials are important for their bioactivities, and there is an extensive research in the synthesis of mesoporous hydroxyapatite derivatives and bioactive glasses.[113-117] The LLC phases of Ca^{2+} systems can serve as a template for the synthesis of these materials. In this chapter, we will focus on the $CaCl_2.xH_2O$-$C_{12}EO_{10}$ system because of its interesting transition to a mesostructured solid complex similar to $LiI.xH_2O$-$C_{12}EO_{10}$ mesophases. The diffraction patterns and POM images of the $CaNO_3xH_2O$-$C_{12}EO_{10}$ system can be found in the related Appendix and will not be discussed any further.

3.3.1. Fresh samples of the $CaCl_2.xH_2O$-$C_{12}EO_{10}$ system

The samples of $CaCl_2.xH_2O$-$C_{12}EO_{10}$ system were prepared in solution as described in the experimental section. The samples were then spin coated either on glass slides or silicon wafers -depending on the characterization technique- and investigated under ambient conditions. Therefore the water concentration in the

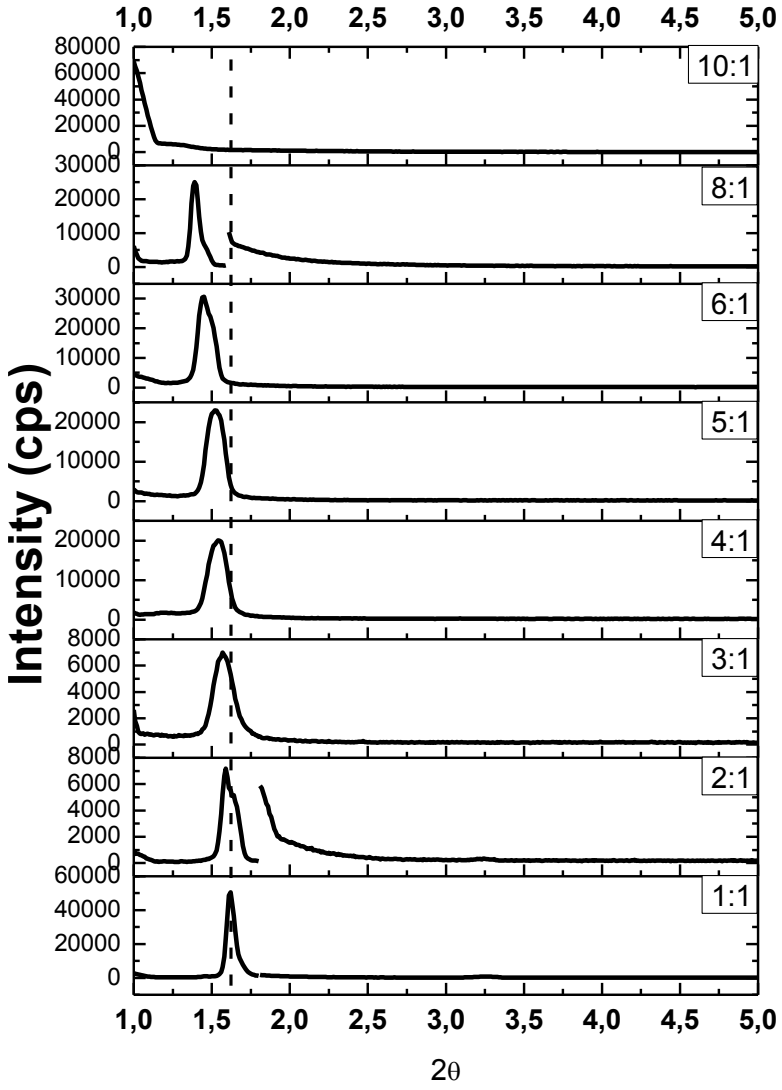

Figure 3.32. XRD patterns of $CaCl_2.xH_2O$ -$C_{12}EO_{10}$ with increasing salt/surfactant mole ratios (as shown in the plots) and corresponding POM images on the right.

samples again varies with the relative humidity of the atmosphere. The samples show LLC mesophases between 1.0 and 8.0 mole ratios of the $CaCl_2/C_{12}EO_{10}$.

Figure 3.32 shows the XRD patterns of the samples with different mole ratios collected at 24^{o}C and 23% RH and the corresponding POM images. The XRD patterns of the samples consist of 2 or 3 diffraction lines at most. Samples with 1.0 and 2.0 salt/surfactant mole ratio have 3 diffraction lines at 55.86 Å (1.63^{o}, 2θ)-52.52Å (1.68, 2θ)– 27.94 Å (3.25, 2θ) and (1.61, 2θ) -(1.67,2θ)-(3.25,2θ), respectively. These diffraction lines can be indexed to a rectangular (hexagonal) columnar phase however as mentioned in section 3.2 the second diffraction line may correspond to water poor layers on the surface of the samples. Other samples give only 1 diffraction line except the samples of 6.0 and 8.0 mole ratios, which has two diffraction lines again at 61.29 Å, 59.63 Å and 63.50 Å, 61.3 Å, respectively. Additional diffraction lines are required to correctly assign the stucture of the mesophase at these concentrations. Nevertheless, the POM images at high salt/surfactant mole ratios provide dark images, therefore the mesophases above 3.0 salt/surfactant mole ratio are assigned as cubic.

The XRD patterns at different concentrations show that the major diffraction line below 2^{o}, *2θ,* shifts to smaller angles with increasing salt concentration in the media. The first diffraction line corresponds to 55.86 Å for the 1.0 salt/surfactant mole ratio and shifts to 63.50 Å in the 8.0 salt/surfactant mole ratios. Note however that we avoid direct comparison of the first diffraction lines between different structures. Nevertheless, the trend is also persistent along both hexagonal and cubic phase. This indicates that additional salt ions increases the distances between the adjacent domains as in $CaCl_2.xH_2O$-$C_{12}EO_{10}$ mesophases. Increasing the salt concentration also results in a phase transition from $\mathbf{H_1}$ to $\mathbf{I_1}$ phase. The intensity of the first diffraction lines changes with salt/surfactant mole ratio. In **Figure 3.32**, the samples with 1.0, 2.0, and 8.0 salt/surfactant mole ratios are blocked with a copper plate. The copper plate reduces the X-ray beam intensity 10 times. Therefore these samples are much more ordered or have larger ordered domains as compared to others. Indeed, the samples show crack patterns at all other mole ratios. This may be related to the reduction of the intensity of the diffraction lines in other samples.

3.3.2. Aged samples of the $CaCl_2.xH_2O$ -$C_{12}EO_{10}$ system

When the spin coated samples, which were prepared from 5 ml homogeneous solutions of $CaCl_2.xH_2O$-$C_{12}EO_{10}$ mixtures, were aged under ambient conditions, a mesocrystalline phase transformation occurs similar to $LiI.xH_2O$-$C_{12}EO_{10}$ system. **Figure 3.33** shows the POM images gathered during the crystallisation. **Figure 3.33 (A)** shows the initiation of a crystal nucleating from a defect site on the glass surface. **Figure 3.33 (B)** shows the growth of these crystals from the edges of the glass slide. **Figure 3.33 (A)** is the fresh sample's appeareance under POM, having crack patterns. Note that, after crystallisation the crack pattern is preserved, **Figure 3.33 (D)**. **Figure 3.34** shows the shapes of the crystals at different concentrations.

The XRD patterns of the aged samples at small and high angles are shown in **Figure 3.35(A)** and (**B)**, respectively. Note that at high angles, there are very limited number of diffraction lines with very weak intensities. The first diffraction line at high angle varies with composition from 12.5^o to 13.3^o, and is absent at 2.0 and 4.0 $CaCl_2/C_{12}EO_{10}$ mole ratios. The other two diffraction lines were only observed for the sample with a 3.0 mole ratio at 16.0^o and 22.4^o. At the same time, the small angle region shows significant changes with aging. The diffraction lines gets broader and weaker in the aged samples similar to the $LiX.xH_2O$-$C_{12}EO_{10}$ systems. The most ordered sample, 2.0 $CaCl_2/C_{12}EO_{10}$ mole ratio, give two diffraction lines corresponding to 66.84 Å and 33.42 Å d-spacings. At high $CaCl_2/C_{12}EO_{10}$ mole ratios, the d-spacing can go up to 69.47 Å, which is unusually large for the salt-$C_{12}EO_{10}$ systems. In general, the d-spacing of the (100) diffraction line is at most 63.40 Å with the addition of extensive amounts of charged surfactants such as CTAB or SDS in the $[Zn(H_2O)_6](NO_3)_2$-$C_{12}EO_{10}$ systems.[73] From the XRD data it can be deduced that the crystallization leads to a more swollen mesophases- mesocrystals. The lack of crystalline diffraction lines related to $CaCl_2$ and its hydrated derivatives indicate that the crystalline shapes are related to the mesostrucures. A few and weak diffractions at high angles may be related to the ordered alkyl and ethylene oxide chains. The FT-IR spectra also support these views (see in the next section).

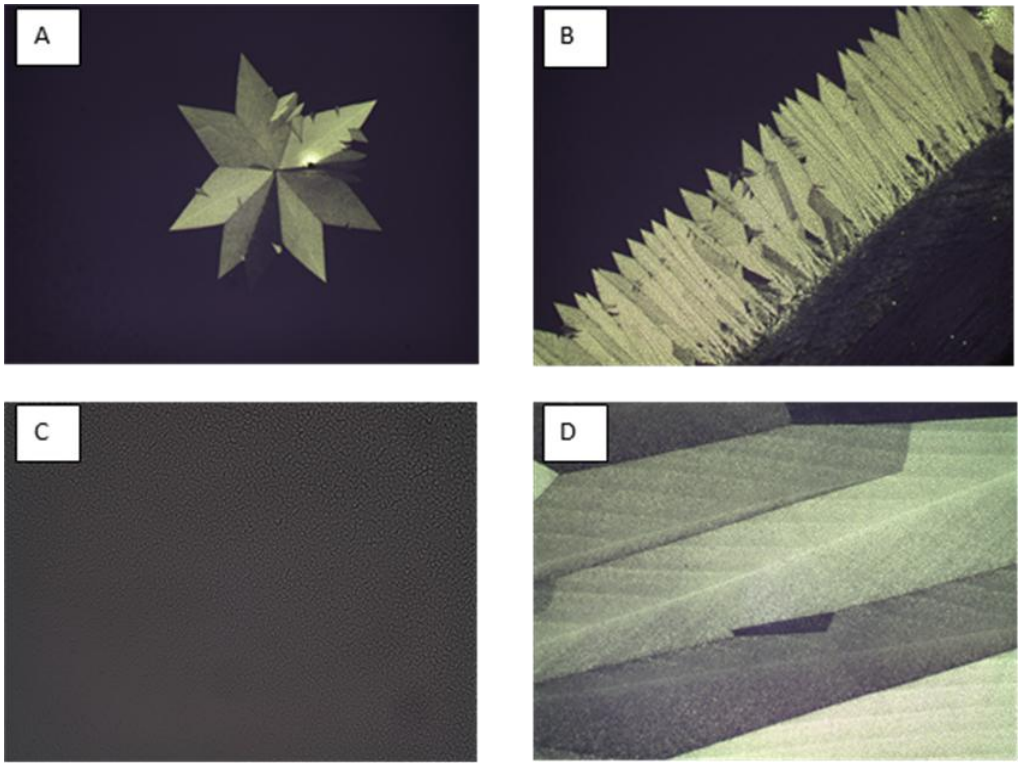

Figure 3.33. POM images of the crystallization process of $CaCl_2.xH_2O$ -$C_{12}EO_{10}$ samples. **A)** growth of a crystal from a defect site **B**) growth from the edge of the sample **C)** fresh sample **D)** aged sample

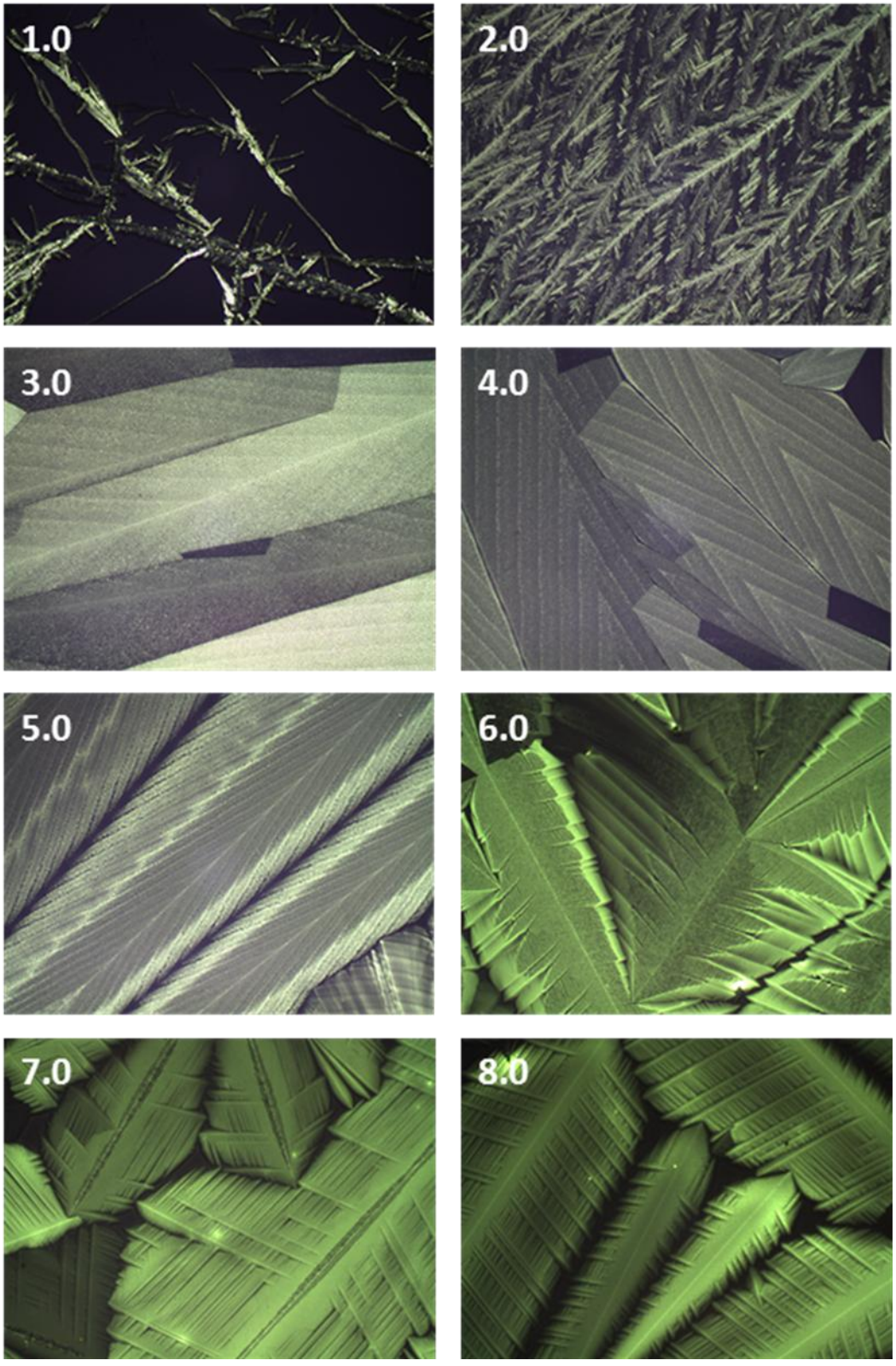

Figure 3.34. POM images of aged samples at different $CaCl_2/C_{12}EO_{10}$ mole ratios.

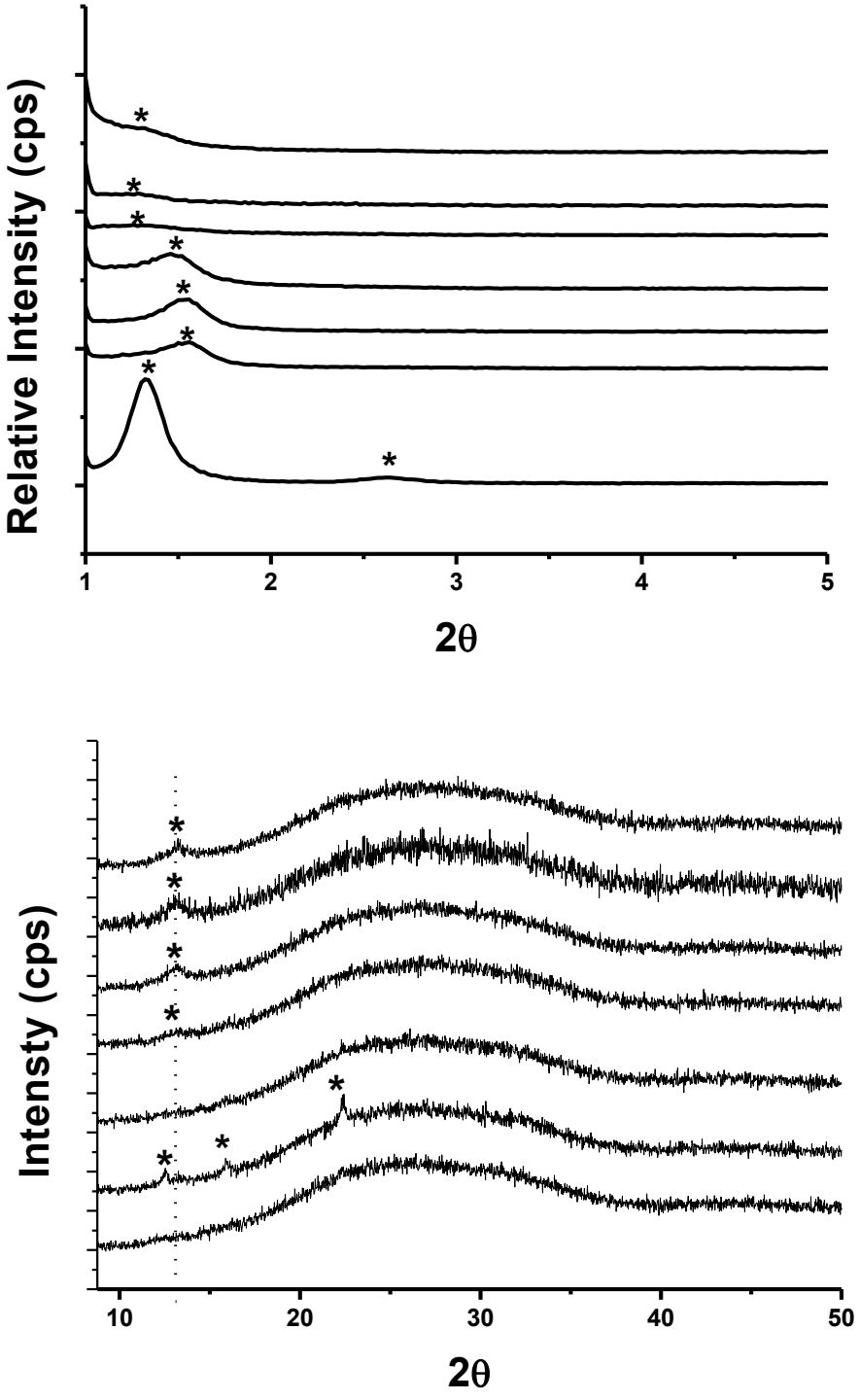

Figure 3.35. XRD patterns of aged samples with crystal like textures under POM. From bottom to up: 1.0, 2.0, 3.0, 4.0 , 5.0 , 6.0, 8.0 and 10.0 $CaCl_2$/ $C_{12}EO_{10}$ mole ratios * marks the visible diffraction lines.

3.3.3. The FT-IR studies of the $CaCl_2.xH_2O$ -$C_{12}EO_{10}$ mesophases

In order to clarify our observations on the phase transition and crystallization we have performed FT-IR spectroscopic measurements at various concentrations and also during the aging process. **Figure 3.36** represent the FT-IR spectra of fresh samples between 1.0 and 5.0 $CaCl_2$/ $C_{12}EO_{10}$ mole ratios. There is a decreasing trend in the ν-CO stretching frequency of the ethoxy backbone with increasing salt concentration, indicating stronger salt-surfactant interactions. The intensity of the water bands at 3000-3700 cm^{-1} region increase with increasing salt concentration. This is also expected in the light of the behavior of alkali salt-surfactant systems. This means that water molecules are mostly in the hydrated form. In spin coated fresh samples the water content was found to be slightly higher (5-7 water/salt) than to Li^+ systems according to our crude approximations based on the relative absorbance of the ν-OH bands to the surfactant peaks. This means that the spin coated samples are highly concentrated in terms of salt/water ratio.

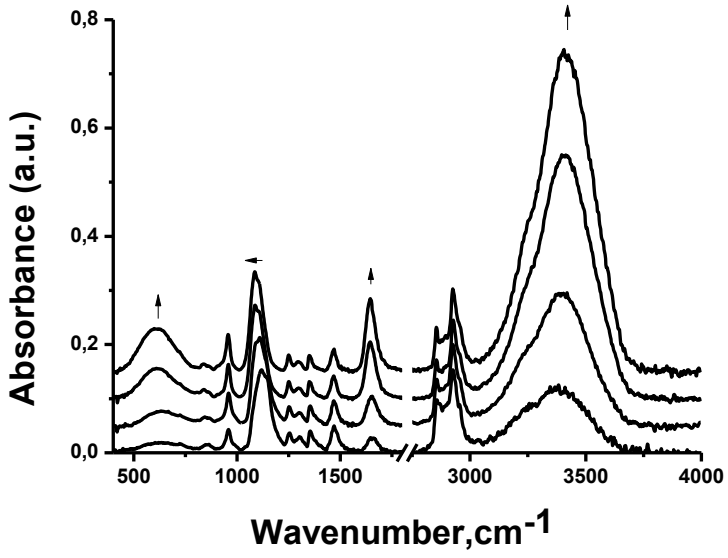

Figure 3.36. FT-IR spectra of $CaCl_2.xH_2O$-$C_{12}EO_{10}$ mesophases at following $CaCl_2/C_{12}EO_{10}$ mole ratios: 1.0, 2.0, 4.0 and 5.0.

As mentioned in earlier section 3.2, the position of the ν-CO stretching is close to the transition metal salt-surfactant systems. On the other hand, the water

bands at 3000-3700 cm^{-1} are found to be at significantly higher wavenumbers due to the lack of covalent coordination of water molecules to the metal center.

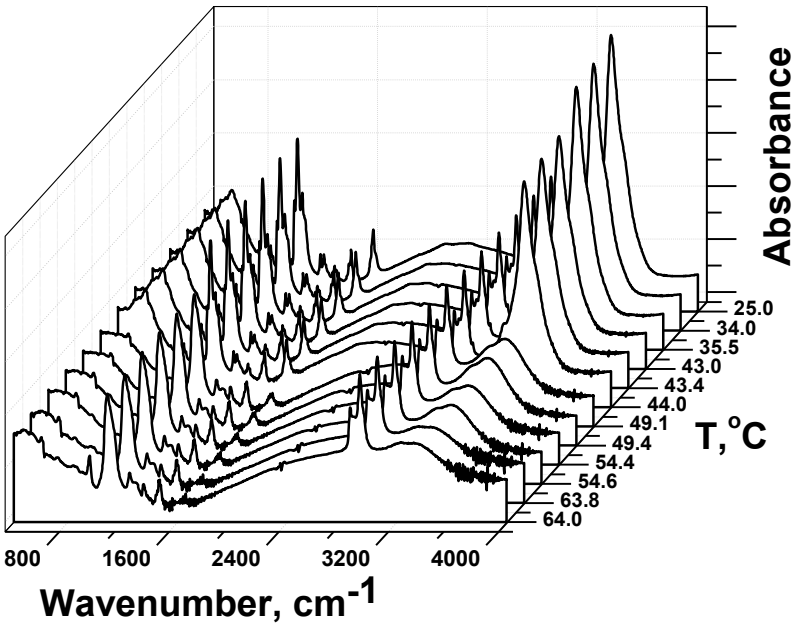

Figure 3.37. FT-IR spectra of 2.0 $CaCl_2/C_{12}EO_{10}$ mole ratio sample during the heating process.

We have followed the stability of the crystals with respect to temperature and humidity. All the aged (crystallized) samples melt at 48°C and all of them –except 2.0 mole ratio- melt at 55% RH at RT. The 2.0 mole ratio sample melts at 60% RH at RT. **Figure 3.37** shows the results of the FT-IR spectra of a crystallized sample of 2.0 $CaCl_2/C_{12}EO_{10}$ mole ratio at various temperatures. Note that the fresh and aged samples have significant differences almost in every region in the spectra. The aged samples have sharp and distinct peaks indicating a solidification of both surfactant and water. Note also that the IR spectrum of crystalline $C_{12}EO_{10}$ is quite different than the aged samples (see Appendix) and especially the ν-CO peaks at 1085 cm^{-1} indicates a strong salt-surfactant interaction. It is seen that during the heating process a sudden change occurs at 49°C. The crystalline water signals at 3100-3700 cm^{-1} broadens together with the surfactant signals. The melting is reversible and the spectral change during cooling is much smoother and allows better monitoring. Therefore we will establish our comments on this experiment

during the cooling process. Note also that the spectra of the aged sample and the spectra of the sample after the cooling process is exactly the same. This allows us monitoring the changes in the spectra at shorter times and lowers the effect of humidity fluctuations during the experiment. In order to simplify the discussion, the spectrum has been divided to four different spectral regions, **2800-3700** cm^{-1}, **1400-1200** cm^{-1}, **1200-1000** cm^{-1}, and **1000-750** cm^{-1}.

3.3.3.1. 2800-3700 cm^{-1} region

This region is occupied by the ν-CH stretchings of the alkyl and ethoxy methylenes, at 2800-3000 cm^{-1}, and the broad water band, between 3000 and 3600 cm^{-1}, **Figure 3.38**. The aged (cooled) sample has distinct and sharp peaks in the water region. There is a relatively sharp ν-OH signal at 3363 cm^{-1}, a shoulder at 3445 cm^{-1} and a small peak at 3212 cm^{-1}. These well defined structures in the water signals indicate the presence of crystalline-like water molecules in the mesocrystals.

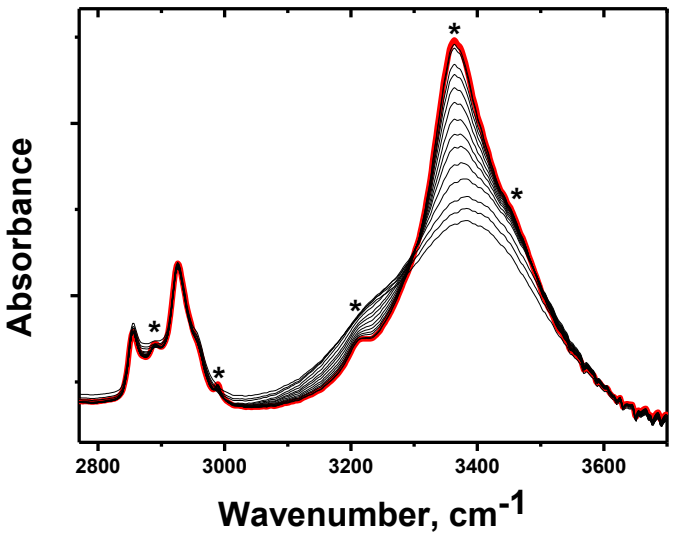

Figure 3.38. FT-IR spectra during the cooling process of 2.0 $CaCl_2/C_{12}EO_{10}$ mole ratio sample. The spectrum in red belongs to the final spectrum of the mesocrystalline phase.

In the 2800-3000 cm^{-1} region the intensity of the peak at 2889 cm^{-1} increases with crystallization. This peak was assigned to ethoxy methylenes[66] and its intensity increases with the formation of LLC phases in transition metal salt – surfactant systems. There is also a new peak emerging at 2989 cm^{-1} in this region, which may indicate the presence of dangling C-H bonds or very acidic O-H bonds. We have prepared samples with D_2O in order to elucidate the origin of this peak. However the water molecules from the air immediately replaces the D_2O molecules and characterisation without a D_2O rich atmosphere seems impossible.

3.3.3.2. 1400-1200 cm^{-1} region

This spectral region is mostly occupied by the peaks due to C-H and C-C bonds and gives important information about the conformation of the ethylene oxide backbone. **Figure 3.39** shows the gauche and trans conformations of C-C and C-O bonds. In the crystalline state, the POE has a helical structure due to the presence of trans(**T**)-gauche(**G**)-trans(**T**) conformation along the -O-CH_2-CH_2-O- segment. Spectral studies on POE+water mixtures show that the C-C bond prefers **G** conformation with increasing water concentration.[118] The C-O bond on the other hand has not a significant preference for the **G** conformation with increasing water concentration. A similar behavior is also observed for the transition metal salt-$C_{12}EO_{10}$ systems. In transition metal salt-$C_{12}EO_{10}$ systems, the ethlylene oxide chains have a higher preference for the **TGT** sequence along the -O-CH_2-CH_2-O- segments as compared to H_2O-$C_{12}EO_{10}$ systems.[66] The conformational differences were attributed to the stronger salt-surfactant interactions via stronger hydrogen bonding arising from coordinated water molecules. The key bands in the 1400-1200 cm^{-1} region are the CH_2 wagging mode for the C-C bond and the CH_2 twisting mode for the C-O bond.[118,119] The **G** conformer was assigned to the 1355-1350 cm^{-1} region and the **T** conformer was assigned to 1335-1325 cm^{-1} region for the C-C bond.[118] For the C-O bond, the **G** conformer was observed at 1310-1290 cm^{-1} and the **T** conformer was observed at 1295-1270 cm^{-1}.[119]

The FT-IR spectra in this region show significant changes together with many isosbestic points during aging. It is seen that the signal at 1350 cm^{-1}, which was assigned to the **G** conformer of the C-C bond[66] looses intensity in the crystallized

phase. While another signal at 1334 cm^{-1} which can be assigned to the **T** conformer of the C-C bond increases. At the same time, the intensity of the **G** conformer of the C-O bond at 1301 cm^{-1} decrease while the signal related to the **T** conformer of this band raises sharply at 1271 cm^{-1} together with a shoulder on the high energy. Both changes indicate that there is a significant increase towards the **T** conformer for both C-C and C-O bonds. However the signals related to **G** conformers does not disappear completely and this means that the ethylene oxide chains are not fully extended.

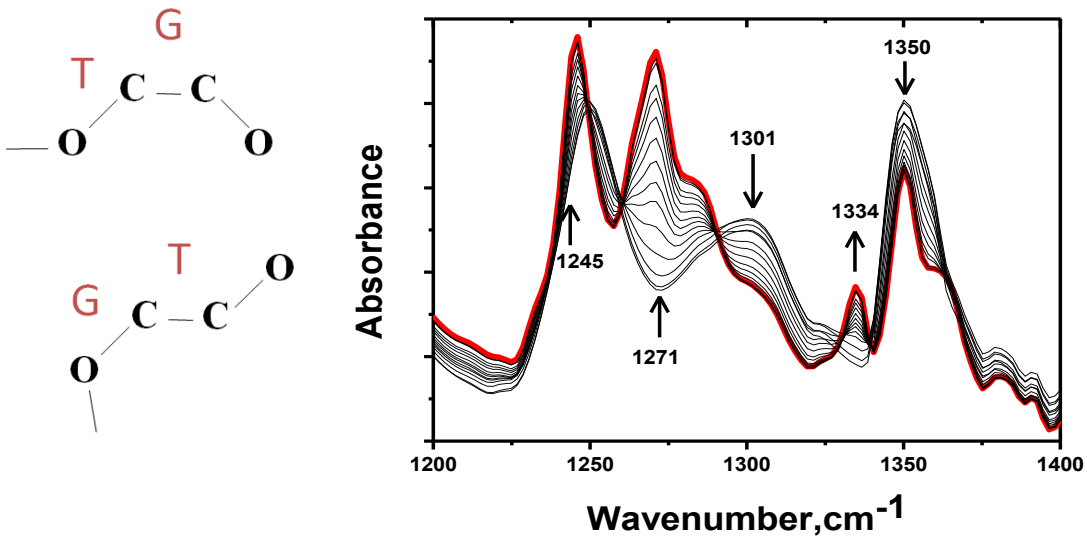

Figure 3.39. FT-IR spectra during the cooling process of 2.0 $CaCl_2$/ $C_{12}EO_{10}$ mole ratio sample. The spectrum in red belongs to the final spectrum of the mesocrystalline phase. Gauche and trans conformations of the C-C and and C-O bond is shown on the left.

The antisymmetric twisting vibrations of the -O-CH_2-CH_2-O- segment at around 1265-1250 cm^{-1} and 1245-1230 cm^{-1} were assigned to **TGG** and **TGT** conformers, respectively.[119]The signal at 1251 cm^{-1} was previously assigned to the **TGG** conformer.[66]In the FT-IR spectra, during the crystallization, the peak at 1251 cm^{-1} shifts to 1245 cm^{-1} and becomes sharper. This means that there is an increase in the **T** conformer of the C-O bond, in accord with the above comments. It was previously mentioned that the C-O bond is not affected by the increase of the

hydrogen bonding as compared to the C-C bond.[118] Basically, it is the **G** conformer of the C-C bond that allows POE-solvent interactions and C-O bond that allows the flexibility.[118] Therefore the variations on the C-C bond are more pronounced in POE-solvent interactions. Overall, this spectral region shows that the population of the **T** conformer for both C-C and C-O bonds increase, which may also explain the increasing distances between the micellar domains.

3.3.3.3. 1200-1000 cm^{-1} region

This region is dominated by the C-O stretching vibrations and does not show conformational dependence.[119] During crystallization it is seen that the signals that are from the C-O stretching bands become visible and well defined. There are also two new signals emerging at 1023 cm^{-1} and 1032 cm^{-1}, which may indicate the presence of direct Ca^{2+}---ethoxy interactions.

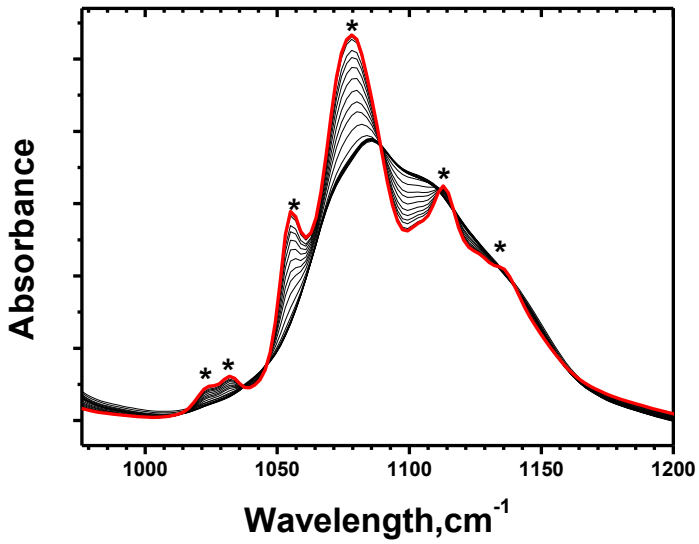

Figure 3.40. FT-IR spectra during the cooling process of 2.0 $CaCl_2/C_{12}EO_{10}$ mole ratio sample. The spectrum in red belongs to the final spectrum of the mesocrystalline phase.

3.3.3.4. 750-1000cm^{-1} region

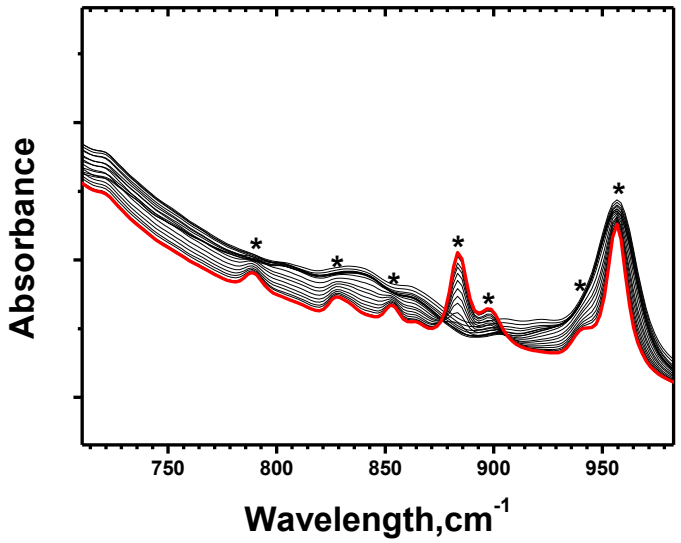

Figure 3.41. FT-IR spectra during the cooling process of 2.0 $CaCl_2$/ $C_{12}EO_{10}$ mole ratio sample. The spectrum in red belongs to the final spectrum of the mesocrystalline phase.

This region also show significant changes with crystallization. Several peaks become well defined and many new peaks emerge most notably at 884 and 898cm^{-1}. However the assignements of this peaks have not yet been achieved.

In conclusion, here we have shown that the concentrated solutions of Ca^{2+} salts can also act as the solvent component in the self-assembly of a nonionic surfactant similar to transition metal aqua complex salts and concentrated solutions of Li^+ salts. We have focused on the $CaCl_2.xH_2O$-$C_{12}EO_{10}$ system which shows a LLC to a mesocrystalline phase transition, which is observed for the first time, to the best of our knowledge. The data including the characterization of the mesophases of $(CaNO_3)_2.xH_2O$ -$C_{12}EO_{10}$ system is indicated in the Appendix.

3.4. Effect of Deliquescence on the Stability of LLC Mesophases

In addition to Li^+ and Ca^{2+} salts we have also scanned other metal salts in search for other salt.xH_2O-surfactant LLC mesophases. The homogeneous 5 ml aqueous solutions of various salts were prepared at salt/surfactant($C_{12}EO_{10}$) mole ratios of 1.0, 2.0, 3.0, 4.0 and 5.0. The solutions were then dropped on glass slides and excess water was allowed to evaporate under open atmosphere at RT and 25-30% RH. During the evaporation, a concentration gradient occurs along the samples which allowed us to monitor the salt/surfactant ratios in between the specified concentrations. In addition, the samples were also spin coated on glass slides at 1000 rpm from the 5 ml solutions. The spin coated samples were then monitored using POM at 25^{o}C and 25 %RH. For samples which are stable and show no sign of crystallisation, the XRD patterns were collected at small angles to determine whether the samples are mesostructurally ordered or not. Among the several samples shown in **Table 3.3** the stable LLC samples were obtained from the following salts: LiCl, $LiNO_3$, LiBr, LiI, $CaCl_2$, and $CaNO_3$. Note however that, the LiI.xH_2O-$C_{12}EO_{10}$ and $CaCl_2$.xH_2O-$C_{12}EO_{10}$ systems exhibit a mesocrystalline phase transformation upon aging. While the $LiClO_4$.xH_2O-$C_{12}EO_{10}$ system is unstable, the $LiClO_4$ salt can induce stable LLC mesophases in a narrow range (1-3) of salt/surfactant mole ratios with $C_{18}EO_{10}$ surfactant. Among other salts, the Na^+ salts except NaI and $NaClO_4$, K^+ salts except KSCN, and Mg^{2+} salts except $MgCl_2$ are unstable and crystallizes rapidly upon spin coating. Note that, the crystallization is most obvious at 2.0 salt/surfactant mole ratio. At 1.0 salt/surfactant mole ratio the surfactant molecules may dissolve the salt species. The NaI.xH_2O-$C_{12}EO_{10}$ system is stable at 3.0 mole ratio, however the XRD patterns show a very low degree of mesostructured order as compared to Li^+ and Ca^{2+}salts. The NaI.xH_2O-$C_{12}EO_{10}$ system is unstable and excess salt is leached out at 4.0 salt/surfactant mole ratio. The $NaClO_4$.xH_2O-$C_{12}EO_{10}$ and KSCN.xH_2O-$C_{12}EO_{10}$ systems are stable at 2.0 salt/surfactant mole ratio but again there is little or no mesostructured order, see **Figure 3.42**. The $MgCl_2$.xH_2O-$C_{12}EO_{10}$ mesophases are stable for a couple of hours with highly ordered LLC mesophases,

see **Figure 3.42**. In summary the Li^+ and Ca^{2+} salts exhibit stable LLC mesophases with $C_{12}EO_{10}$ while Na^+, K^+ and Mg^{2+} salts are in general unstable. These results are summarized in **Table 3.3**. **Type I** salts are usually stable over a broad range of salt concentrations and exhibit LLC mesophases. **Type II** salts are stable at low salt concentrations and exhibit little or no mesostructured order. **Type III** salts crystallize rapidly.

Table 3.3. Table shows whether the cation-anion couple (the salt) is successful in forming a water-salt surfactant LLC mesophase. The numbers indicate **I)** stable LC phase, **II)** LC texture was monitored under POM but the structure breaks down after a while, see also related XRD data at small angle **III)** Salt crystallizes out. (-) indicates: not-studied. *LiI.xH_2O -$C_{12}EO_{10}$ mesophases are able to keep the water but also exhibit transition to a mesocrystalline phase. ** $CaCl_2.xH_2O$-$C_{12}EO_{10}$ systems exhibit a transition from LLC to a mesocrystalline phase.

	$CH_3CO_2^-$	Cl^-	Br^-	I^-	NO_3^-	ClO_4^-	SCN^-	F^-
Li^+	-	I	I	I*	I	III	-	-
Na^+	III	III	III	II	III	II	III	-
K^+	-	III	-	III	III	-	II	-
Ca^{2+}	-	I**	-	-	I	-	-	-
Mg^{2+}	-	I	-	-	III	-	-	-

The trends among different salts can be explained when the hygroscopic tendency of the salt is taken into account. The surfactant molecules are unable to keep the water without salts, therefore one needs to look at the salts ability to do so. The salts ability to keep the water is directly summarized in its hygroscopic tendency and deliquiescence behaviour. Most hygroscopic salts can exhibit deliquescence where the salt crystals are dissolved spontaneously by the adsorbed water molecules from the air. Deliquescence occurs if the equilibrium vapor pressure of the saturated solution is lower than the vapor pressure of the air at that relative humidity. **Table 3.4** shows a list of deliquescence relative humidities

(%DRH) of some salts. Among all monovalent salts, it is seen on **Table 3.3** that Li^+ salts have very low %DRH levels as compared to Na^+ and K^+ salts. **Type I** salts such as LiCl, LiBr, LiI and $LiNO_3$ have %DRH levels lower than 20% - which is also lower than our experimental conditions, 20-25%. This may explain the higher stability of Li^+ containing LLC mesophases. Among the **Type II** salts, %DRH values of NaI and $NaClO_4$ salts are 38.17% and 43-46%, respectively (for the other

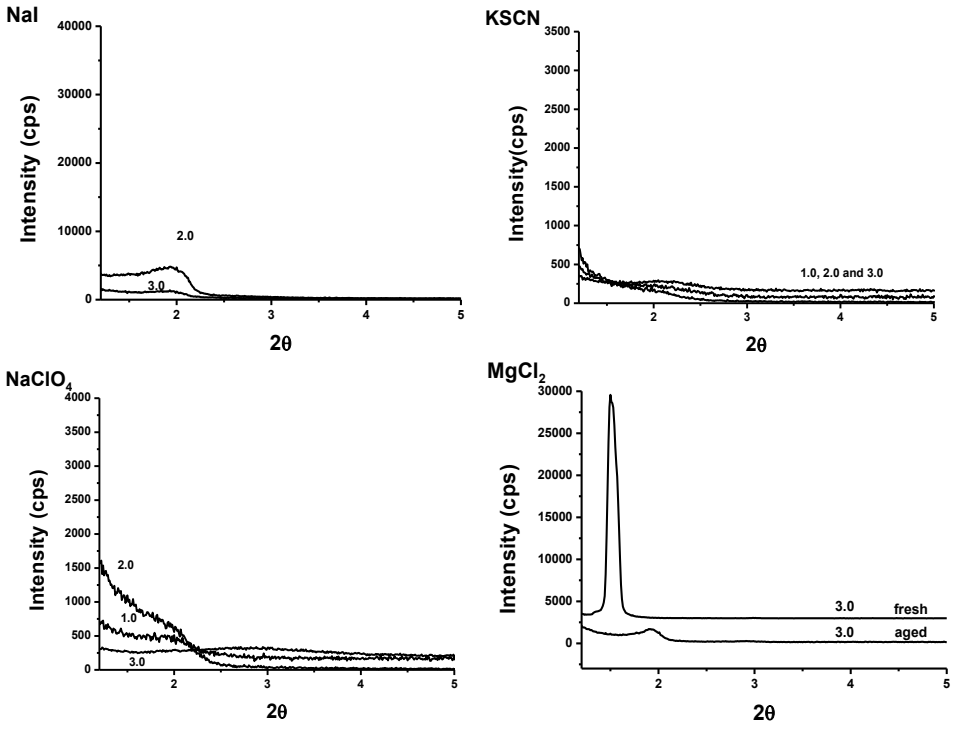

Figure 3.42. XRD patterns of stable samples of NaI, KSCN, $NaClO_4$ and $MgCl_2$ systems at different salt/surfactant mole ratios.

Type II salt KSCN we were not able to find the %DRH value in the literature). It is also seen that all **Type III** salts have %DRH levels higher than 50%. This may explain the instant crystallisation of the salt species in **Type III** salt systems. On the other hand **Type II** salt systems are stable at low concentrations (2-3 salt/surfactant mole ratio) with little or no mesostructured order.

The divalent salts should be considered separately because the cation(II)----ethyleneoxide chain interactions are much stronger in these systems as compared to monovalent salts, see for FTIR discussions in section 3.2. For divalent salts we

have studied the $CaCl_2$, $CaNO_3$, $MgCl_2$, $MgNO_3$ salts. The difference between the %DRH values of $Mg(NO_3)_2$ and $Ca(NO_3)_2$ is small- 52% and 51%, respectively, but the differences in the LC state are significant. The samples of $Mg(NO_3)_2.xH_2O$-$C_{12}EO_{10}$ systems rapidly crystallizes when spin coated but slowly crystallizes when dropped, the $Ca(NO_3)_2.xH_2O$-$C_{12}EO_{10}$ systems are stable. The chloride salts of Ca^{2+} and Mg^{2+} are more stable and have lower %DRH levels as compared to nitrate salts, 33% and 31% respectively. The samples of $MgCl_2.xH_2O$-$C_{12}EO_{10}$ leaches out salt crystals at 4.0 salt/surfactant mole ratio. However, the samples below this composition (1.0, 2.0 and 3.0) shows a mesocrystalline phase transformation similar to LiI and $CaCl_2$ salt systems. On the other hand, the $CaCl_2.xH_2O$-$C_{12}EO_{10}$ system is more stable and the $CaCl_2$ salt never crystallizes out. The $CaCl_2.xH_2O$-$C_{12}EO_{10}$ system also transforms to a mesocrystalline phase as a salt-water-surfactant complex, see section 3.4. As a result, the trends among different divalent salts correlate with the %DRH values. However small deviations in the DRH levels have more significant effects on phase stability. It seems that, the divalent cation has stronger interaction with the hydrophilic segment and salt-surfactant interactions contribute more to the phase behaviour as compared to the monovalent cations.

In order to check further whether the hygrospocity is a prerequest for the LLC mesophase formation, we prepared mixtures of $H_3PO_4.xH_2O$-$C_{12}EO_{10}$ and NaOH $.xH_2O$-$C_{12}EO_{10}$. The $H_3PO_4.xH_2O$-$C_{12}EO_{10}$ systems exhibited stable hexagonal LLC mesophases, see **Figure 3.44**. The $NaOH.xH_2O$-$C_{12}EO_{10}$ systems are very reactive to the dissolved CO_2 from the air forming Na_2CO_3 and $NaHCO_3$ crystals which have high DRH% levels. **Figure 3.43** shows the FT-IR spectra of the fresh NaOH samples. The ν-CO stretching of the carbonate and bicarbonate ions are indicated on the plot. The ν-CO stretching band of carbonate increases in time while those of bicarbonate decreases. Note also that, even the freshly coated sample have significant amount of carbonate. A closed chamber with CO_2-free atmosphere and controlled humidity is necessary to study the $NaOH.xH_2O$-$C_{12}EO_{10}$ system.

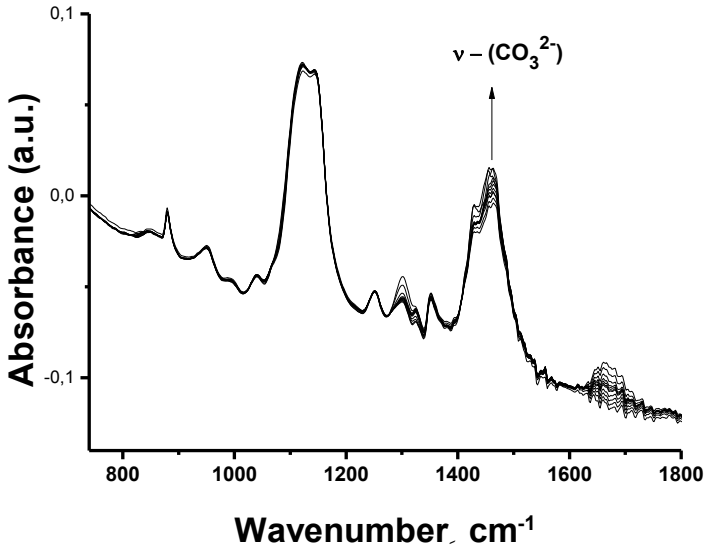

Figure 3.43. FT-IR spectra of fresh 3.0NaOH-1.0$C_{12}EO_{10}$ in time.

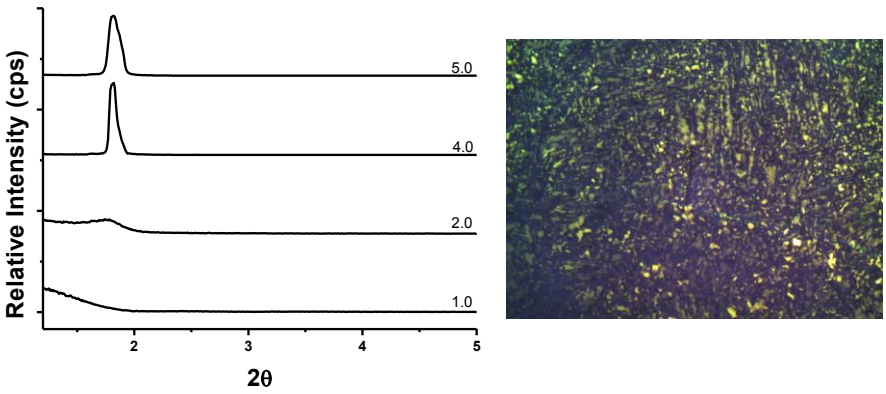

Figure 3.44. XRD patterns of $H_3PO_4.xH_2O$-$C_{12}EO_{10}$ system at different salt/surfactant mole ratios and POM image of 4.0$H_3PO_4.xH_2O$-1.0$C_{12}EO_{10}$ sample.

In conclusion, it is seen that there is a relation between the hygroscopicity of the salt and the air stability of the mesophase. Additional factors may also contribute to the phase behavior such as; the effect of anion, salt concentration,

temperature, pressure, relative humidity, hyrdophilicity of the surfactant molecule and most importantly the soft confinement effect. For instance, a more hydrophobic surfactant induces LLC mesophase formation in the presence of $LiClO_4$ at low salt concentrations. Additionally, Type II salts may exhibit LLC mesophases at higher humidity levels. The ability of the salt to keep the water species, may also be an indication for the role of the salt on the phase behaviour of a ternary system. If the salt-water interactions are weak, the ternary phase diagrams may exhibit a narrower range of LLC regions. However, at the current moment such an investigation includes rigorous work for the construction of ternary phase diagrams for each salt system. Further investigations are necessary to elucidate the nature of the LLC mesophase formation in salt.xH_2O-surfactant and salt-H_2O-surfactant systems and its stability. Nevertheless, it may be argued that, any particle, which can strongly interact with the water molecules, can induce spontaneous LLC mesophase formation under proper conditions.

Table 3.4 Deliquescence relative humidity of various salts at 25.0°C -except otherwise noted.

Salt*	%DRH [120]
H_2O	100
K_2SO_4	100
$KClO_3$	98.0
$CaHPO_4.2H_2O$	97.0
KH_2PO_4	96.6
KNO_3	95.0-91.0
$NH_4H_2PO_4$	93.0
$Na_2C_2H_4O_6.2H_2O$	92.0
$ZnSO_4.7H_2O$	88.5
$BaCl_2.2H_2O$	88.0 (24.5°C)
$Na_2CO_3.10H_2O$	87.0
KCl	89.0-84.5
$C_{12}H_{22}O_{17}$	85.0
$(NH_4)SO_4$	83.0-81.1
KBr	79.0
NH_4Cl	79.3-77.0
CH_3.COONa	77.0
$CO(NH_2)_2$	76.7-76.0
NaCl	76.5-75.0
$NaNO_3$	76.0-74.0
$K_2C_4H_4O_6.1/2H_2O$	75.0
$LiClO_4$	~70[121]
KI	68.86[122]
NH_4NO_3	63.5
NaBr	57.0
NaBr-KBr mixture	56.0
$C_6H_{12}O_6.\ 1/2H_2O$	55.0 (27°C)
NH,Cl-NaBr misture	54.0
NaNO,-KBr mixture	54.0
$Mg(NO_3)_2.6H_2O$	52.0 (24.5°C)
KBr-$CO(NH_2)_2$ mixture	51.0
$Ca(NO_3)_2.\ 4H_2O$	51.0
$NaClO_4$	43-46[121,123]
$K_2CO_3.2H_2O$	43.0
NaI	38.17[122]
$MgCl_2.\ 6H_2O$	33.0
$CaCl_2.\ 6H_2O$	31.0
CH_3COOK	19.0
LiI	17.56[122]
$(CH_3COO)_2Ca.\ H_2O$	17.0
LiCl . H_2O	13.0
$(CH_3COO)_2$Ca-Cane sugar misture	13.0
$LiNO_3$	12.86[124]
H_3PO_4 . $1/2H_2O$	9.0
NaOH	6.5
LiBr	6.37[122]
P_2O_5	0

*In Table 3.2, we have indicated the Type I salts with blue, Type II salts with green and Type III salts with red color. Other salts were not investigated except NaOH which is air reactive. A correlation between the %DRH levels and LC stability can be inferred from this table.

3.5. Applications and Future Perspective

All of the LLC mesophases mentioned in previous chapters including the mesostructured solid phases are potential candidates as templates for the synthesis of metal containing mesoporous and mesostructured materials. In this direction, a molten salt assisted self-aasembly synthesis of metal oxide-silica hybrid films has been established in our laboratory.[70] We have used the molten phase of $[Zn(H_2O)_6(NO_3)_2]$ and $[Cd(H_2O)_4(NO_3)_2]$ and shown that the silica walls of mesoporous thin films can be uniformly coated with ZnO and CdO with a record metal oxide/silica weight percentage of 60% and and 71%, respectively.[70] The films then can easily be converted to their sulphur and selenium analogues MS-SiO_2 and MSe-SiO_2 (M is Zn and Cd), respectively, under H_2S and H_2Se atmospheres.[106] The molten salt assisted synthesis strategies are currently in progress in our laboratory for the synthesis of mesoporous CaO containing silica films and mesoporous metal titanate films. The development of these materials are important for CO_2 capture and Li ion electrode applications, respectively. The availibility of the stable LLC mesophases of H_3PO_4 and CaX_2 ($X = Cl^-$ and NO_3^-) salts with non-ionic surfactants provides oppurtunities for the synthesis of porous hydroxyapatite films. The mixtures of these two salts have been prepared and preliminary experiments have been performed. We believe that our discoveries on the origin of salt-surfactant LLC mesophases will inspire the synthesis of novel metal containing hybrid materials.

The Li^+ mesophases can be also be good candidates as electrolyte materials in electrochemical applications. Electrolyte materials are basically responsible for the transport of ions in between the electrodes in electrochemical devices and high ionic conductivity is a prerequest for a good electrolyte material. In general an electrolyte material can be a solid, liquid or gel depending on the device setup. In electrochemical devices, where liquid electrolytes are used, it is important to be able to convert the liquid electrolyte to a gel by maintaining the high ionic conductivity. The gel electrolytes can overcome the problems related to the leakage and vaporisation. [125] The aqueous gel electrolytes have been investigated to found

usage in many electrochemical applications including rechargeable batteries, electrochemical capacitors,[126] solar cells.[127]LC materials as gel electrolytes have also been investigated due to their high conductivity and anisotropic properties.[128-133]

In this direction, we have investigated the ionic conductivity properties of Li^+ contaning LLC mesophases.[103] The LLC gel materials were prepared by mixing salt, surfactant and water. The mixtures transform to LLC mesophases by constant shaking and homogenizing in closed vials at temperatures above the melting point of the composition, see experimental section for details. The ionic conductivity measurements were performed with an experimental setup that avoids the leakage of materials and evaporation of water, see **Figure 2.1**. One of the stainless steel electrodes was contacted to the working electrode (of the potentiostat) and the other steel electrode was contacted to the reference-counter electrode couple. The stainless steel electrodes were unreactive with samples and maintain good conduction. The ionic conductivities of some samples were measured several times to check the repreducibility of our results. Overall, the error margin is found to be lower than 10% of the measured resistance. The conductivity of the samples that are held in contact the electrochemical cell may decrease in time, ~10-20%, most probably due to the reorganization of the surfactant molecules at the electrode interface. The ionic conductivities were measured with an AC impedance spectroscopy. The Z_{real} was taken as the sample resistance at $Z_{imaginary} = 0$ in the Nyquist Plot, see Chapter 2 for an example. Basically, Nyquist Plot gives the variation of the imaginary and real components of impedance on the same graph. The resistance datum was then converted to ionic conductivity using the equation, $\sigma = K/R_s$, where σ is the ionic conductivity in Scm^{-1}, K is the cell constant in cm^{-1} and R_s is the resistance data in ohms gathered from the sample. The cell constant was calculated as 0.59 cm^{-1},using a standart 0.1M KCl solution at RT, whose ionic conductivity (σ) is known. The heating and cooling experiments were performed by inserting the sample vial in temperature controlled water bath and ethanol bath, respectively. At each temperature step, the sample was allowed to equilibrate with the conditions 5 to 10 minutes. The variation in resistance was continuously monitored during this process and resistance data was recorded when a constant reading was achieved.

The ionic conductivities of the of the $LiNO_3$-$C_{12}EO_{10}$-H_2O with $LiNO_3/C_{12}EO_{10}$ mole ratios of 5, 6 and 7 and a LiCl-$C_{12}EO_{10}$-H_2O with a $LiCl/C_{12}EO_{10}$ mole ratio of 5 were measured as a function of temperature.[103] **Figure 3.45** shows our results on the ionic conductivity of these samples with respect to temperature. It is seen that ionic conductivities exhibit a nearly Arrhenius type relation with the temperature. Among these samples highest conductivity was recorded as 2.0 x 10^{-2} Scm^{-1}. Higher conductivities might be achieved at higher water contents but the excess water will tend to evaporate under ambient conditions, see section 3.4 for details about the water content of the mesophases. The mesophases exhibit high ionic conductivities even below 0°C. For measurements below -13°C a different measurement setup with lower cell constant is required. **Figure 3.46** shows the relation of ionic conductivity with salt and water compositions. It is seen that in both systems the conductivity increase with increasing salt and water concentration. The highest conductivity at RT was recorded as 7.0 x 10^{-3} Scm^{-1} among the samples investigated in this study.[103]

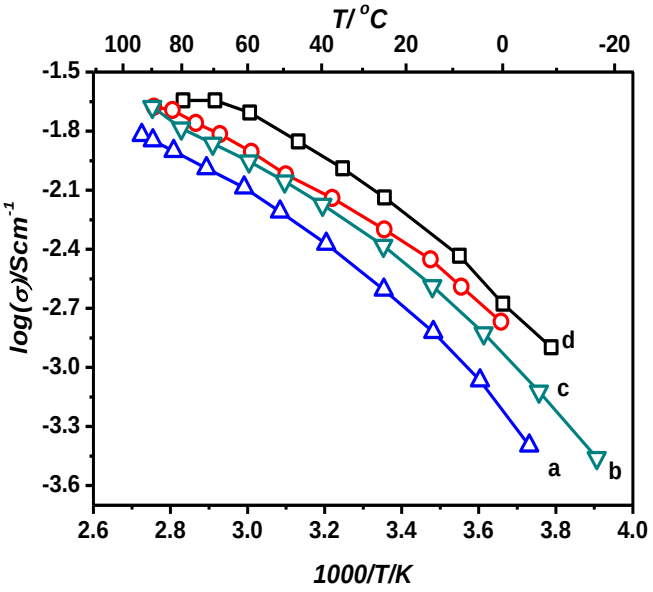

Figure 3.45.[*] The logarithm of the conductivity versus 1000/T plots of the samples: a) $5LiNO_3$-$C_{12}EO_{10}$-$15H_2O$, b) $6LiNO_3$-$C_{12}EO_{10}$-$18H_2O$, c)$7LiNO_3$-$C_{12}EO_{10}$-$21H_2O$, and d)5LiCl-$C_{12}EO_{10}$-$25H_2O$.[103]

[*] Reprinted from Albayrak, C., Cihaner, A. & Dag, Ö. A New, Highly Conductive, Lithium Salt/Nonionic Surfactant, Lyotropic Liquid-Crystalline Mesophase and Its Application. *Chemistry – A European Journal* 18, 4190-4194 (2012), with permission from John Wiley and Sons (2012).

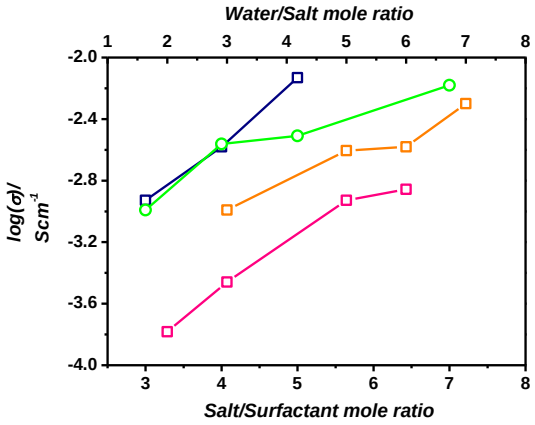

Figure 3.46.[*] Conductivity vs. composition relations for several samples. (a) and (b) belongs to the bottom x-axis whereas (c) and (d) belongs to top x-axis. In the bottom axis water/salt mole ratio is kept constant at 3 mole ratio and in the top axis salt/surfactant ratio is kept constant, (c) at 3.0 and (d) at 5.0. (a) and (d) for the LiCl-$C_{12}EO_{10}$-H_2O and (b) and (c) for the $LiNO_3$ -$C_{12}EO_{10}$-H_2O samples.[103]

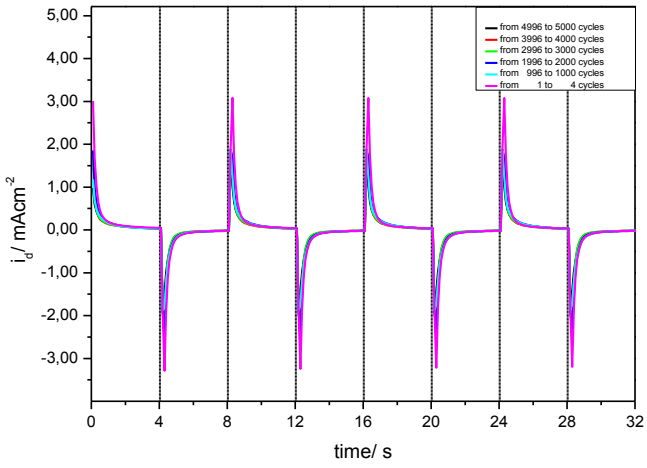

Figure 3.47.[*] Current profile of a sample 4.0LiCl-1.0$C_{12}EO_{10}$-16.0H_2O sandwiched between ITO glasses which were previously coated with Poly (4,7-di-2,3-dihydrothieno[3,4-b][1,4]dioxin-5-yl-2,1,3-benzoselenadiazole) and poly (3,4 diethleyedioxythiophene) during 5000 switches.[103]

[*] Adapted from Albayrak, C., Cihaner, A. & Dag, Ö. A New, Highly Conductive, Lithium Salt/Nonionic Surfactant, Lyotropic Liquid-Crystalline Mesophase and Its Application. *Chemistry – A European Journal* 18, 4190-4194 (2012), with permission from John Wiley and Sons (2012).

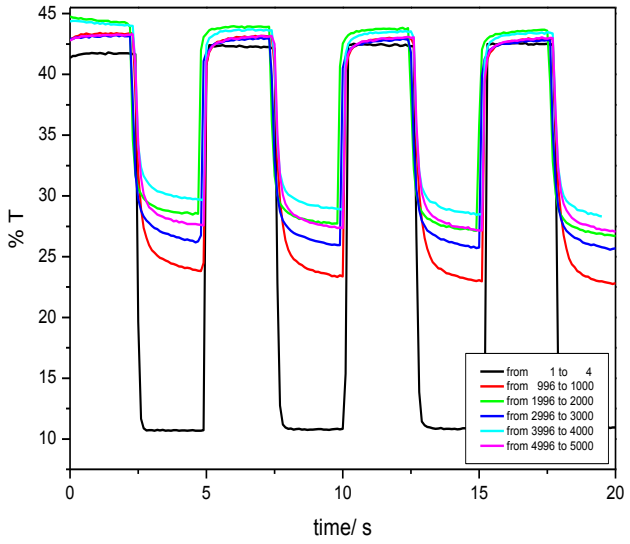

Figue 3.48.[*] Optical activity profile of a sample 4.0LiCl-1.0$C_{12}EO_{10}$-16.0H_2O sandwiched between ITO glasses which were previously coated with Poly (4,7-di-2,3-dihydrothieno[3,4-b][1,4]dioxin-5-yl-2,1,3-benzoselenadiazole) and poly (3,4-diethleyedioxythiophene) during 5000 switches.[103]

We have also performed tests on a polymer electrochromic device.[103] Poly (4,7-di-2,3-dihydrothieno[3,4-b][1,4]dioxin-5-yl-2,1,3-benzoselenadiazole)[99], exhibiting green color when neutralized and transmissive sky blue when oxidized, and poly (3,4-diethleyedioxythiophene), showing dark blue and transmissive sky blue upon oxidation, were coated separately on ITO electrodes in 0.1 M $LiClO_4$ dissolved CH_2Cl_2 and acetonitrile solutions, respectively by applying varying voltage using cyclic voltametry.The LLC material was sandwiched between the coated electrodes and allowed to equilibrate for half an hour. Two different potentials were applied at -1.0V and 1.2V at a residance time of 4s. The electrochemical response of the device was monitored for 5000 cycles ($2x10^4$ s). The switching behaviour is given in **Figure 3.47** and **Figure 3.48**. Note that, the devices does not loose its redox potential significantly (maintains 66.3% of its

[*] Adapted from Albayrak, C., Cihaner, A. & Dag, Ö. A New, Highly Conductive, Lithium Salt/Nonionic Surfactant, Lyotropic Liquid-Crystalline Mesophase and Its Application. *Chemistry – A European Journal* 18, 4190-4194 (2012), with permission from John Wiley and Sons (2012).

electro activity after 5000th switch) and it also maintaines 46% of its optical activity at 610 nm.[103]

In addition to the material applications, it is also worthwhile to mention that the self-assembly of surfactants in molten salts and concentrated electrolyte solutions are almost unexplored. This thesis work enlightens the origin of the LLC mesophase formation in these systems. However, the physical chemistry of surfactants in solvents spans a much larger area involving potential applications in organic and inorganic synthesis. For instance, the presence of microemulsions and inverted micellar systems in molten salt mesophases is waiting to be investigated. These mesophases can also be good candidates in the fundamental study of the behaviour of molten salt and concentrated electrolyte solutions under soft confinement.

4. Conclusions

In this thesis we shed light on the origin of self-assembly of surfactants into liquid crystalline mesophases, in salt-water-surfactant mixtures. We showed that the transition metal aqua complex salts of the form $[M(H_2O)_m]X_n$ -where M is a transition metal and X is a counter-ion, such as NO_3^-, ClO_4^- and Cl^- acts as the solvent component of the mesophase and organizes the surfactant molecules into LLC mesostructures such as hexagonal, cubic, bicontinuous cubic, and micellar. The first binary phase diagram of the $[Zn(H_2O)_6](NO_3)_2$-$C_{12}EO_{10}$ system were constructed at RT. The phase behavior of the $[Zn(H_2O)_6](NO_3)_2$-$C_{12}EO_{10}$ system is very similar to H_2O-C_mEO_n systems, except at subzero temperatures. An LLC to ordered mesostructured solid transition was observed for the first time in a LLC phase at -52^{o}C with a glass transition. The system was found to be stable down to -190^{o}C (lower temperatures could not be monitored). The confinement of the ions in the soft mesostructure prevents the crytallisation of the salt with a drastic decrease in freezing point by 88^{o}C, where freezing forms not the crystalline form but a glassy form of the salt. Further investigations are necessary to elucidate the nature of this interesting phenomenon.

Our experiments on alkali salts showed that the concentrated solutions of alkali metal salts can also act as the solvent component similar to molten transition metal aqua complex salts. The LC phases of various Li^+ salts were studied –LiCl, $LiClO_4$, LiBr, LiI, $LiNO_3$- and a ternary phase diagram for the $LiNO_3$-H_2O-C_mEO_n was constructed. The phase behaviour indicates that the water/salt mole ratios can be lowered down to 2 (lower than the solubility limit (4.4) of this salt in water). The high salt concentrations in these systems show that the self-assembly of surfactant occurs via the collaborative act of salt-water couple. This findings shifts the current perspective on the effects of salts in the surfactant self-assembly. At high salt concentrations the system becomes highly responsive to the presence of salt species and the salt-water couple should be considered as the solvent. We observed a Hofmeister series effect on the phase behaviour of different anions in $LiX.H_2O$-$C_{12}EO_{10}$ systems. The mesophases go into a phase transition from hexagonal to

cubic mesophases with increasing chaotropicity of the anion. The ClO_4^- ion containing mesophases were unstable with $C_{12}EO_{10}$ surfactant. However, stable mesophases were obtained with a more hydrophobic surfactant, $C_{18}EO_{10}$. It seems that the perchlorate makes the surfactant molecule too hydrophilic and the usage of a more hydrophobic surfactant balances this effect. However, further evidences are required at this point. In $LiI.H_2O$-$C_{12}EO_{10}$ systems, a phase transition from LLC to ordered mesostructured crystalline solid occurs, where the salt-surfactant-water triple acts together without disrupting the mesophase. The samples diffract at both small and high angles similar to zeolite crystals, indicating mesocrystallinity, crystallinity in the walls.

The $LiX.H_2O$-$C_{12}EO_{10}$ mesophases show very high ionic conductivity (compared to current polyelectrolytes) at RT, 7.0×10^{-3} S/cm at RT and maximum conductivity of 2.0×10^{-2} S/cm at 90°C. The mesophases can be potentially important as gel electrolytes in electrochemical devices, such as electrochromic devices. We have extended our investigations further to include Ca salts. Similar to other metal salt systems, concentrated solutions of Ca salts ($Ca(NO_3)_2$ and $CaCl_2$) exhibited LLC mesophases with hexagonal and cubic structures. In the $Ca(NO_3)_2$ systems, upon heating and the evaporation of water, the samples solidify without salt crystallisation. In the $CaCl_2$ systems a mesostructured crystalline solid phase similar to $LiI.H_2O$-$C_{12}EO_{10}$ systems was observed below 55% RH at RT. To the best our knowledge these are the first examples of such transitions.

The investigation has also been extended to include the following compounds: NaCl, NaBr, NaI, NaAc, $NaClO_4$, NaSCN, $NaNO_3$, KCl, KNO_3, KI, KSCN, $MgCl_2$, and $Mg(NO_3)_2$, H_3PO_4, and NaOH. Among these compounds, the H_3PO_4 systems exhibited stable LLC mesophases with $C_{12}EO_{10}$ under ambient and open atmospheric conditions. The LLC mesophases of $MgCl_2$ systems were found to be stable for a couple of hours. The NaI, $NaClO_4$ and KSCN systems can be stable at low salt concentrations with little or no mesostructured order. The stability of the samples under open atmosphere is found to be correlated with the hygroscopic property of the salt species. Further investigations are necessary to elucidate the nature of the LLC mesophase formation in $Salt.xH_2O$-Surfactant and Salt-H_2O-Surfactant systems and its stability.

It can be concluded that the soft confinement depresses the melting points of the molten hydrated salts and enhances the solubilities of alkali and alkaline earth metals salts. These findings expands our understandings on the salt-surfactant LLC mesophase to include many more salts, acids, and bases. We believe these findings will increase the interest in the salt-surfactant self-assembly and create a new media for the synthesis of nanostructured materials. In this content, the LLC mesophases of acids and bases need to be explored that may open up new synthetic strategies for advance functional materials for various applications.

5. Appendix

5.1. POM images

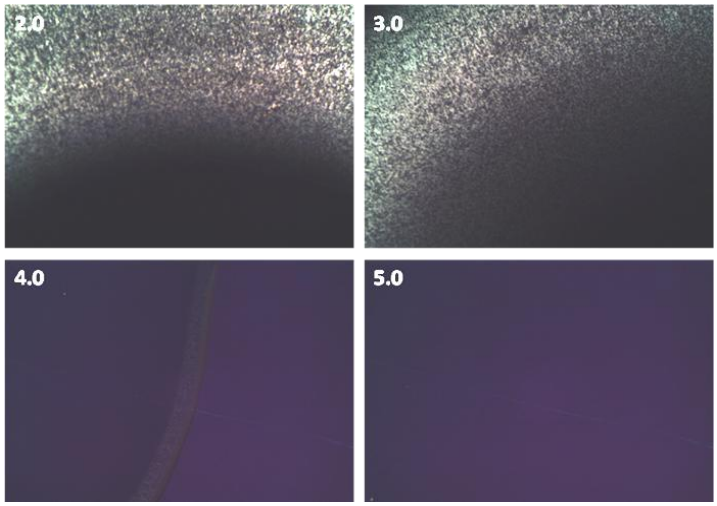

Figure 5.1. POM images showing the $\mathbf{H_1}$ to $\mathbf{I_1}$ transition in $Ca(NO_3)_2.xH_2O$-$C_{12}EO_{10}$ mesophases at indicated $Ca(NO_3)_2/C_{12}EO_{10}$ mole ratios.

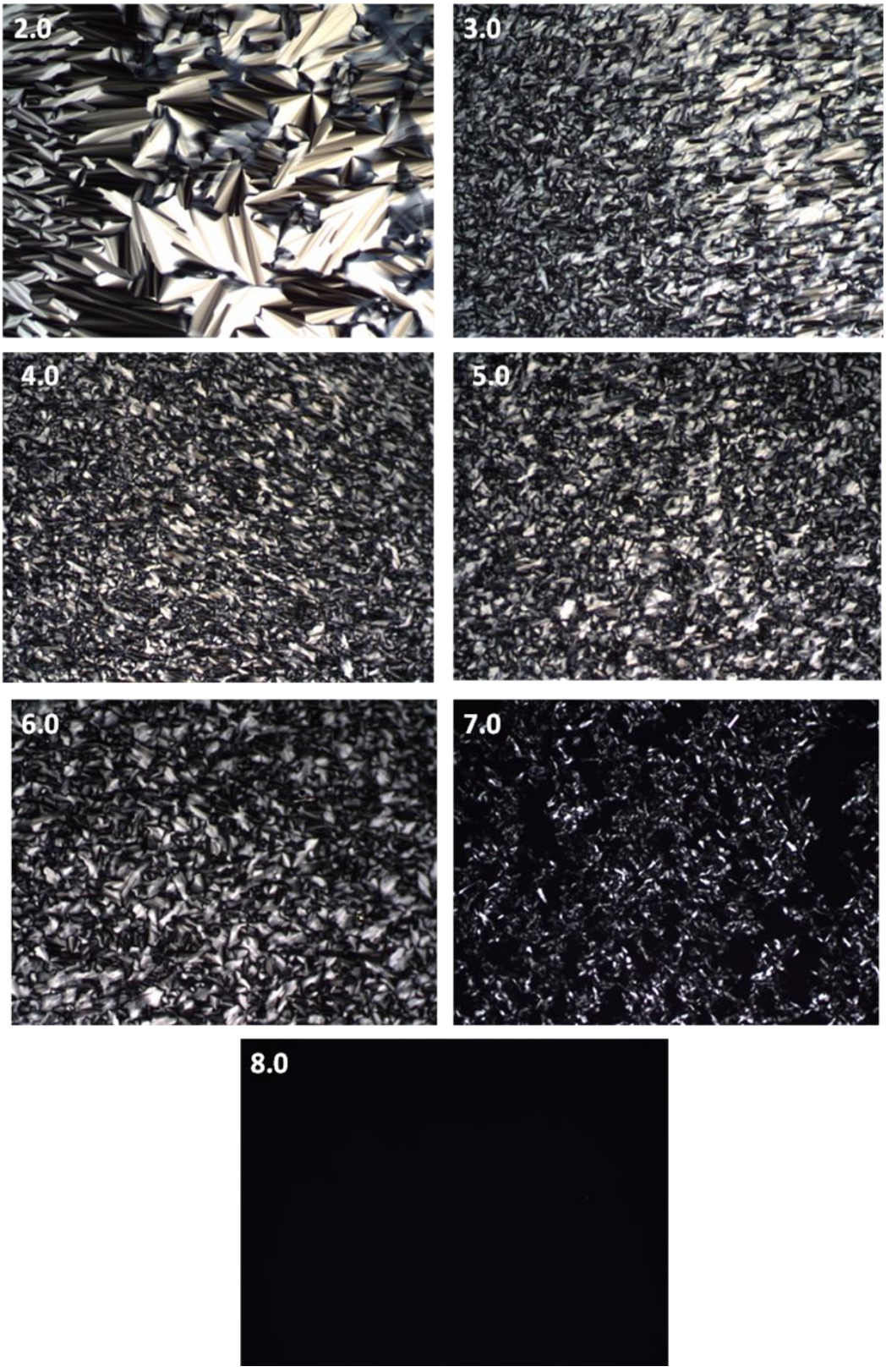

Figure 5.2. POM images of $LiNO_3.xH_2O$-$C_{12}EO_{10}$ system at 30% RH at RT.

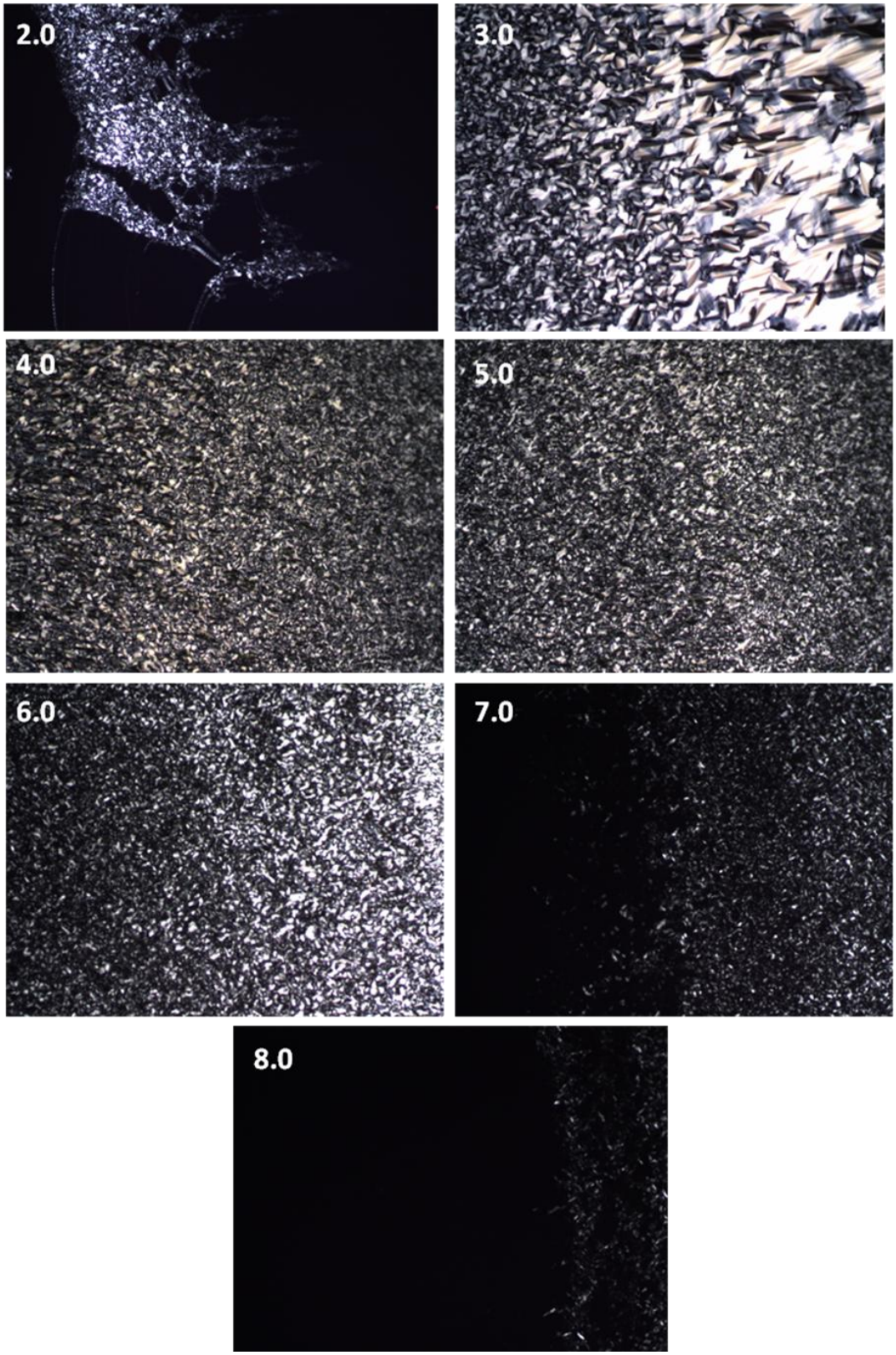

Figure 5.3. POM images of $LiCl.xH_2O$-$C_{12}EO_{10}$ system at 30% RH at RT.

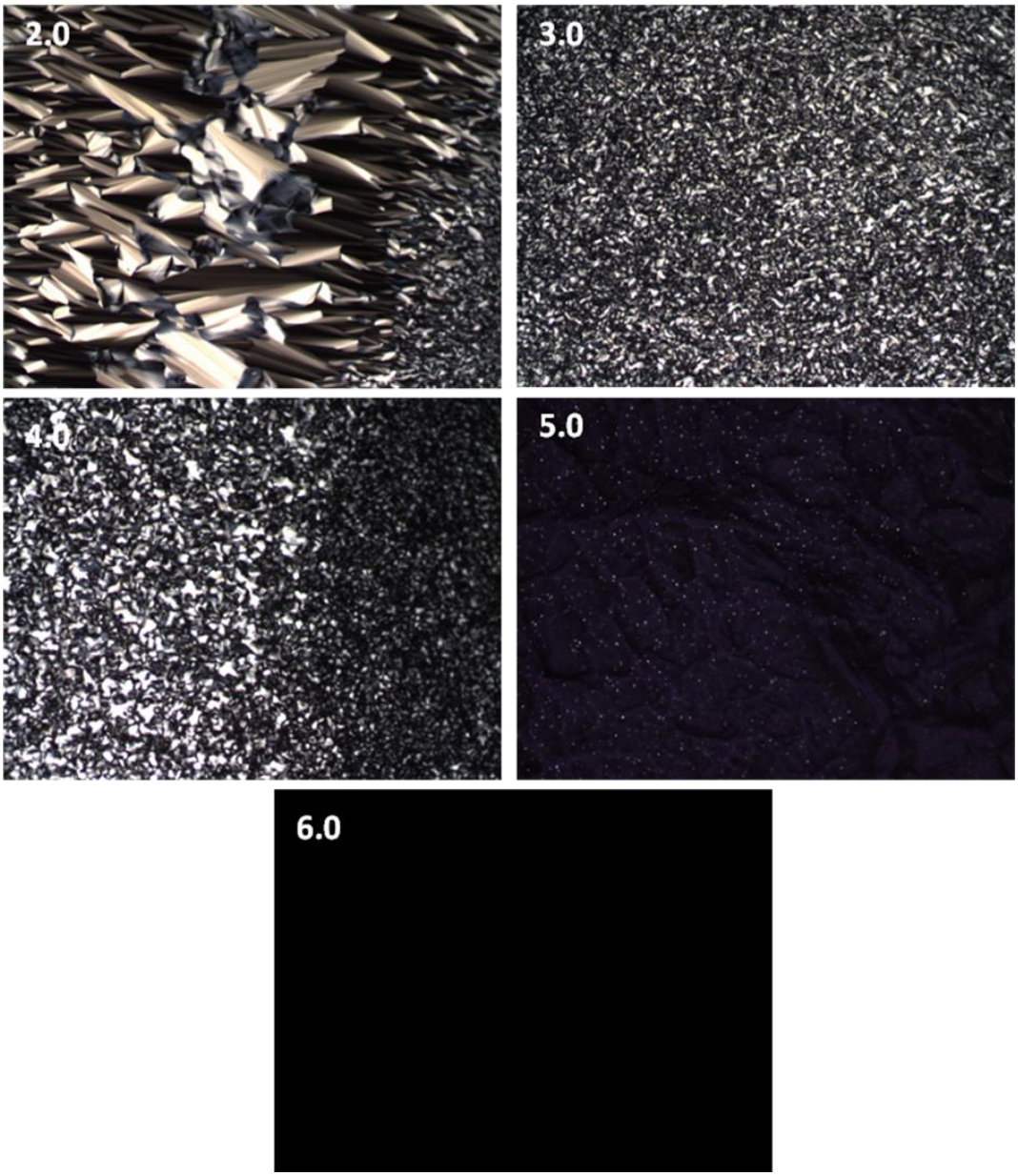

Figure 5.4. POM images of $LiBr.xH_2O$-$C_{12}EO_{10}$ system at 30% RH at RT

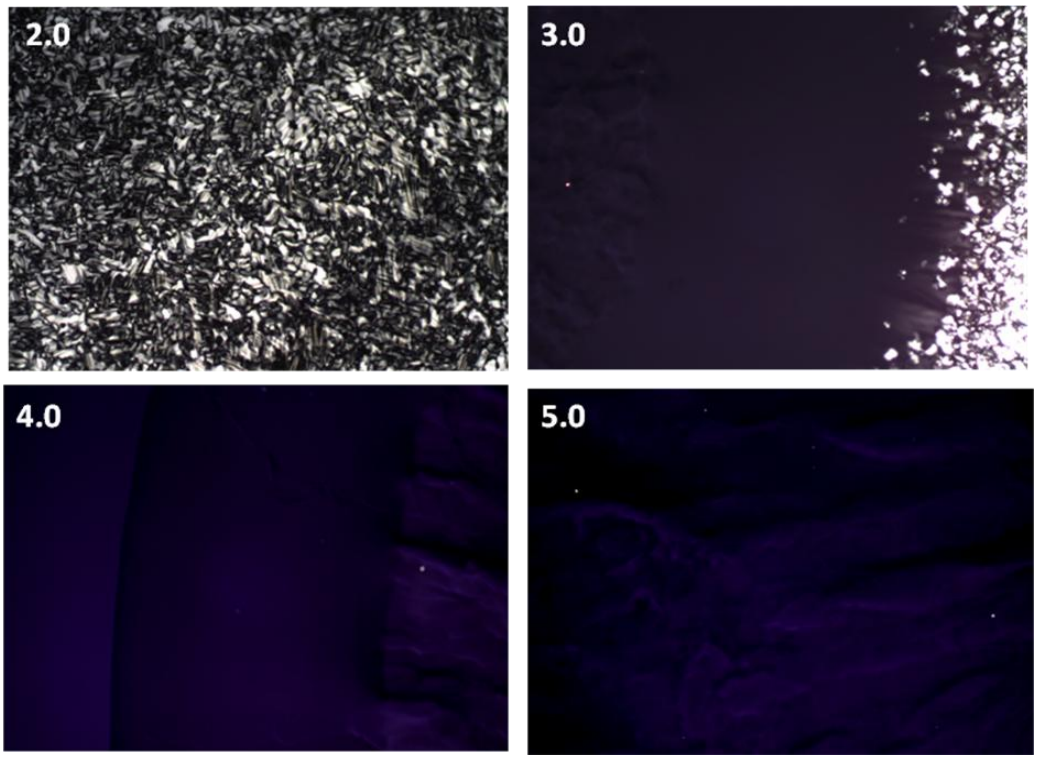

Figure 5.5. POM images of $LiBr.xH_2O$-$C_{12}EO_{10}$ system at 30% RH at RT

5.2. XRD Patterns

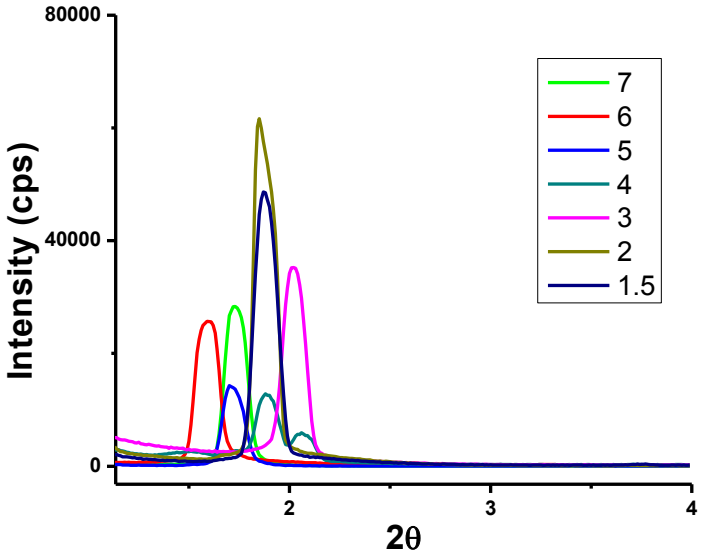

Figure 5.6. XRD Patterns of $Ca(NO_3)_2.H_2O$-$C_{12}EO_{10}$ system at different mole ratios.

5.3. DSC Thermographs

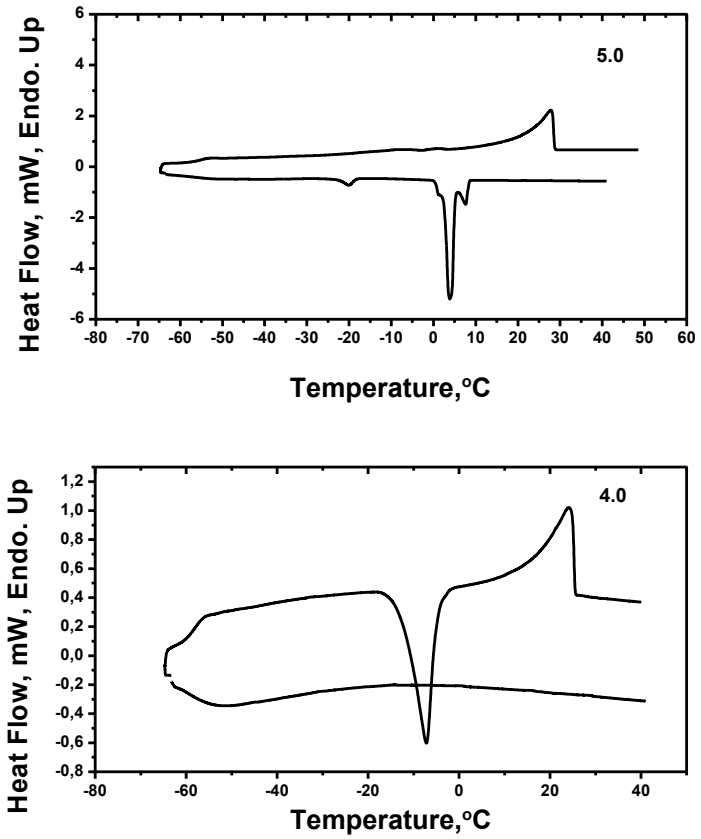

Figure. 5.7. DSC thermographs of $[Zn(H_2O)_6](NO_3)_2$- $C_{12}EO_{10}$ samples at indicated salt/surfactant mole ratios.

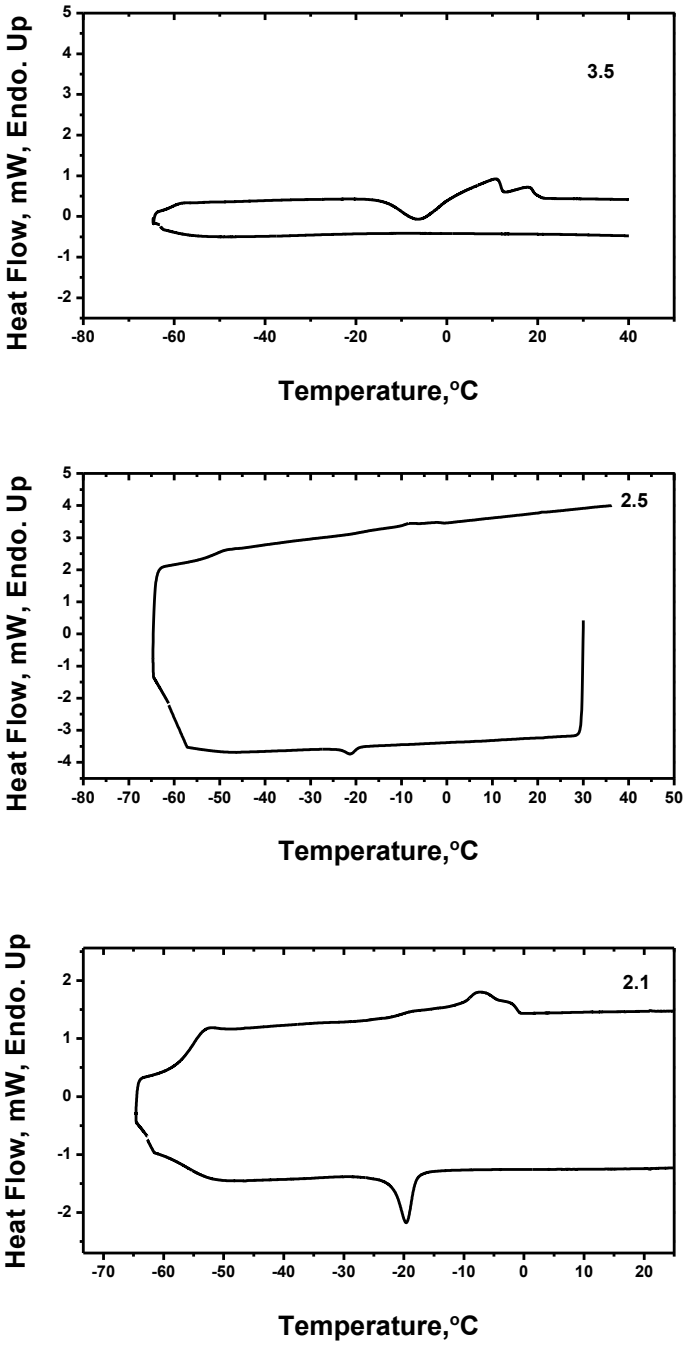

Figure. 5.8. DSC thermographs of $[Zn(H_2O)_6](NO_3)_2$- $C_{12}EO_{10}$ samples at indicated salt/surfactant mole ratios.

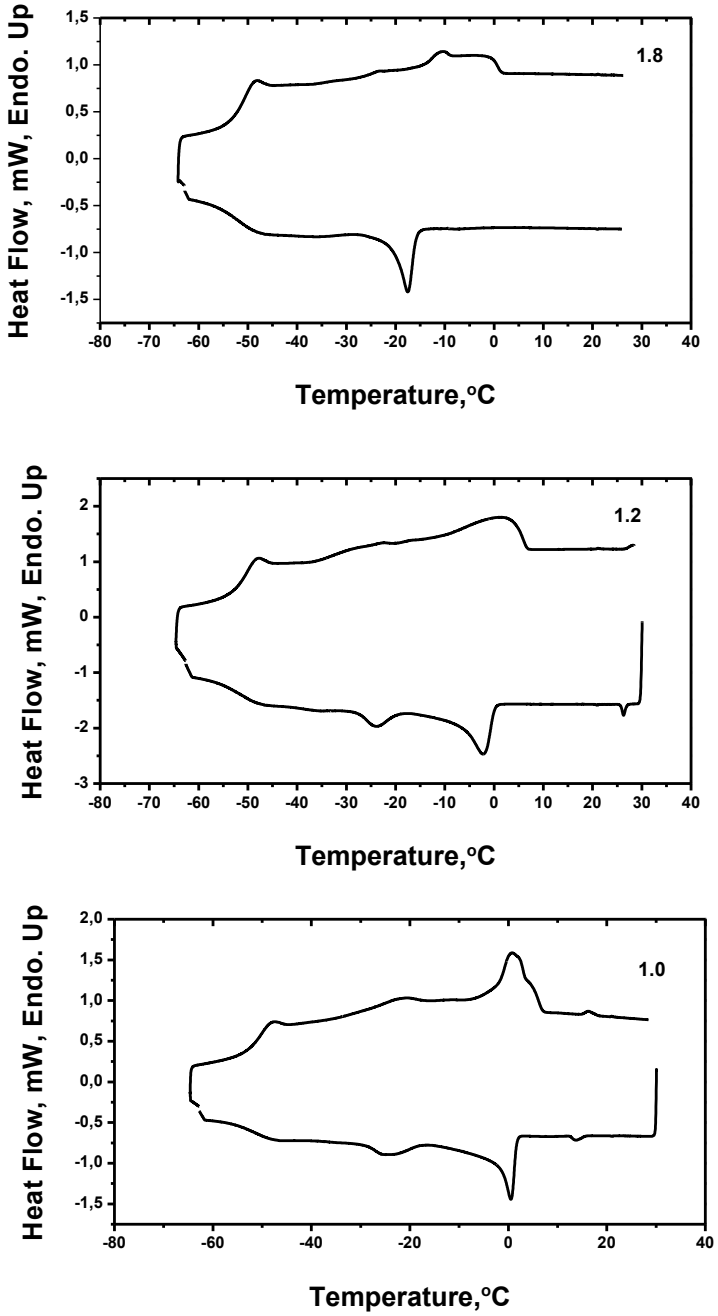

Figure. 5.9. DSC thermographs of $[Zn(H_2O)_6](NO_3)_2$- $C_{12}EO_{10}$ samples at indicated salt/surfactant mole ratios.

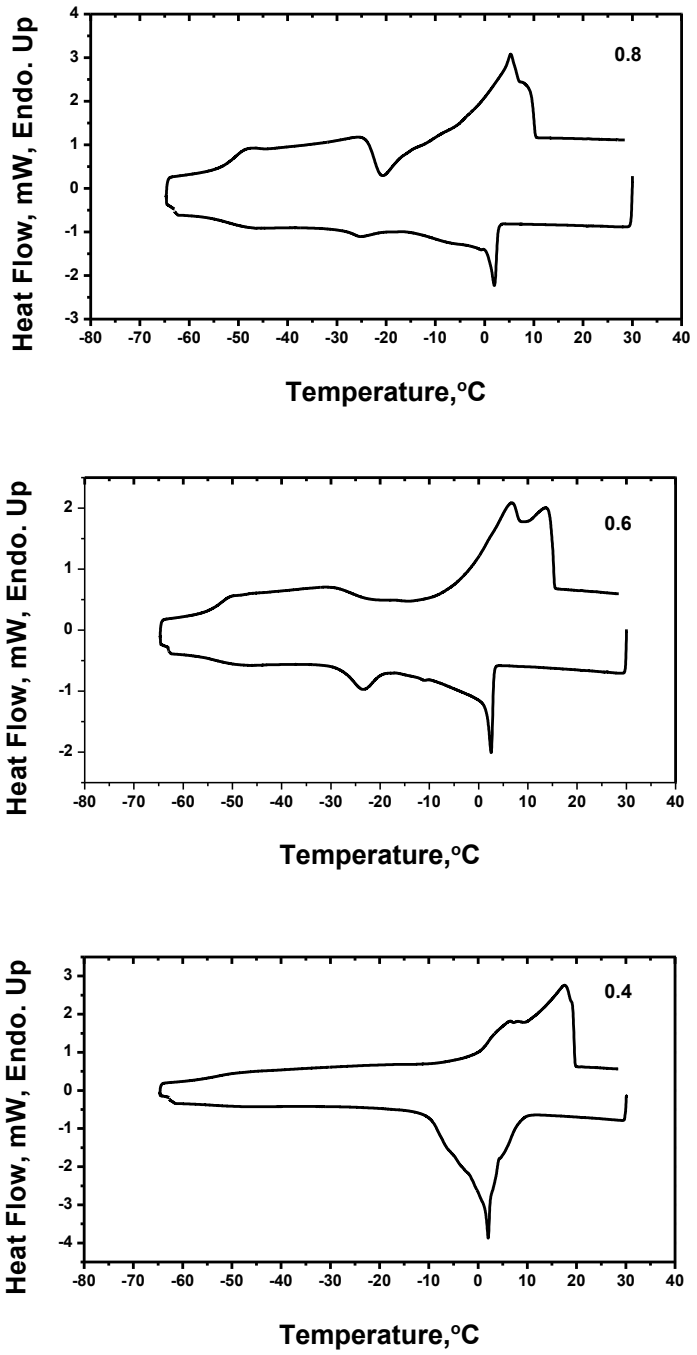

Figure. 5.10. DSC thermographs of $[Zn(H_2O)_6](NO_3)_2$- $C_{12}EO_{10}$ samples at indicated salt/surfactant mole ratios.

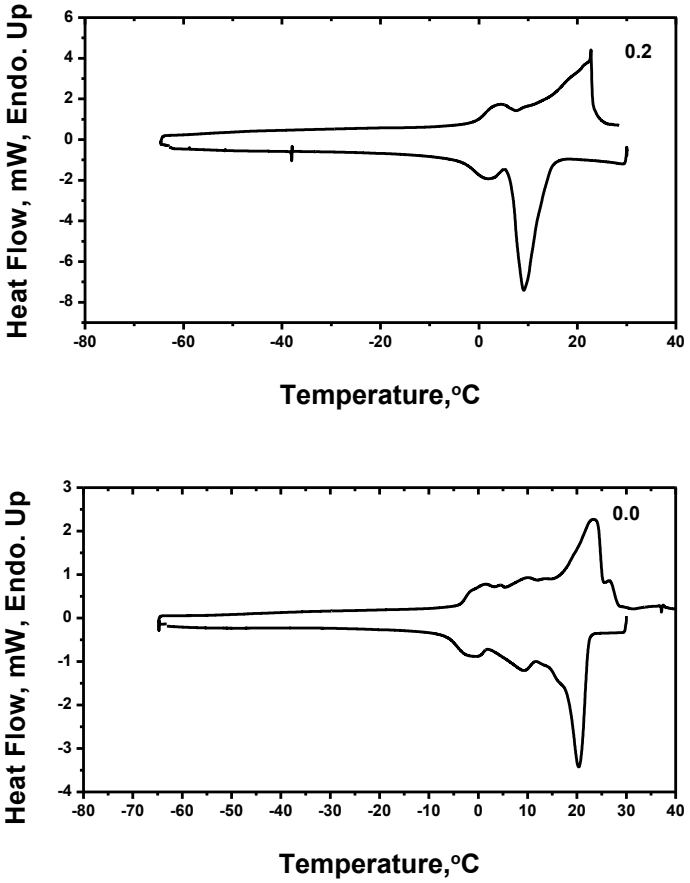

Figure. 5.11. DSC thermographs of $[Zn(H_2O)_6](NO_3)_2$- $C_{12}EO_{10}$ samples at indicated salt/surfactant mole ratios.

5.4. FT-IR spectra

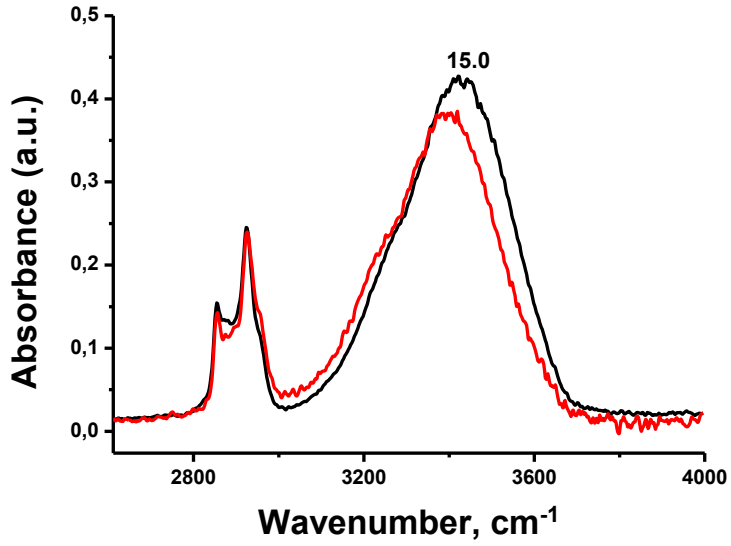

Figure 5.12. FT-IR spectra of 3.0LiCl-15.0H_2O-1.0$C_{12}EO_{10}$ (indicated with 15.0) and 2.0$CaCl_2$.xH_2O-1.0$C_{12}EO_{10}$ samples.

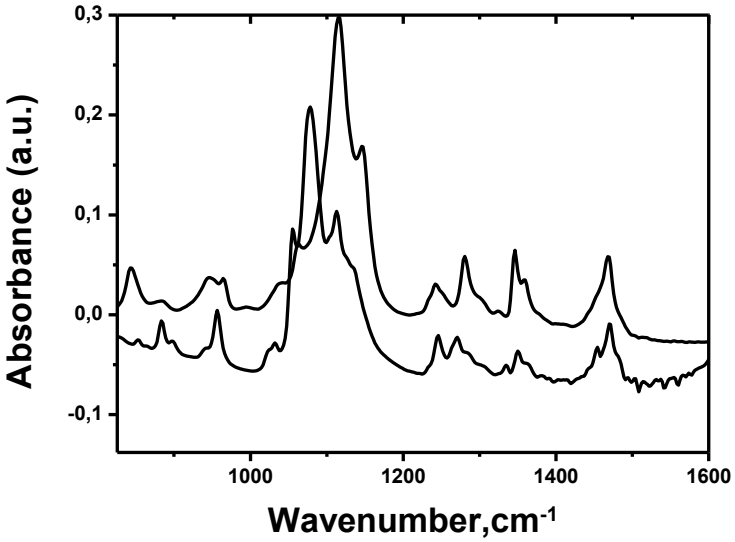

Figure 5.13. FT-IR spectra of the mesocrystals of $CaCl_2$.H_2O-$C_{12}EO_{10}$ (bottom) and crystalline $C_{12}EO_{10}$ (top).

5.5. Abbreviations

RT: Room temperature

RH: Relative humidity

DRH: Deliquescent relative humidity

CMC: Critical micelle concentration

CPP: Critical packing parameter

H_1: Hexagonal

I_1: Cubic

V_1: Bicontinuous cubic

L_1: Micellar

L_α: Lamellar

T_g: Glass transition

LLC: Lyotropic liquid crystal

LC: Liquid crystal

TLC: Thermotropic liquid crystal

FT-IR: Fourier transform infrared

DSC: Differential scanning calorimetry

POM: Polarized optical microscope

$C_{12}EO_{10}$: Decaethylene glycol monododecyl ether, surfactant

T: Trans conformation

G: Gauche conformation

6. References

1. Evans, D.F. Self-organization of amphiphiles. *Langmuir* 4, 3 (1988).

2. Frank, H.S. & Evans, M.W. Free volume and entropy in condensed systems III. Entropy in binary liquid mixtures; partial molal entropy in dilute solutions; structure and thermodynamics in aqueous electrolytes. *The Journal of Chemical Physics* 13, 507-532 (1945).

3. Silverstein, T.P. The real reason why oil and water don't mix. *Journal of Chemical Education* 75, 116 (1998).

4. Chandler, D. Interfaces and the driving force of hydrophobic assembly. *Nature* 437, 640-647 (2005).

5. Bowron, D.T., Filipponi, A., Roberts, M.A. & Finney, J.L. Hydrophobic hydration and the formation of a clathrate hydrate. *Physical Review Letters* 81, 4164-4167 (1998).

6. Lee, B. Solvent reorganization contribution to the transfer thermodynamics of small nonpolar molecules. *Biopolymers* 31, 993-1008 (1991).

7. Krister Holmberg, B.J., Bengt Kronberg, Björn Lindman. *Surfactants and Polymers in Aqueous Solution*, (John Wiley & Sons, Ltd, 2003).

8. Mitchell, D.J., Tiddy, G.J.T., Waring, L., Bostock, T. & McDonald, M.P. Phase behaviour of polyoxyethylene surfactants with water. Mesophase Structures and partial miscibility (cloud points). *Journal of the Chemical Society, Faraday Transactions 1: Physical Chemistry in Condensed Phases* 79, 975-1000 (1983).

9. Hyde, S.T. (ed.) *Handbook of Applied Surface and Colloid Chemistry*, (John Wiley & Sons, Ltd., 2001).

10. Collings, P.J. & Hird, M. *Introduction to Liquid Crystals Chemistry and Physics*, (Taylor and Francis, Ltd., 1997).

11. Israelachvili, J.N. 20 - Soft and biological structures. in *Intermolecular and Surface Forces (Third Edition)* 535-576 (Academic Press, San Diego, 2011).

12. Alexandridis, P., Olsson, U. & Lindman, B. Structural polymorphism of amphiphilic copolymers: six lyotropic liquid crystalline and two solution phases in a poly(oxybutylene)-b-poly(oxyethylene)-water-xylene system. *Langmuir* 13, 23-34 (1997).

13. Alexandridis, P., Olsson, U. & Lindman, B. A record nine different phases (four cubic, two hexagonal, and one lamellar lyotropic liquid crystalline and two micellar solutions) in a ternary isothermal system of an amphiphilic block copolymer and selective solvents (water and oil). *Langmuir* 14, 2627-2638 (1998).

14. Araos, M.U. & Warr, G.G. Self-assembly of nonionic surfactants into lyotropic liquid crystals in ethylammonium nitrate, a room-temperature ionic liquid. *Journal of Physical Chemistry B* 109, 14275-14277 (2005).

15. Forrest, B.J. & Reeves, L.W. New lyotropic liquid-crystals composed of finite nonspherical micelles. *Chemical Reviews* 81, 1-14 (1981).

16. Funari, S.S., Holmes, M.C. & Tiddy, G.J.T. Intermediate lyotropic liquid-crystal phases in the $C_{16}EO_6$/water system. *Journal of Physical Chemistry* 98, 3015-3023 (1994).

17. Chevalier, Y. & Zemb, T. The structure of micelles and microemulsions. *Reports on Progress in Physics* 53, 279-371 (1990).

18. Israelachvili, J. The science and applications of emulsions - an overview. *Colloids and Surfaces a-Physicochemical and Engineering Aspects* 91, 1-8 (1994).

19. Dong, R. & Hao, J. Complex fluids of poly(oxyethylene) monoalkyl ether nonionic surfactants. *Chemical Reviews* 110, 4978-5022 (2010).

20. Greaves, T.L. & Drummond, C.J. Ionic liquids as amphiphile self-assembly media. *Chemical Society Reviews* 37, 1709-1726 (2008).

21. Hollamby, M.J. et al. Surfactant aggregation in CO_2/heptane solvent mixtures. *Langmuir* 25, 12909-12913 (2009).

22. Liu, J.C. et al. Solubility of the non-ionic surfactant tetraethylene glycol n-laurel ether in supercritical CO_2 with n-pentanol. *Fluid Phase Equilibria* 187, 247-254 (2001).

23. Seguin, C., Eastoe, J., Clapperton, R., Heenan, R.K. & Grillo, I. Alternative non-aqueous water-miscible solvents for surfactants. *Colloids and Surfaces a-Physicochemical and Engineering Aspects* 282, 134-142 (2006).

24. Seguin, C., Eastoe, J., Heenan, R.K. & Grillo, I. Controlling aggregation of nonionic surfactants using mixed glycol media. *Langmuir* 23, 4199-4202 (2007).

25. Warnheim, T. & Jonsson, A. Phase-diagrams of alkyltrimethylammonium surfactants in some polar-solvents. *Journal of Colloid and Interface Science* 125, 627-633 (1988).

26. Evans, H., Tildesley, D.J. & Leng, C.A. Theories of cloud-curve phase-separation in nonionic alkyl polyoxoethylene micellar solutions. *Journal of the Chemical Society-Faraday Transactions Ii* 83, 1525-1541 (1987).

27. Tasaki, K. Poly(oxyethylene)-water interactions: A molecular dynamics study. *Journal of the American Chemical Society* 118, 8459-8469 (1996).

28. Nibu, Y. & Inoue, T. Phase behavior of aqueous mixtures of some polyethylene glycol decyl ethers revealed by DSC and FT-IR measurements. *Journal of Colloid and Interface Science* 205, 305-315 (1998).

29. Nibu, Y. & Inoue, T. Solid-liquid phase behavior of binary mixture of tetraethylene glycol decyl ether and water. *Journal of Colloid and Interface Science* 205, 231-240 (1998).

30. Nibu, Y., Suemori, T. & Inoue, T. Phase behavior of binary mixture of heptaethylene glycol decyl ether and water: formation of phase compound in solid phase. *Journal of Colloid and Interface Science* 191, 256-263 (1997).

31. Hofmeister, F. *Arch. Exp. Pathol. Pharmakol.* 24, 247 (1888).

32. Cacace, M.G., Landau, E.M. & Ramsden, J.J. The Hofmeister series: salt and solvent effects on interfacial phenomena. *Quarterly Reviews of Biophysics* 30, 241-277 (1997).

33. Collins, K.D. & Washabaugh, M.W. The Hofmeister effect and the behavior of water at interfaces. *Quarterly Reviews of Biophysics* 18, 323-422 (1985).

34. Zhang, Y.J. & Cremer, P.S. Interactions between macromolecules and ions: the Hofmeister series. *Current Opinion in Chemical Biology* 10, 658-663 (2006).

35. Bostrom, M., Williams, D.R.M. & Ninham, B.W. Why the properties of proteins in salt solutions follow a Hofmeister series. *Current Opinion in Colloid & Interface Science* 9, 48-52 (2004).

36. Gurau, M.C. et al. On the mechanism of the Hofmeister effect. *Journal of the American Chemical Society* 126, 10522-10523 (2004).

37. Leontidis, E. Hofmeister anion effects on surfactant self-assembly and the formation of mesoporous solids. *Current Opinion in Colloid & Interface Science* 7, 81-91 (2002).

38. Sharma, K.S., Patil, S.R. & Rakshit, A.K. Study of the cloud point Of $C_{12}E_n$ nonionic surfactants: effect of additives. *Colloids and Surfaces a-Physicochemical and Engineering Aspects* 219, 67-74 (2003).

39. Weckstrom, K. & Zulauf, M. Lower consolute boundaries of a poly(oxyethylene) surfactant in aqueous-solutions of mono-valent salts. *Journal of the Chemical Society-Faraday Transactions I* 81, 2947-2958 (1985).

40. Blankschtein, D., Thurston, G.M. & Benedek, G.B. Phenomenological theory of equilibrium thermodynamic properties and phase-separation of micellar solutions. *Journal of Chemical Physics* 85, 7268-7288 (1986).

41. Rodriguez, C. & Kunieda, H. Effect of electrolytes on discontinuous cubic phases. *Langmuir* 16, 8263-8269 (2000).

42. Iwanaga, T., Suzuki, M. & Kunieda, H. Effect of added salts or polyols on the liquid crystalline structures of polyoxyethylene-type nonionic surfactants. *Langmuir* 14, 5775-5781 (1998).

43. Zheng, L.Q., Minamikawa, H., Harada, K., Inoue, T. & Chernik, G.G. Effect of inorganic salts on the phase behavior of an aqueous mixture of heptaethylene glycol dodecyl ether. *Langmuir* 19, 10487-10494 (2003).

44. Inoue, T., Yokoyama, Y. & Zheng, L.-Q. Hofmeister anion effect on aqueous phase behavior of heptaethylene glycol dodecyl ether. *Journal of Colloid and Interface Science* 274, 349-353 (2004).

45. Kahlweit, M., Lessner, E. & Strey, R. phase-behavior of quaternary systems of the type H_2O-oil-nonionic surfactant inorganic electrolyte .2. *Journal of Physical Chemistry* 88, 1937-1944 (1984).

46. Firman, P., Haase, D., Jen, J., Kahlweit, M. & Strey, R. On the effect of electrolytes on the mutual solubility between H_2O and nonionic amphiphiles. *Langmuir* 1, 718-724 (1985).

47. Kahlweit, M. et al. General patterns of the phase-behavior of mixtures of H_2O, nonpolar-solvents, amphiphiles, and electrolytes .1. *Langmuir* 4, 499-511 (1988).

48. Kahlweit, M., Strey, R., Schomacker, R. & Haase, D. General patterns of the phase-behavior of mixtures of H_2O, nonpolar-solvents, amphiphiles, and electrolytes .2. *Langmuir* 5, 305-315 (1989).

49. Kahlweit, M., Strey, R. & Haase, D. Phase behavior of multicomponent systems water-oil-amphiphile-electrolyte. 3. *The Journal of Physical Chemistry* 89, 163-171 (1985).

50. Çelik, Ö. & Dag, Ö. A new lyotropic liquid crystalline system: Oligo(ethylene oxide) surfactants with [$M(H_2O_n)X_m$] transition metal complexes. *Angewandte Chemie-International Edition* 40, 3800 (2001).

51. Binnemans, K. Ionic liquid crystals. *Chemical Reviews* 105, 4148-4204 (2005).

52. Ray, A. Micelle formation in pure ethylene glycol. *Journal of the American Chemical Society* 91, 6511-6512 (1969).

53. Siegel, D.P. Fourth-order curvature energy model for the stability of bicontinuous inverted cubic phases in amphiphile-water systems. *Langmuir* 26, 8673-8683 (2010).

54. Turner, D.C., Wang, Z.G., Gruner, S.M., Mannock, D.A. & McElhaney, R.N. Structural study of the inverted cubic phases of di-dodecyl alkyl-beta-d-glucopyranosyl-rac-glycerol. *Journal De Physique Ii* 2, 2039-2063 (1992).

55. Zhou, W.J., Gu, W.Q., Xu, Y.J., Pecinovsky, C.S. & Gin, D.L. Assembly of acidic amphiphiles into inverted hexagonal phases using an L-alanine-based surfactant as a structure-directing agent. *Langmuir* 19, 6346-6348 (2003).

56. Fennel D. Evans, H.W. *The Colloidal Domain: Where Physics, Chemistry, Biology, and Technology Meet (Advances in Interfacial Engineering)*, (Wiley-VCH, 1999).

57. Ozin, G.A., Arsenault, A.C. & Codemartiri, L. *Nanochemistry a chemical approach to nanomaterials*, (The Royal Society of Chemistry Cambridge, 2009).

58. Kresge, C.T., Leonowicz, M.E., Roth, W.J., Vartuli, J.C. & Beck, J.S. Ordered mesoporous molecular-sieves synthesized by a liquid-crystal template mechanism. *Nature* 359, 710-712 (1992).

59. Attard, G.S., Glyde, J.C. & Goltner, C.G. Lıquıd-crystalline phases as templates for the synthesis of mesoporous silica. *Nature* 378, 366-368 (1995).

60. De Vos, D.E., Dams, M., Sels, B.F. & Jacobs, P.A. Ordered mesoporous and microporous molecular sieves functionalized with transition metal complexes as catalysts for selective organic transformations. *Chemical Reviews* 102, 3615-3640 (2002).

61. Soler-Illia, G.J.d.A.A., Sanchez, C., Lebeau, B. & Patarin, J. Chemical strategies to design textured materials: from microporous and mesoporous oxides to nanonetworks and hierarchical structures. *Chemical Reviews* 102, 4093-4138 (2002).

62. Wan, Y. & Zhao, D.Y. On the controllable soft-templating approach to mesoporous silicates. *Chemical Reviews* 107, 2821-2860 (2007).

63. Okur, H.I., Turker, Y. & Dag, Ö. Synthesis of stable mesostructured coupled semiconductor thin films: meso-CdS-TiO_2 and meso-CdSe-TiO_2. *Langmuir* 26, 538-544 (2010).

64. Turker, Y. & Dag, Ö. Synthesis of mesostructured metal sulfide films using $[M(H_2O)_n](NO_3)_2$: P85 (M = Cd(II) and Zn(II)) liquid crystalline mesophases. *Journal of Materials Chemistry* 18, 3467-3473 (2008).

65. Dag, Ö., Alayoglu, S. & Uysal, I. Effects of ions on the liquid crystalline mesophase of transition-metal salt : surfactant (C_nEO_m). *Journal of Physical Chemistry B* 108, 8439-8446 (2004).

66. Çelik, Ö. A new lyotropic liquid crystalline system: oligo(ethylene oxide) surfactants with transition metal complexes ($M(H_2O)_nX_m$) and the synthesis of mesoporous metal sulfides, Master Thesis, Bilkent University (2001).

67. Demirors, A.F., Eser, B.E. & Dag, Ö. Liquid crystalline mesophases of pluronics (L64, P65, and P123) and transition metal nitrate salts ($[M(H_2O)_6](NO_3)_2$). *Langmuir* 21, 4156-4162 (2005).

68. Albayrak, C., Gulten, G. & Dag, Ö. Phase separation in liquid crystalline mesophases of $[Co(H_2O)_6]X_2$: P65 systems (X = NO_3^-, Cl^-, or ClO_4^-). *Langmuir* 23, 855-860 (2007).

69. Akdogan, Y., Uzum, C., Dag, Ö. & Coombs, N. Synthesis of solid solutions of Cd1-xZnxS nanocrystals in the channels of mesostructured silica films (vol 16, pg 2048, 2006). *Journal of Materials Chemistry* 16, 2853-2853 (2006).

70. Karakaya, C., Turker, Y., Albayrak, C. & Dag, Ö. Assembly of molten transition metal salt-surfactant in a confined space for the synthesis of mesoporous metal oxide-rich metal oxide-silica thin films. *Chemistry of Materials* 23, 3062-3071 (2011).

71. Tura, C., Coombs, N. & Dag, Ö. One-pot synthesis of CdS nanoparticles in the channels of mesosructured silica films and monoliths. *Chemistry of Materials* 17, 573-579 (2005).

72. Dag, Ö., Samarskaya, O., Coombs, N. & Ozin, G.A. The synthesis of mesostructured silica films and monoliths functionalised by noble metal nanoparticles. *Journal of Materials Chemistry* 13, 328-334 (2003).

73. Albayrak, C., Soylu, A.M. & Dag, Ö. Lyotropic liquid-crystalline mesophases of $[Zn(H_2O)_6](NO_3)_2$-$C_{12}EO_{10}$-CTAB-H_2O and $[Zn(H_2O)_{(6)}](NO_3)_{(2)}$-$C_{12}EO_{10}$-SDS-$H_2O$ systems. *Langmuir* 24, 10592-10595 (2008).

74. Albayrak, C., Soylu, A.M. & Dag, Ö. The role of charged surfactants in the thermal and structural properties of lyotropic liquid crystalline mesophases of $[Zn(H_2O)_{(6)}](NO_3)_{(2)}$-$C_nEO_m$-$H_2O$. *Journal of Colloid and Interface Science* 341, 109-116 (2010).

75. Christenson, H.K. Confinement effects on freezing and melting. *Journal of Physics-Condensed Matter* 13, R95-R133 (2001).

76. Findenegg, G.H., Jahnert, S., Akcakayiran, D. & Schreiber, A. Freezing and melting of water confined in silica nanopores. *Chemphyschem* 9, 2651-2659 (2008).

77. Jackson, C.L. & McKenna, G.B. The melting behavior of organic materials confined in porous solids. *Journal of Chemical Physics* 93, 9002-9011 (1990).

78. Jackson, C.L. & McKenna, G.B. The glass-transition of organic liquids confined to small pores. *Journal of Non-Crystalline Solids* 131, 221-224 (1991).

79. Jahnert, S. et al. Melting and freezing of water in cylindrical silica nanopores. *Physical Chemistry Chemical Physics* 10, 6039-6051 (2008).

80. Vargas-Florencia, D., Petrov, O. & Furo, I. Inorganic salt hydrates as cryoporometric probe materials to obtain pore size distribution. *Journal of Physical Chemistry B* 110, 3867-3870 (2006).

81. Jackle, J. Models of the glass-transition. *Reports on Progress in Physics* 49, 171-231 (1986).

82. Zhang, J., Liu, G. & Jonas, J. . *Journal of Physical Chemistry* 96, 3478-3480 (1992).

83. Schuller, J., Melnichenko, Y.B., Richert, R. & Fischer, E.W. Dielectric studies of the glass-transition in porous-media. *Physical Review Letters* 73, 2224-2227 (1994).

84. Binder, K., Horbach, J., Vink, R. & De Virgiliis, A. Confinement effects on phase behavior of soft matter systems. *Soft Matter* 4, 1555-1568 (2008).

85. Chi, P., Wang, Z., Li, B.H. & Shi, A.C. Soft confinement-induced morphologies of diblock copolymers. *Langmuir* 27, 11683-11689 (2011).

86. Cramer, C., Cramer, T., Kremer, F. & Stannarius, R. Measurement of orientational order and mobility of a nematic liquid crystal in random nanometer confinement. *Journal of Chemical Physics* 106, 3730-3742 (1997).

87. Ruths, M., Steinberg, S. & Israelachvili, J.N. Effects of confinement and shear on the properties of thin films of thermotropic liquid crystal. *Langmuir* 12, 6637-6650 (1996).

88. Eggers, D.K. & Valentine, J.S. Molecular confinement influences protein structure and enhances thermal protein stability. *Protein Science* 10, 250-261 (2001).

89. Blochowicz, T. et al. Accelerated dynamics of supercooled glycerol in soft confinement. *Chemical Physics Letters* 475, 171-174 (2009).

90. He, F., Wang, L.M. & Richert, R. Dynamics of supercooled liquids in the vicinity of soft and hard interfaces. *Physical Review B* 71(2005).

91. Wang, L.M., He, F. & Richert, R. Intramicellar glass transition and liquid dynamics in soft confinement. *Physical Review Letters* 92(2004).

92. Turnbull, D. & Cohen, M.H. Free-volume model of the amorphous phase: glass transition. *The Journal of Chemical Physics* 34, 120-125 (1961).

93. Macfarlane, D.R. & Angell, C.A. An emulsion technique for the study of marginal glass-formation in molecular liquids. *Journal of Physical Chemistry* 86, 1927-1930 (1982).

94. Sharma, R.C., Bhatia, K. & Gaur, H.C. Volumetric properties of molten hydrated salts. 2. zinc nitrate hexahydrate + alkali metal nitrates. *Journal of Chemical & Engineering Data* 24, 183-185 (1979).

95. Angell, C.A. Glass-forming composition regions and glass transition temperatures for aqueous electrolyte solutions. *J. Chem. Phys.* 52, 1058 (1970).

96. Angell, C.A. Liquid fragility and the glass transition in water and aqueous Solutions. *Chemical Reviews* 102, 2627-2650 (2002).

97. Cook, L. Investigation of the hygroscopic and morphological properties of atmospheric aerosols. Master Thesis, Bucknell University (2011).

98. Bard, A.J. & Faulkner, L.R. *Electrochemical Methods: Fundamentals and Applications*, (John Wiley & Sons, Inc., 2001).

99. Cihaner, A. & Algı, F. A novel neutral state green polymeric electrochromic with superior n- and p-doping processes: closer to red-blue-green (RGB) display realization. *Advanced Functional Materials* 18, 3583-3589 (2008).

100. Cihaner, A. & Algı, F. A processable rainbow mimic fluorescent polymer and its unprecedented coloration efficiency in electrochromic device. *Electrochimica Acta* 53, 2574-2578 (2008).

101. Dag, Ö., Alayoglu, S., Tura, C. & Celik, O. Lyotropic liquid-crystalline phase of oligo(ethylene oxide) surfactant/transition metal salt and the synthesis of mesostructured cadmium sulfide. *Chemistry of Materials* 15, 2711-2717 (2003).

102. Dag, Ö., Samarskaya, O., Tura, C., Gunay, A. & Celik, O. Spectroscopic investigation of nitrate-metal and metal-surfactant interactions in the solid $AgNO_3/C_{12}EO_{10}$ and liquid-crystalline $[M(H_2O)_n](NO_3)_2/C_{12}EO_{10}$ systems. *Langmuir* 19, 3671-3676 (2003).

103. Albayrak, C., Cihaner, A. & Dag, Ö. A new, highly conductive, lithium salt/nonionic surfactant, lyotropic liquid-crystalline mesophase and its application. *Chemistry – A European Journal* 18, 4190-4194 (2012).

104. Albayrak, C., Özkan, N. & Dag, O. Origin of lyotropic liquid crystalline mesophase formation and liquid crystalline to mesostructured solid transformation in the metal nitrate salt−surfactant systems. *Langmuir* 27, 870-873 (2010).

105. Angell, C.A. A new class of molten salt mixtures the hydrated dipositive ion as an independent cation Species. *Journal of the Electrochemical Society* 112, 1224 (1965).

106. Türker, Y., Karakaya, C. & Dag, Ö. Fabrication of mesoporous metal chalcogenide nanoflake silica thin films and spongy mesoporous CdS and CdSe. *Chemistry – A European Journal* 18, 3695-3705 (2012).

107. Burikov, S.A., Dolenko, T.A., Velikotnyi, P.A., Sugonyaev, A.V. & Fadeev, V.V. The effect of hydration of ions of inorganic salts on the shape of the raman stretching band of water. *Optics and Spectroscopy* 98, 235-239 (2005).

108. Terpstra, P., Combes, D. & Zwick, A. Effect of salts on dynamics of water - a raman-spectroscopy study. *Journal of Chemical Physics* 92, 65-70 (1990).

109. Currey, J. Biomaterials - sacrificial bonds heal bone. *Nature* 414, 699-699 (2001).

110. Fredericks, D.C. et al. Cellular. interactions and bone healing responses to a novel porous tricalcium phosphate bone graft material. *Orthopedics* 27, S167-S173 (2004).

111. Hing, K.A., Best, S.M., Tanner, K.E., Bonfield, W. & Revell, P.A. Mediation of bone ingrowth in porous hydroxyapatite bone graft substitutes. *Journal of Biomedical Materials Research Part A* 68A, 187-200 (2004).

112. Yan, X.X., Yu, C.Z., Zhou, X.F., Tang, J.W. & Zhao, D.Y. Highly ordered mesoporous bioactive glasses with superior in vitro bone-forming bioactivities. *Angewandte Chemie-International Edition* 43, 5980-5984 (2004).

113. Schmidt, S.M. et al. Surfactant based assembly of mesoporous patterned calcium phosphate micron-sized rods. *Microporous and Mesoporous Materials* 94, 330-338 (2006).

114. Wang, H., Zhai, L., Li, Y. & Shi, T. Preparation of irregular mesoporous hydroxyapatite. *Materials Research Bulletin* 43, 1607-1614 (2008).

115. Yao, J. et al. Hydroxyapatite nanostructure material derived using cationic surfactant as a template. *Journal of Materials Chemistry* 13, 3053-3057 (2003).

116. Ye, X., Cai, S., Xu, G., Dou, Y. & Hu, H. Synthesis of mesoporous hydroxyapatite thin films using F127 as templates for biomedical applications. *Materials Letters* 85, 64-67 (2012).

117. Zhao, Y.F. & Ma, J. Triblock co-polymer templating synthesis of mesostructured hydroxyapatite. *Microporous and Mesoporous Materials* 87, 110-117 (2005).

118. Begum, R. & Matsuura, H. Conformational properties of short poly(oxyethylene) chains in water studied by IR spectroscopy. *Journal of the Chemical Society-Faraday Transactions* 93, 3839-3848 (1997).

119. Matsuura, H. & Fukuhara, K. Vibrational spectroscopic studies of conformation of poly(oxyethylene) .2. conformation spectrum correlations. *Journal of Polymer Science Part B-Polymer Physics* 24, 1383-1400 (1986).

120. Obrien, F.E.M. The control of humidity by saturated salt solutions. *Journal Of Scientific Instruments and of Physics in Industry* 25, 73 (1948).

121. Zhang, Y.-H. & Chan, C.K. Observations of water monomers in supersaturated $NaClO_4$, $LiClO_4$, and $Mg(ClO_4)_2$ droplets using raman spectroscopy. *The Journal of Physical Chemistry A* 107, 5956-5962 (2003).

122. Greenspan, L. Humidity fixed points of binary saturated aqueous solutions. *Journal of Research of the National Bureau of Standards - A. Physics and Chemistry* 81A, 89 (1976).

123. Zhao, L.-J., Zhang, Y.-H., Wang, L.-Y., Hu, Y.-A. & Ding, F. FTIR spectroscopic investigations of supersaturated $NaClO_4$ aerosols. *Physical Chemistry Chemical Physics* 7, 2723-2730 (2005).

124. Pearce, J.N. & Nelson, A.F. The vapor pressures of aqueous solutions of lithium nitrate and the activity coefficients of some alkali salts in solutions of high concentration At 25°. *Journal of the American Chemical Society* 54, 3544-3555 (1932).

125. Bai, Y. et al. High-performance dye-sensitized solar cells based on solvent-free electrolytes produced from eutectic melts. *Nature Materials* 7, 626-630 (2008).

126. Choudhury, N.A., Sampath, S. & Shukla, A.K. Hydrogel-polymer electrolytes for electrochemical capacitors: an overview. *Energy & Environmental Science* 2, 55-67 (2009).

127. Law, C.H. et al. Water-based electrolytes for dye-sensitized solar cells. *Advanced Materials* 22, 4505-4509.

128. Hoshino, K. et al. Ion-conductive liquid crystals: formation of stable smectic semi-bilayers by the introduction of perfluoroalkyl moieties. *Macromolecular Chemistry and Physics* 203, 1547-1555 (2002).

129. Judeinstein, P. & Roussel, F. Ionic conductivity of lithium salt/oligo (ethylene oxide)-based liquid-crystal mixtures: The effect of molecular architecture on the conduction process. *Advanced Materials* 17, 723-+ (2005).

130. Kishimoto, K. et al. Nanostructured anisotropic ion-conductive films. *Journal of the American Chemical Society* 125, 3196-3197 (2003).

131. Li, J. et al. Anisotropic ion conductivity in liquid crystalline diblock copolymer membranes with perpendicularly oriented PEO cylindrical domains. *Macromolecules* 40, 8125-8128 (2007).

132. Ohtake, T. et al. Liquid-crystalline ion-conductive materials: Self-organization behavior and ion-transporting properties of mesogenic dimers containing oxyethylene moieties complexed with metal salts. *Macromolecules* 33, 8109-8111 (2000).

133. Yoshio, M. et al. One-dimensional ion-conductive polymer films: alignment and fixation of ionic channels formed by self-organization of polymerizable columnar liquid crystals. *Journal of the American Chemical Society* 128, 5570-5577 (2006).